Failure Assessment of Cast Iron Water Mains Using Fracture Mechanics

by

© Suborno Debnath

A thesis submitted to the

School of Graduate Studies

in partial fulfillment of the requirement for the degree of

Master of Engineering

Faculty of Engineering & Applied Science

Memorial University of Newfoundland

June 2019

St. John’s, Newfoundland, Canada

ABSTRACT

Cast iron was one of the most dominated materials for municipal water mains in the last century. Cast iron pipes are being gradually replaced by ductile iron, steel or plastic pipe due to their poor performance. However, a significant portion of cast iron pipelines is still in service for the municipal water distribution system. Many of these pipelines are deteriorated due to corrosion and often fail. The remaining strength assessment of these pipelines is required for maintaining the integrity of municipal water distribution systems. Researchers employed conventional continuum mechanics approach for the assessment of cast iron water mains. However, the continuum mechanics based modelling was found to be unsuccessful explaining some failure mechanisms observed in the field. The fracture mechanics approach could be used to investigate the failure mechanism of the pipelines. The major challenges in the application of fracture mechanics include i) availability of a tool for calculating the fracture parameters and ii) availability of material parameter for fracture mechanics based strength assessment. In this study, mechanical properties for cast iron pipe materials are explored for fracture mechanics based strength assessment. Uniaxial tensile tests are conducted to understand the stress–strain response for stress–deformation analysis to calculate the fracture parameter. The influence of the rate of loading on stress–strain behavior and loading-unloading responses are investigated. Fracture toughness is also determined by using a simplified chevron notch method. The parameters obtained from the test are used in finite element analysis to determine the fracture parameters of cast iron pipes. Numerical techniques for finite element modelling are developed for the assessment of fracture parameter (i.e., stress intensity factor). The stress intensity factors for different shapes of corrosion defects are examined. The employed fracture mechanics approach is found to successfully explain the failure mechanism of cast iron pipes observed in the field.

ACKNOWLEDGEMENTS

First of all, I would like to take the opportunity to acknowledge the help and support of several individuals who have contributed in many different ways to the work. I would like to express my sincere and heartfelt gratitude to Dr. Ashutosh Sutra Dhar for his proper guidance and valuable suggestions, sincere supervision, and co-operation throughout the research work. I have been very fortunate that Dr. Dhar is my supervisor, and I have learnt many lessons in working under his guidance that I will remember for the rest of my life. Thank you very much for being my guide, mentor and role model.

I would also like to thank Dr. Kshama Roy, Dr. Rajib Dey, Mr. Abu Hena Muntakim, Mr. Ripon Karmaker, Mr. Anan Morshed and Mr. Diponkar Saha for their invaluable suggestions, insightful guidance and continuous encouragement throughout the program. I owe a debt of gratitude to Dr. Kshama Roy, for encouraging me to hone my leadership skills by involving and volunteering in different societies. He assisted me with every aspect of my graduate student life and also with any kind of help that I needed.

I would also like to thank the staff and technicians, especially Mr. Steve Steele and Mr. David Snook, who have helped me during my research. Furthermore, I highly appreciate the support given by the research and administration staff of the Faculty of Engineering and Applied Science, Memorial University who helped me in different ways.

I would not have been able to undertake this work without the financial support of the Natural Sciences and Engineering Research Council of Canada (NSERC), the Faculty of Engineering and Applied Science and the School of Graduate Studies.

I cannot express with words my gratitude towards my parents, brother and close friends, for encouraging and supporting me throughout this journey.

Table of Contents

CHAPTER 5

List of Figures

List of Tables

CHAPTER 1

Introduction

1.1 Background and Motivation

Cast iron pipeline is found in all parts of the world that fulfill the basic needs by transporting fluid. First authentically recorded cast iron pipe was laid at Langensalza, Germany in 1962, although its full-scale use was started long ago in 1664 at Versailles, France (Koeble and Hogan 1967). It was first installed in the USA at the beginning of the nineteenth century that was imported from England and Scotland and grew rapidly in the 1890s (Koeble and Hogan 1967). In Canada, first cast iron pipeline was built in 1853, the largest pipeline in that time around the world (Finkel 2018). Since then, the cast iron pipeline is one of the dominating infrastructures that transmit fluid. At present, the age of cast iron pipe ranges from around fifty years to over hundred years, many of which are in replacement era.

The aged pipelines require fitness-for-services (FFS) assessment as these are prone to failure. However, failure assessment tools for FFS assessment of cast iron pipes are not well developed and are not able to predict the failure modes observed in the field. Folkman (2018) conducted a comprehensive survey of different municipalities in the USA and Canada to identify the failure modes of water mains. Figure 1.1 provides a summary of different failure modes observed (Folkman 2018). As seen in this figure, circumferential cracking is the major failure mode for cast iron water mains. Circumferential cracking may occur due to bending stress developed by the loss of bedding support, differential ground movement, or axial stress due to temperature change.

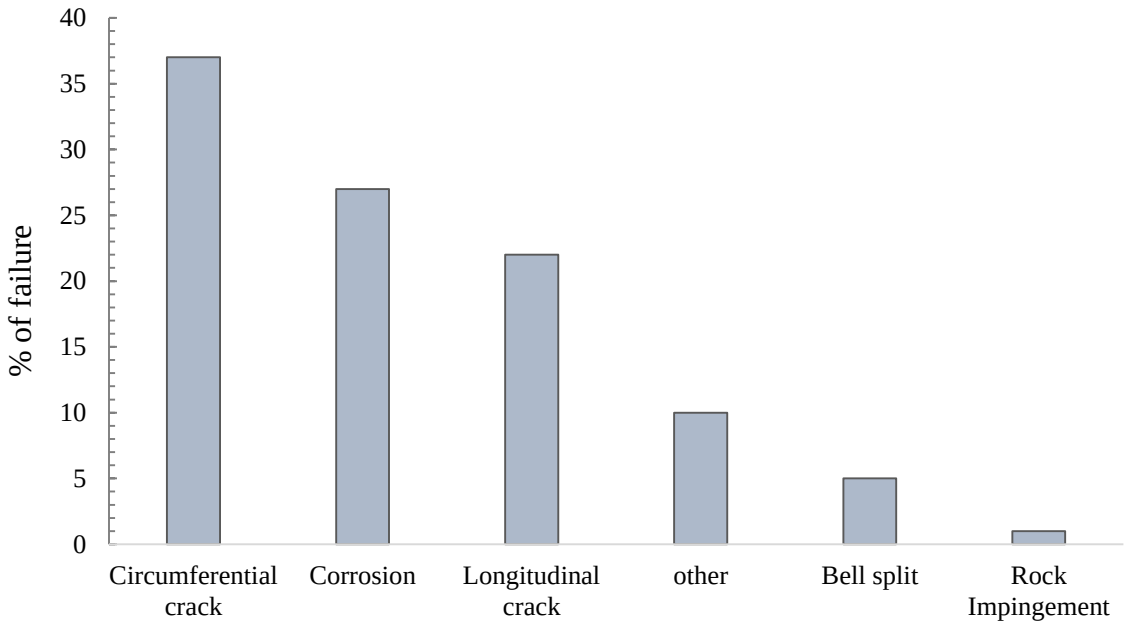

Figure 1.1: Distribution of failure mode (Folkman 2018)

Pipelines are subjected to non-uniform bedding when the backfill material contains a significant portion of fine soil that can be eroded under gravity or carried by the water flow and creates a void around the pipe (Figure 1.2). If it continues and causes progressive volume loss, settlement may occur (Kamel et al. 2008) leading to longitudinal bending. Balkaya et al. (2012) and Liyanage and Dhar (2018) conducted continuum based finite element analysis and revealed that longitudinal stress developed due to bending is insufficient to cause circumferential cracking of the water mains. An erosion void along with localized concentrated support might cause a stress leading to cracking (Liyanage and Dhar 2018).

Corrosion is identified as one of the major problems in the water transportation system, which reduce the strength of the pipeline. Pipelines can corrode internally or externally. Soil-pipeline system acts as an electrochemical cell and creates external corrosion. Internal corrosion occurs due to the influence of water.

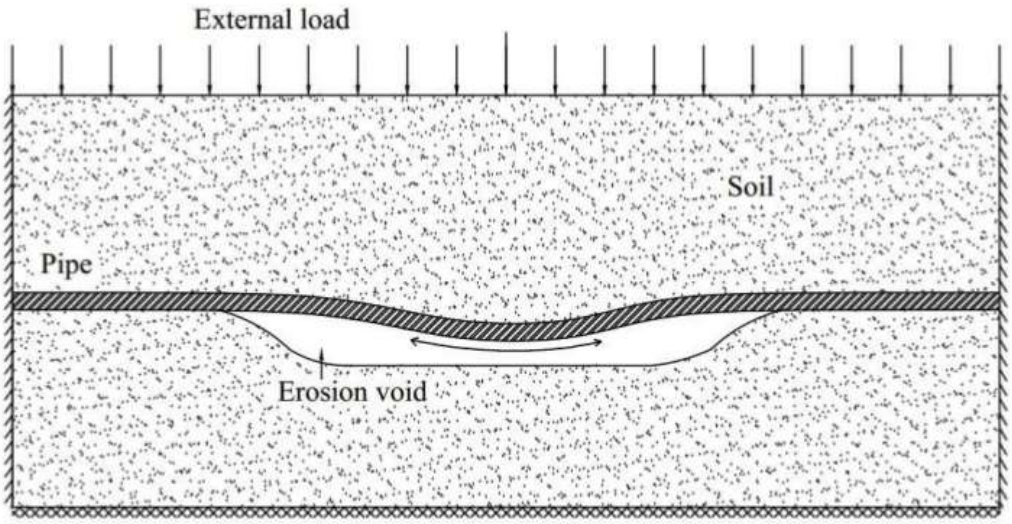

Figure 1.2: Pipeline subjected to non-uniform bedding (Liyanage 2016)

Both types of corrosion lead to leakage that affect the safety of the pipe and causes water losses. Marker et al. (2005) reveals that corrosion pit on the pipe wall may be the cause of circumferential cracking of cast iron water mains observed in the field. Liyanage and Dhar (2017) employed finite element modelling and showed that although corrosion pit causes redistribution of stresses around the pit, the developed stress is not significant to cause circumferential cracking. A corrosion pit along with an erosion void and a localized concentrated force can lead to circumferential cracking (Liyanage and Dhar 2018). Corrosion of the pipe can lead to the development of sharper notch and/or crack-like defects on the pipe wall (Conlin and Paker 1991). The effect of corrosion notch and/or crack like defect can be modelled through the application of fracture mechanics. However, fracture mechanics has not been applied extensively for studying the failure mechanism of cast iron water main. The major challenges in the application of fracture mechanics include: i) unavailability of the material parameter (fracture toughness) required for failure assessment ii) unavailability of tools for assessing fracture parameter (i.e., stress intensity factor). This research focuses on addressing the challenges for cast iron water mains.

1.2 Objectives

The major objective of the current research is to develop tools for fracture mechanics based failure assessment of cast iron water mains. An experimental program is undertaken to develop material parameters for fracture mechanics based assessment, and a three-dimensional finite element modelling technique is used to develop fracture parameters for different shapes of defects. The specific objectives of this research are:

- Identify parameters for cast iron pipe materials for stress–deformation analysis to calculate fracture parameters
- Develop finite element (FE) modelling technique to determine the fracture parameter for buried cast iron water mains
- Assess the fracture parameters for different corrosion defects of a buried pipe.
- Evaluate existing equation for fracture assessments for in-air pipe and develop improved methods for buried pipes.

1.3 Outline of the thesis

This thesis is prepared in manuscript format. The outcome of the study is presented in five chapters and one appendix (Appendix A). The outline is as follows:

- Chapter 1 highlights the backgrounds, motivation and objectives of the research work.

- Chapter 2 presents a brief review. However, as the thesis is prepared in manuscript format, the problem-specific literature reviews are provided in Chapters 3 and 4.

- Chapter 3 presents the material properties for fracture mechanics based strength assessment of cast iron water mains. This chapter has been submitted to a journal paper as a technical paper for review. A part of this research work has been published in the 71st Canadian Geotechnical Conference, GeoEdmonton 2018, Edmonton, Alberta, Canada, September 23–26, 2018 (attached in Appendix A).

- Chapter 4 presents the assessment of stress intensity factor for buried cast iron water pipes using Abaqus FE software. This research work has been prepared for submission to the 72nd Canadian Geotechnical Conference.

- Chapter 5 summarizes the outcomes of the research and recommendations for future studies.

As the thesis is prepared in manuscript format, the references cited in Chapters 3 and 4 are listed at the end of each chapter. The references cited in Chapters 1 and 2 are listed in the 'Reference' section at the end of the thesis.

Co-Authorship: The research presented in this thesis has been performed by the author of this thesis, Mr. Suborno Debnath under the supervision of Dr. Ashutosh Sutra Dhar. He also prepared the draft manuscript. Some test data from Ali are used for validation of FE model for SENB tests and compare with some test data obtained from the current research. Ali's data are properly cited within the text and figures, as applicable.

CHAPTER 2
Literature Review

2.1 Introduction

As the thesis has been written in manuscript format, problem-specific literature review is presented in Chapters 3 and 4. This chapter provides a brief overview of mechanical properties of cast iron, theoretical background of fracture mechanics, failure mechanism of cast iron pipeline and additional previous research relevant to the present study. In this thesis, unless stated otherwise, pipelines refer to water main pipelines.

2.2 Cast iron

Cast iron is an iron alloy that has more than 2% carbon as the main alloying element and 1– 3% silicon with a wide variety of properties (Arias-Gonzalez et al. 2016). Mechanical properties of cast iron, i.e., tensile and compressive strength, Poison's ratio, ductility, Young's modulus, and fracture toughness depend strongly on its microstructure. Research undertaken to determine the material parameters for cast iron materials, reveals the wide variation of the parameters (Yamamoto et al. l983, Caproco Corrosion 1985, Conlin and Baker 1991, Ma and Yamada 1994, Rajani et al. 2001, Seica et al. 2004). Table 2.1 shows a summary of the material parameter of cast iron reported by different researchers. Variability in the material properties of cast iron are also observed in the material database available in CES EduPack Software (Granta 2018). CES EduPack has been developed by Granta Design Limited, a leading materials information technology company in Cambridge, UK that includes material data collected for over twenty years in collaboration with leading materials and process data providers (i.e., American Society of Mechanical Engineers (ASME), ASM International, M-Base Engineering & Software GmBH,

ecoinvent, UK Steel (EEF), Firehole Technologies Inc., HIS, Metallic Materials Properties Development and Standardization (MMPDS), MI-21, NIMS etc.). Mechanical properties, i.e., tensile strength, compressive strength, yield strength, Young's modulus, fracture toughness, and fatigue strength are obtained from CES EduPack software are shown in Figures 2.1–2.6. Data for cast iron in the figures consist of the data presented in Table 2.1.

Table 2.1. Comparison of mechanical properties of cast iron (Seica et. al. 2004)

Type of cast iron	Reference	Age (years)	Tensile strength (MPa)	Modulus of rupture (MPa)	Fracture toughness (MPa√m)
Pit	Rajani et. al. (2000)	64 –115	33 – 267	132 –378	5.7 – 13.7
Pit and Spun	Conlin and Baker (1991)	Out of service pipes	137 – 212	n/a	10.5 – 15.6
Pit and Spun	Seica et. al. (2004)	50 – 124	47 – 297	164 – 349	n/a
Spun	Yamamoto et. al. (1983)	22 – 79	100 – 150	20 – 250	n/a
Spun	Caproco Corrosion (1985)	22 – 28	70 – 217	n/a	n/a
Spun	Ma and Yamada (1994)	21 – 32	40 – 320	120 – 320	n/a
Spun	Rajani et. al. (2000)	22 – 61	135 – 305	194 – 445	10.3 – 15.4

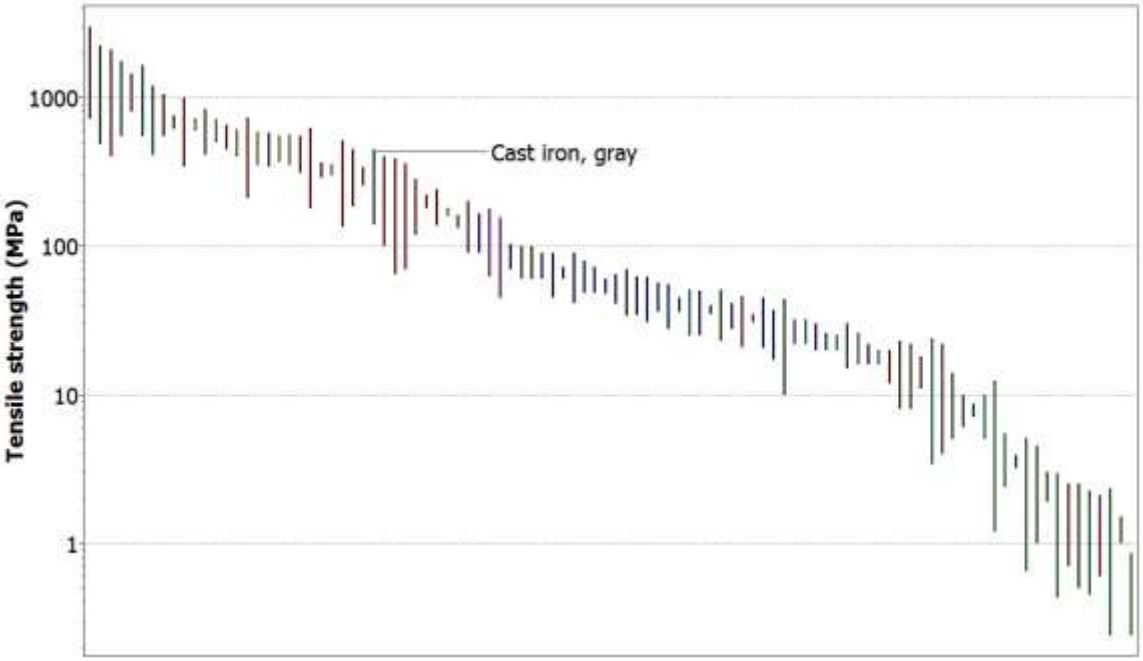

Figure 2.1. The tensile strength of cast iron (CES EduPack)

Figure 2.2. The compressive strength of cast iron (CES EduPack)

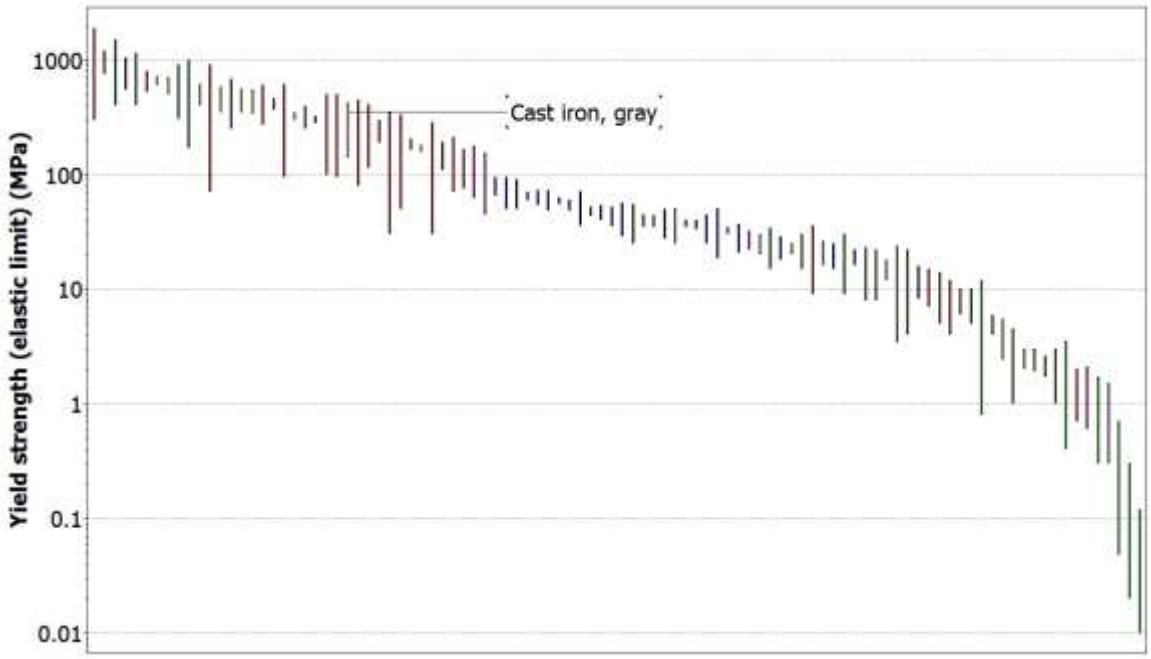

Figure 2.3. The yield strength of cast iron (CES EduPack)

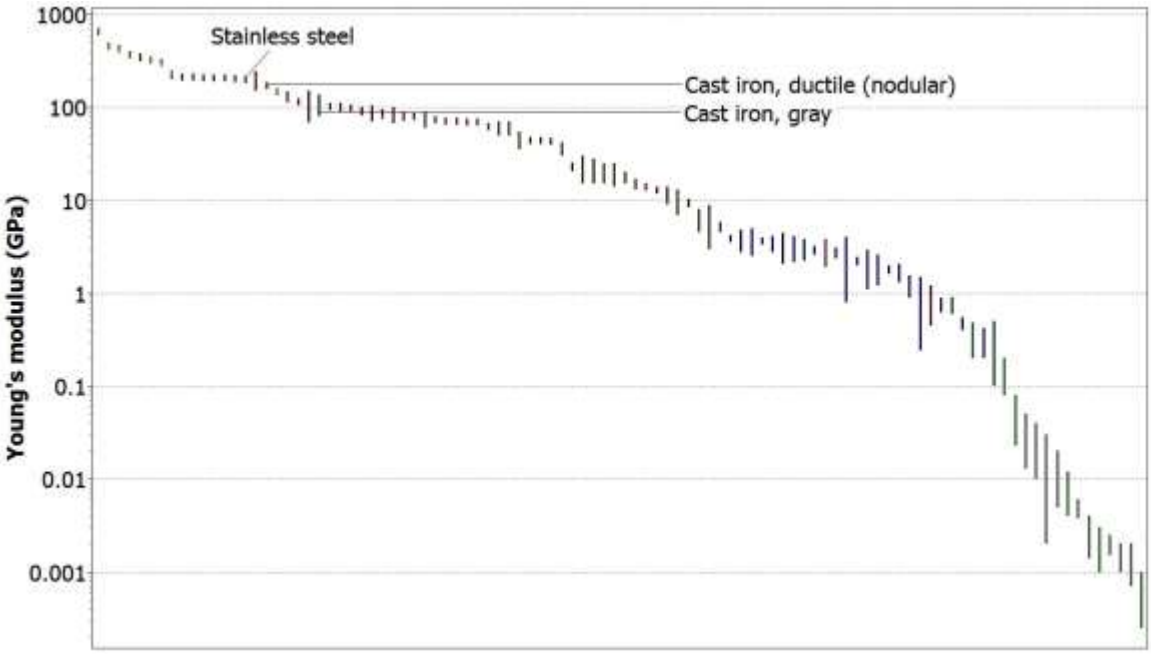

Figure 2.4. Young's modulus of cast iron (CES EduPack)

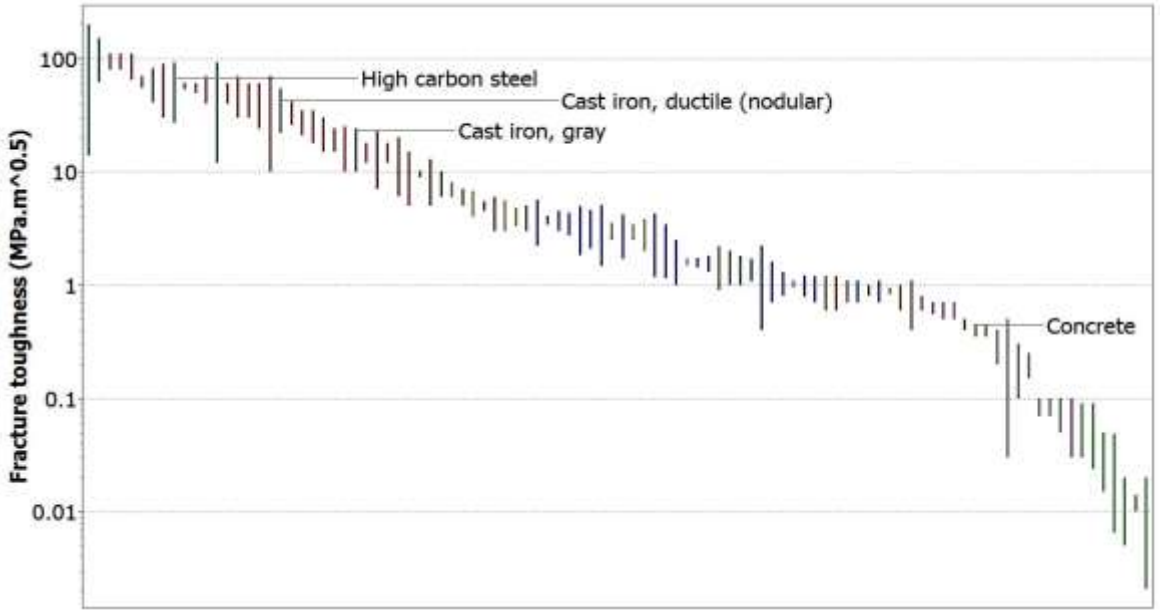

Figure 2.5. Fracture toughness of cast iron (CES EduPack)

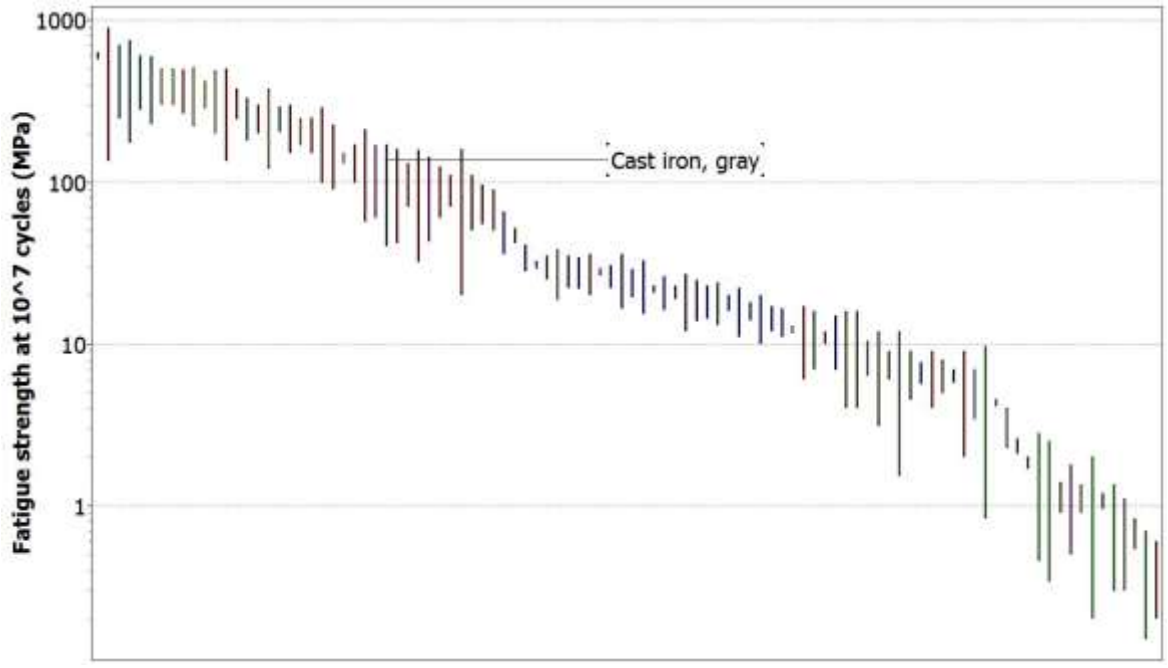

Figure 2.6. Fatigue strength of cast iron (CES EduPack)

2.3 Failure Mechanisms of Cast Iron Pipelines

Folkman (2018) conducted an extensive study on the failure mechanisms of pipeline in North America. Folkman (2018) showed that circumferential crack, longitudinal crack, corrosion (internal or external), bell splitting, manufacturing defects and human error are mainly responsible for the failure of cast iron pipes. These pipe failures are briefly discussed below.

2.3.1 Circumferential crack

Circumferential crack occurs due to high longitudinal stress on the pipe wall that may be caused by bending of the pipe (Talbot, 1926) and/or axial tension resulting from temperature change (Jesson et al. 2010). The bending may be caused due to rock impingement, loss of bedding support, ground movement, differential settlement, expansive soils or changes in water temperature. Small diameter pipe (< 200 mm in diameter) is more vulnerable on circumferential crack, responsible for up to 80% of the failures (Rajani and McDonald 1995). Corrosion pits and graphitization may influence the circumferential crack. About 90% of the circumferential failures are reported to occur with the presence of a corrosion pit (Makar et al. 2001).

2.3.2 Longitudinal crack

Excessive circumferential stress due to internal water pressure along with geostatic stress causes a longitudinal crack. Large diameter pipes are mainly affected by longitudinal crack (Makar et al. 2001). External loading like geostatic stress, snow load, and traffic load accelerate the process of longitudinal cracking.

2.3.3 Corrosion

Corrosion is one of the predominate factors that reduces the service life of cast iron water mains. Metal loss occurs due to an attack by the environment on pipeline materials. About 28% of

water main failure is reported to occur due to corrosion of pipelines (Folkman 2018). There are several types of corrosion. Uniform or general corrosion occurs when the whole pipeline deteriorates at approximately the same rate. Localized corrosion causes pit holes on the pipe wall which is considered as the worst type of corrosion. Makar et al. (2005) conducted a parametric study, varying pit diameter under different types of loading conditions, i.e., water pressure, frost load, temperature changes, loss of support, soil properties and wall thickness. This study reported that pitting corrosion creates stress concentration that may induce crack. Intergranular corrosion may also occur at or near the grain boundaries.

2.3.4 Bell splitting

Bell splitting is a common failure mode in small diameter pipe (Makar et al. 2001). It occurs due to temperature variation. Molten lead is used to pour the joint of cast iron that has different thermal co-efficient of expansion and behave differently than cast iron. As a result, cracks may develop just below the bell of the pipe when excess stress is produced due to thermal expansion (Makar et al. 2001).

2.3.5 Spiral Cracking

Spiral cracking failure is generally observed in medium diameter (380 mm-500 mm of diameter) pipes when subjected to a combinational of loads, i.e., internal pressure and bending stress (Makar et al. 2001). Firstly, crack initiates in the circumferential direction then it propagates in the longitudinal direction that makes a spiral shape.

2.3.6 Manufacturing defects

Cast iron is manufactured by different techniques to improve its quality. It often shows some manufacturing defects. Spun cast iron shows fewer defects than pit cast iron (Makar et al.

2001). Porosity is one of the most common defects found in pit cast iron. Another manufacturing defect is inclusions that weaken the pipe metal and may create stress concentration. Ferrosilicon that is not fully dissolved creates spherical inclusion when it cools rapidly (Makar et al. 2001). Pinholes, form by chemical reactions between oxidized metal and carbon which can affect the strength of cast iron. Besides, foreign materials may be present due to insufficient cleaning of molds.

2.3.7 Human factors

Several human factors were found to contribute toward the failure of cast iron water mains. The human factor includes improper design, poor installation, third-party damage from excavation or repairing and negligence in maintenance.

The current study has focused on assessing the cracking due to corrosion of cast iron water mains.

2. 4. Fracture Mechanics Concepts

Pipeline failure occurs due to loss of strength and/or extreme loading. A failure occurs when the pipe wall stress exceeds the strength of the pipe material. The conventional method employs continuum theory to calculate wall stresses that is compared with the strength of materials. Seica and Packer (2004), Makar and McDonald (2007), Ji et al. (2015), Zhang et al. (2017), Liyanage and Dhar (2017 & 2018) and others employed different technique utilizing the continuum mechanics theory to calculate the pipe wall stress for cast iron pipeline. However, a higher circumferential stress was calculated using these methods, which does not explain the reason for the circumferential cracking of water mains observed in the fieldPipe with corrosion notches and crack-like defects, may fail at a stress, below its yield strength, where failure would not normally be expected (Dowling 2013). Researchers are now employing fracture mechanics for

failure assessment of pipes. Fracture mechanics has been widely used in recent times and was found as a more appropriate way to explain failure mechanism (Fahimi et al. 2016, Wang et al. 2017, Mondal 2017).

The concept of fracture mechanics initially introduced by Inglis (1913) and later developed by Griffith (1921), Westergaard (1939) and Irwin (1957). The stress intensity factor (SIF) is introduced as a measure of the severity of the stress near the crack. The SIF is defined by

$$K = \lim_{r,\theta \to 0} \sigma \sqrt{2\pi r} \quad \text{[2.1]}$$

This equation is generally expressed as

$$K = F\,\sigma\sqrt{\pi a} \quad \text{[2.2]}$$

Where K is the stress intensity factor for a particular mode of cracking, a is the initial crack length, F is a geometric factor, and σ is the nominal stress at failure.

Another parameter is also used for fracture assessment of linear elastic material, which is the strain energy release rate. The strain energy release rate, G is related with K by the following equation,

$$G = \frac{K^2}{E'} \quad \text{[2.3]}$$

E' can be obtained from the material's elastic modulus E, and Poisson's ratio, v. If the thickness of a structure in the z direction is small relative to other directions, the normal and shear stress and their gradients are often assumed to be zero in the z-direction and the stress is defined as plane stress. If the thickness in the z direction is large relative to other directions, plane strain condition exists where the strain in z direction is zero (Terfas, 2010).

For plane stress condition

$$E' = E \quad \text{[2.4]}$$

For plane strain condition

$$E' = \frac{E}{1-\nu^2} \quad \text{…….[2.5]}$$

The above approach is applicable for linear elastic material and termed as linear elastic fracture mechanics (LEFM). For low toughness materials, i.e., brittle material, the region of yielding (plastic zone) is not excessively large and LEFM is applicable. For ductile material showing higher toughness, LEFM may not be applicable. Elastic-plastic fracture mechanics (EPFM) is required for assessing the ductile material. As cast iron is a brittle material, the LEFM approach is applicable for the assessment of cast iron water main.

2.5 Summary

An overview of cast iron material, failure modes, and failure assessment technique is presented in this chapter. The physical and mechanical properties of cast iron are reported to vary significantly, which is due to the variation of metallurgy. It is thus important to understand the microstructure to predict the strength behaviour of the pipe material. Failure of cast iron water mains is found to be associated with corrosion and crack. The conventional continuum mechanics is often not successful in predicting the failure mechanism in the cast iron pipe. Fracture mechanics is being utilized to better understand the failure mechanism of the water mains. As cast iron is a brittle material, LEFM can be used for assessing the cast iron pipes.

CHAPTER 3

Material Properties for Fracture Mechanics based Strength Assessment of Cast Iron Water Mains

3.1. Introduction

Cast iron was extensively used as the dominant material for municipal water mains until the middle of the twentieth century. Although cast iron pipes are no longer manufactured or used for water mains, a huge volume of cast iron pipes exists in the water distribution system in North America (Folkman 2018). These aged infrastructures are subjected to deterioration due to corrosion and are susceptible to leakage and breakage. Determining the strength of the deteriorating water mains which is required for developing a rehabilitation and replacement strategy of these structures has been a challenge for municipalities. The conventional method of assessing the strength of the pipes is to compare the ultimate tensile and compressive strengths with the maximum stresses in the pipe wall. The stress experienced by the pipe wall is calculated using the theory of continuum mechanics (Seica and Packer 2004, Makar and McDonald 2007, Ji et al. 2015, Zhang et al. 2017a, Liyanage and Dhar 2017 & 2018).

Old cast iron pipe failures are associated with through-wall notches caused by corrosion and sharper crack-like defects caused by a stress-dependent corrosion (Conlin and Baker 1991). For the pipe with corrosion notches and crack-like defects, the stress to cause failure was reported to be significantly less than the nominal tensile strength of the pipe material (Jesson et al. 2010).

Rajani and Kleiner (2010) applied the fracture mechanics approach to explain these failures in cast iron pipes. Fracture mechanics-based strength assessment methods of deteriorating pipelines has been widely explored in recent years and was found to reasonably explain the observed failure mechanism (i.e., Fahimi et al. 2016, Wang et al. 2017, Mondal 2018). In fracture mechanics, the strength of a material against crack initiation and crack propagation is expressed using the fracture toughness of the material that is calculated using stress–deformation analyses of the structure. However, very limited information is currently available for cast iron water main materials on the fracture toughness and the parameters for stress–deformation analysis (i.e., Young's modulus, E and Poisson's ratio,ν).

The objective of the current study is to address the existing gaps in the material properties and develop an effective method for determination of parameters for fracture mechanics based strength assessment of cast iron water mains. The properties for two cast iron water mains exhumed from two nearby cities (City of St. John's and City of Mount Pearl) in the Province of Newfoundland and Labrador in Canada are determined through an experimental program. Uniaxial tensile tests are performed with samples extracted from the pipe walls to examine the stress–strain responses under monotonic loads and loading-unloading-reloading cycles applied at various strain rates. Electronic strain gauges are used to measure the axial strain and lateral strain for calculation of Poisson's ratio during uniaxial tensile tests. For determination of the fracture toughness, a simplified approach of the single-edge-notch bending (SENB) test is used through validation of the method using finite element analysis. The specimens are scanned using a scanning electron microscope (SEM) to examine the graphite flakes and chemical compositions of the pipe materials. Finite element analysis is then performed for the fracture mechanics based strength assessment of

water mains subjected to pitting corrosions using the parameters determined from the experimental program.

3.2. Fracture parameters

. The fracture toughness is a critical value of the parameters: the stress intensity factor (K), strain energy release rate (G), J-integral (J) or crack tip opening displacement (δ), used to describe the stress field around the crack tip. The stress intensity factor and strain energy release rate is generally used for brittle materials that follow linear elastic fracture mechanics principles. The stress intensity factor, K, is a measure of the stress field near a crack tip, which combines far-field stress and crack dimensions as given in Eq. 3.1:

$$K = Y\sigma\sqrt{\pi a} \tag{3.1}$$

where K = stress intensity factor for a particular mode of cracking

a = initial crack length

Y = a geometric factor

σ = nominal stress at failure

The strain energy release rate, *G*, is a measure of energy available for an increment of a crack and is defined as in Eq. 3.2:

$$G = -\frac{\partial \pi}{\partial a} \tag{3.2}$$

where π indicates the potential energy under the applied loading.

The stress intensity factor (K) and/or the strain energy release rate (G) are calculated using stress–deformation analyses of the structure. The calculated K or G are then compared with the critical value of the parameters (K_c or G_c), i.e., the fracture toughness.

However, natural variations of the properties of cast iron are well recognized. The structure of cast iron depends on its heterogeneous microstructure, alloying elements, cooling conditions, the rate of the casting, casting method, and inoculants. Discontinuity of the matrix occurs due to the presence of free graphites. Shape and dimension of the graphite play an important role in tensile strength because these produce notch effect and exclude parts in the matrix (Collini et al. 2008). The strength of cast iron is reported to be inversely proportional to the graphite contents (Angus 1976, Yamamoto et al. l983). Collini et al. (2008) showed that the stress intensity factor (SIF) dramatically decreases with the increase of free graphite. The size and the shape of the free graphite flakes depend on the cooling rate during the manufacture of cast iron pipes. These flakes act as a void and form natural cracks which tend to produce a brittle fracture (Marker et al. 2000). A moderate cooling rate forms a more pearlitic microstructure which has less tensile strength than the ferritic microstructure that is formed by a fast cooling rate (Marker et al. 2000, Lacaze et al. 2016). The strength of cast iron also depends on whether it is vertically or horizontally cast. Horizontally cast (spun) material has higher strength than vertically (pit) cast material (Marker et al. 2007).

Collini et al. (2008) showed that tensile and fatigue strength of gray cast iron of the same grade varies from foundry to foundry. Rajani et al. (2000) conducted an assessment of microstructure, tensile strength, four-point bending strength, and fracture toughness of pit and spun cast iron pipe materials, supplied by eight cities in Canada and eight cities in the USA. This study reveals that tensile strength and fracture toughness varies extensively from one city to another. Seica and Packer (2004) examined cast iron properties by conducting the tension test, compression test, ring bearing test, and pipe bending test and came to the conclusion that mechanical properties show significant variation and should not be assumed for the determination of pipe strength.

Mohebbi et al. (2010) studied the role of microstructure on the fracture toughness and fatigue behavior and reported that fracture toughness remains almost constant for the same type of microstructure, specifically the pearlite structure. Jesson et al. (2013) studied a 150-year-old pipeline and showed that the strength of cast iron decreases with the increase of graphite depth. For the strength assessment of cast iron water mains having extensively variable material properties, a statistical characterization of the material properties can be performed with available data. In this regard, tests of available pipe materials can be conducted to enrich the existing data base with additional data.

Researchers examined uniaxial stress-strain behavior of cast iron pipe materials using coupon samples extracted from pipes (Conlin and Baker 1991, Seica and Packer 2004, Makar and McDonald 2007, Collini et al. 2008, Zhang et al. 2017a). The tensile strength and the compressive strength are found to range from 125-246 MPa and 325-400 MPa, respectively. The stress–strain responses of the material in both tensile and compressive loading were nonlinear. The modulus of elasticity and Poisson's ratio of the materials were not reported from these tests. However, these parameters are required for stress–deformation analysis, particularly for application of linear elastic fracture mechanics (LEFM). Water mains are also subjected to repeated loading and unloading applied at different rates during pressure surge, temporary shut-down, temperature change, and repeating surface loads. Information on cyclic stress–strain response is currently not available for the assessment of pipes subjected to the repeated loading. While stress–strain response of cast iron pipe materials are assumed to be independent on the rates of loading, no experimental evidence is currently available to validate the assumption. In the current research, a laboratory testing program is undertaken to investigate the stress-strain response of cast iron pipe materials under monotonic and repeating loading with various rate of loading.

3.3. SEM Scanning

To investigate the graphite flakes, chemical composition, and the type of cast iron, specimens are scanned by a scanning electron microscope (SEM) in the SEM lab at Memorial University of Newfoundland, Canada. Firstly, specimens are sectioned by using a blade designed for metallography work to ensure the least possible amount of damage. Grinding and polishing of the surface are then completed by using a Struers TegraForce-5 machine (Figure 3.1).

Figure 3.1. Struers TegraForce-5 machine for grinding and polishing

A properly polished specimen is required for observation of inclusions of graphite in cast iron. The samples are physically examined and scanned using the 'Phenom ProX desktop scanning electron microscope' (Figure 3.2). Distributions of elements in the specimen are analyzed using 'optional elemental mapping and line scan' software. Element identification is completed by fully integrated energy dispersive spectrometer (EDS) of the SEM machine.

Figure 3.2. Phenom ProX desktop scanning electron microscope" (Quanta 400)

Types of graphite flakes vary between pit and spun cast iron because, during solidification, carbon is separated from iron and produce different shapes of flakes. The graphite flake of cast iron is divided into different types according to ASTM (2017), as shown in Table 3.1. SEM scanning showed both of the specimens as type VII graphite form, i.e., long and individual flake, which are gray cast iron. Generally, Type D graphite flakes are present in spun cast iron, formed by rapidly cooling and type A (uniform distribution, random orientation) or C (superimposed flake sizes, random orientation) graphite flakes are present in pit cast iron that is formed by slower cooling rates. Type B flakes (rosette pattern) are found from fairly rapid cooling. In the SEM tests, both of the specimens showed a very fine pattern of flakes with the surrounding areas without graphite (Figure 3.3), similar to Type D, and therefore, are classified as a spun cast iron.

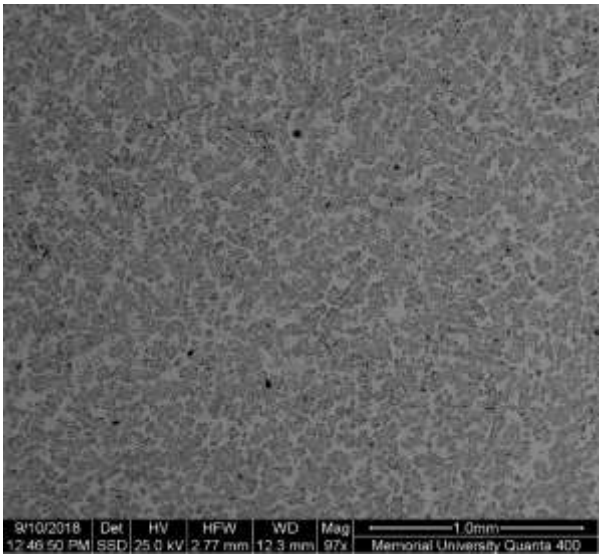

(a) Sample 1

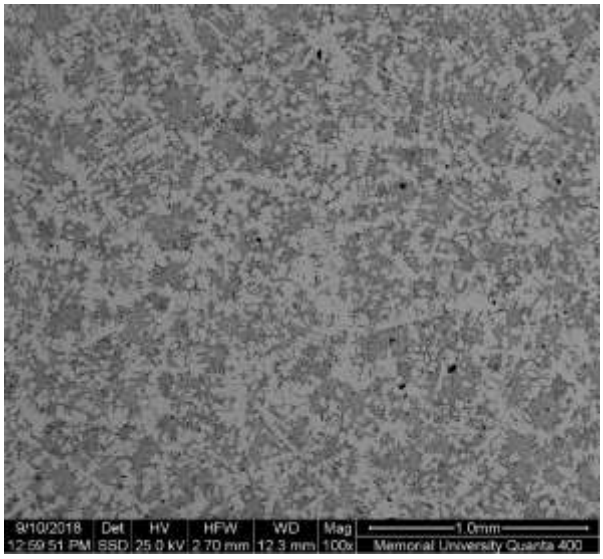

(b) Sample 2

Figure 3.3. Microstructure spun cast iron after polishing (100x magnification)

In each sample, four areas are selected to determine the chemical composition (Figure 3.4) where three small areas or blocks (around 45 to 65 µm by 25 µm in size) containing different observed patterns of graphite, denoted by Areas 1, 2 and 3, are used to understand the local variabilities of material composition. Table 3.2 shows that for Sample 1 (supplied by the City of Mount Pearl), the lowest amount of carbon (i.e., 4.43%) and the highest amount of iron (i.e., 74.49%) is found in Area 1. However, in Area 2, the percentage of carbon is much higher (21.36%) where the amount of iron is reduced to 64.17%. Sample 2 (collected from the City of St. John's) also shows similar patterns (Table 3.2). The test results show that the amount of iron compound of Sample 1 is less than that in Sample 2. Due to the large variation in localized area, an approximate 650 µm block, denoted as Area 4 is considered to obtain carbon equivalent over a larger area. The carbon equivalent of Sample 1 and 2 obtained from Area 4 are 18.85% and 18.35% respectively, which are very similar.

Table 3.1. Description of Graphite Flakes (ASTM A 247 − 17, Marker et al. 2000)

Graphite Form[a]	Flake type	Flake description
	A	Uniformly distributed, apparently randomly oriented flakes
	B	Rosette pattern of graphite flakes
Type	C	Randomly oriented flakes of widely varying sizes
VII	D	A very fine pattern of flakes surrounding areas without graphite
	E	Graphite flakes have preferred orientation and appear in quasi-regular pattern

[a]In ASTM A247 − 17, graphite form is classified as (1) spheroidal graphite; (2) imperfect spheroidal graphite; (3) temper graphite; (4) compact graphite; (5) grab graphite; (6) exploded graphite; or (7) flake graphite. Pictures of both flake types and forms can be found in ASTM A247 – 17.

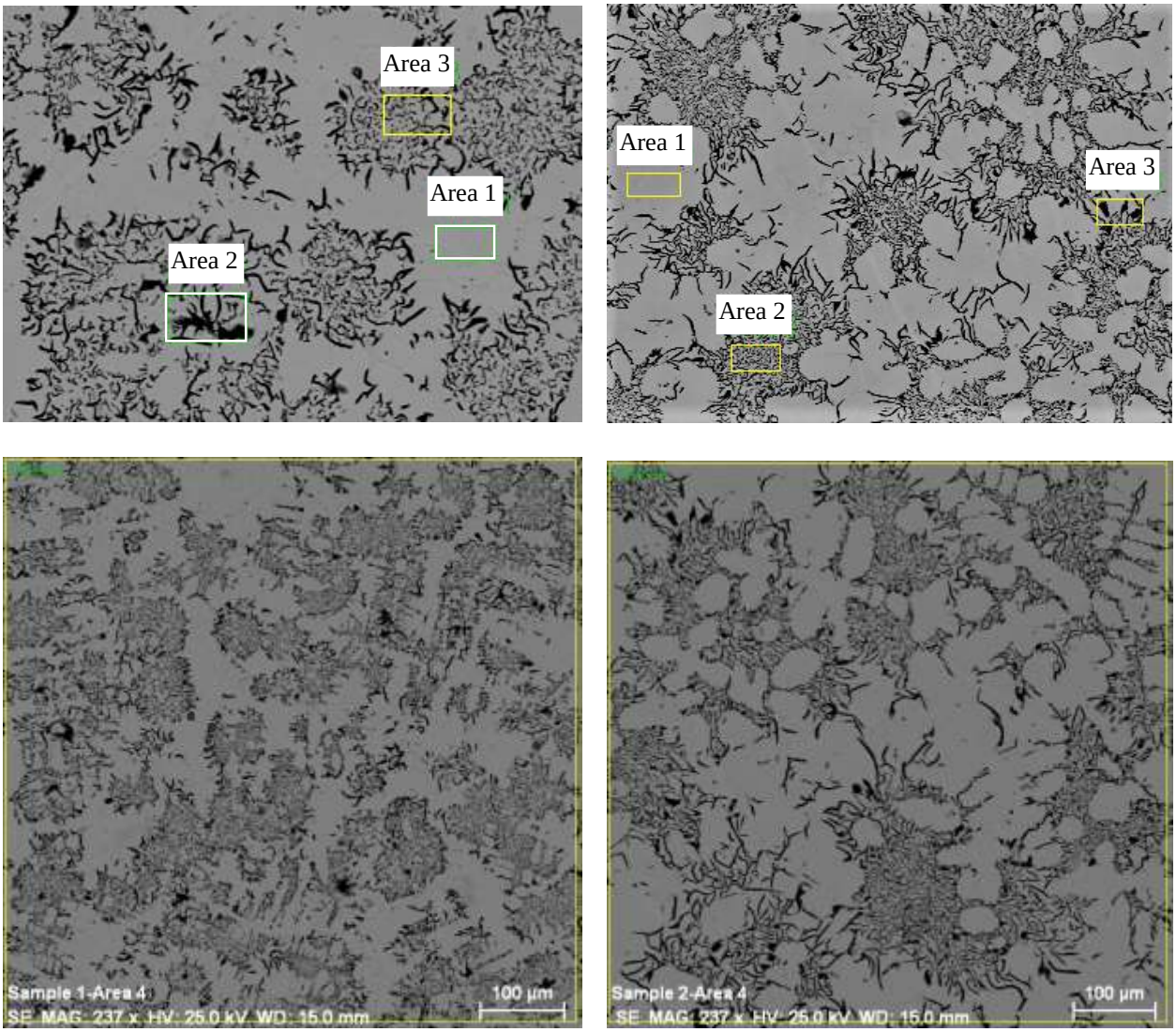

(a) Sample 1 (b) Sample 2

Figure 3.4. The selected area to determine the chemical composition

Table 3.2. Chemical composition (% by weight) of Sample 1 and Sample 2

Foundry	Spectrum	Fe	C	Si	Mn	P	S	Cu	Ca	Ti	K
Sample 1	Area-1	74.49	4.43	1.24	0.75	0.98	0.00	0.13	0.00	0.00	0.00
	Area-2	64.17	21.36	1.18	1.48	0.00	0.55	0.14	0.02	0.05	0.01
	Area-3	70.20	11.59	1.36	0.77	0.13	0.02	0.09	0.03	0.00	0.01
	Mean value:	69.62	12.46	1.26	1.00	0.37	0.19	0.12	0.02	0.02	0.00
	Sigma	5.19	8.50	0.10	0.41	0.54	0.31	0.03	0.01	0.03	0.00
	Sigma mean	2.99	4.91	0.06	0.24	0.31	0.18	0.01	0.01	0.01	0.00
	Area-4	73.65	18.28	1.31	1.61	0.39	0.06	0.18	0.02	0.09	0.01
Sample 2	Area-1	75.17	4.22	1.25	0.89	0.98	0.00	0.18	0.00	0.01	0.01
	Area-2	72.77	15.03	1.30	0.96	0.00	0.00	0.19	0.00	0.02	0.00
	Area-3	69.04	19.63	1.06	0.93	0.09	0.00	0.12	0.01	0.01	0.01
	Mean value:	72.33	12.96	1.20	0.93	0.36	0.00	0.16	0.00	0.01	0.01
	Sigma	3.09	7.91	0.13	0.04	0.54	0.00	0.04	0.00	0.00	0.01
	Sigma mean	1.78	4.57	0.07	0.02	0.31	0.00	0.02	0.00	0.00	0.00
	Area-4	75.27	17.85	1.33	1.66	0.15	0.07	0.27	0.00	0.02	0.00

3.4. Tensile tests

3.4.1. Test description

Tensile tests are performed on specimens extracted from the two separate exhumed cast iron water mains (obtained from the City of Mount Pearl and the City of St. John's). Multiple tensile coupons are cut from the pipe by using a water jet. Corrosion (such as graphitization) and other materials flaws (air inclusions, foreign body inclusions, etc.) visible on the coupons, particularly within the gauge length, are removed. ASTM (2016) recommends two types of dog-bone shaped specimens (flat and round) for the tension test. Seica and Packer (2004) showed that both flat and round tensile coupons provide reliable results and therefore either type of coupons can be used for the tensile test of cast iron. All the tensile tests in this study are performed on flat coupon specimens prepared according to ASTM (2016) specifications (Figure 3.5).

Figure 3.5. ASTM E E8 / E8M –16a recommended tension specimen

The length of the test specimens is parallel to the length of the cast iron pipeline. An INSTRON (5585H) (Figure 3.6) machine is used for the test. Thirteen coupons are exhumed from the pipe supplied by the City of Mount Pearl (Sample 1) and thirty-three specimens are exhumed from the pipe collected from the City of St. John's (Sample 2). Dimensions of all specimens are measured within the gauge length before the tests. The coupons are loaded in tension until failure and the data are collected using a computer-controlled data acquisition system. Displacement control tests are carried out by moving the crosshead of the INSTRON machine at various displacement rates to examine the effects of the rate of loading. In a few tests, the load is applied up to a certain level and unloaded and then reloaded to examine the loading-unloading-reloading responses. An extensometer is attached to measure the axial deformation and strain. A biaxial strain gauge is also used in a few specimens to verify the strain measured by the extensometer and for the examination of Poisson's ratio.

Figure 3.6. Tensile test by INSTRON (5585H) machine

3.4.2. Strain rate effect

Figure 3.7 presents the stress–strain responses obtained during the tests with specimens extracted from different locations of Sample 1 (pipe extracted from the City of Mount Pearl). A wide variation of stress–strain response is observed in this figure for tests conducted at various loading rates. The variations in the stress–strain response could be due to variation in the materials properties for the specimens extracted from different locations or could be due to the variation in the rate of loading. However, as seen in Figure 3.7, the stress–strain responses for tests conducted at the same loading rate are also different. Therefore, the differences in the responses are likely due to the variability in the material properties. To validate this argument, two other tests are conducted with specimens extracted from close vicinity of the same pipe (Sample 1). Tests are conducted at different displacement rates (i.e., 0.5 mm/min and 1 mm/min), which are arbitrarily chosen based on previous test results. For one of the specimens, the displacement rate is changed

during the test. A displacement rate of 0.5 mm/min is applied up to a stress level of 85 MPa and then it is increased to 20 mm/min and continued until failure. Test results are plotted in Figure 3.8. In this figure, the stress–strain responses are not affected by the change of displacing rate from 0.5 mm/min to 20 mm/min, indicating no effect of the rate of loading. The responses for the tests conducted at 0.5 mm/min and 1 mm/min are also very close, which is due to extracting the specimens from close vicinity. Therefore, it can be concluded that the stress–strain response of cast iron pipe material is not affected by the rate of loading. The variability observed in Figure 3.7 is due to variation in the material property even for the same pipe. A similar conclusion regarding the effect of rate of loading can be drawn for Sample 2 where the stress–strain responses with tests conducted at various displacement rates are very close to each other (Figure 3.9).

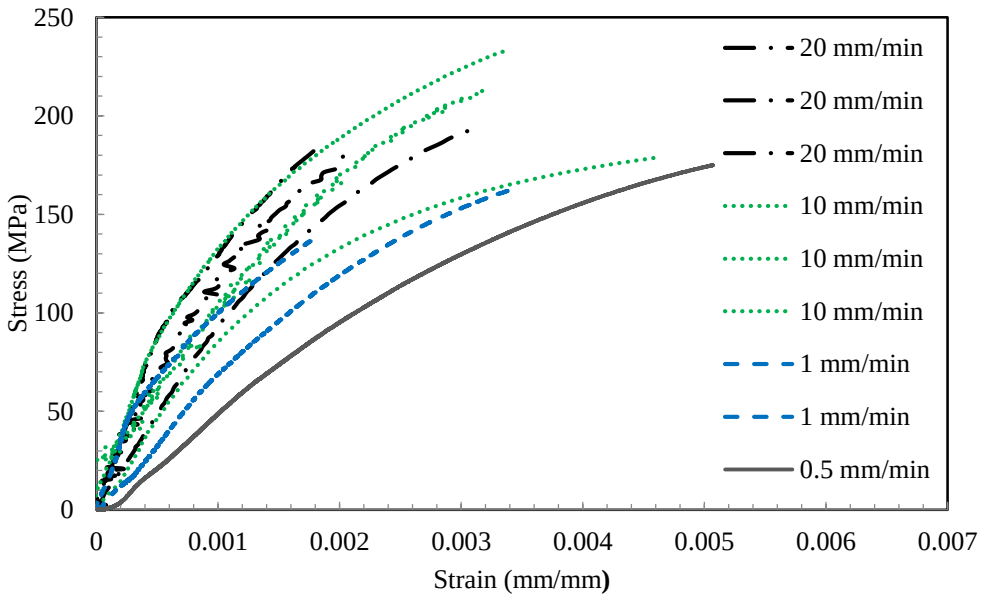

Figure 3.7. Stress–strain response of Sample 1 at various strain rate (After Ali 2017)

The ultimate strength of Sample 1 was found to vary from around 150 MPa to around 230 MPa with the average and the standard deviation as 185 MPa and 27 MPa, respectively. Sample 2 shows almost similar ultimate strength which is around 250 MPa. The failure strains at the ultimate

strength vary from 0.002 to 0.007 for Sample 1 whereas the failure strain fluctuation in Sample 2 is very small (0.0034 to 0.0038). The result of SEM scanning (Table 3.2) reveals that the percentage of iron compared to carbon equivalent is more in Sample 2 than Sample 1. As a result, the tensile strength is expected to be higher in Sample 2, which is consistent with the test results.

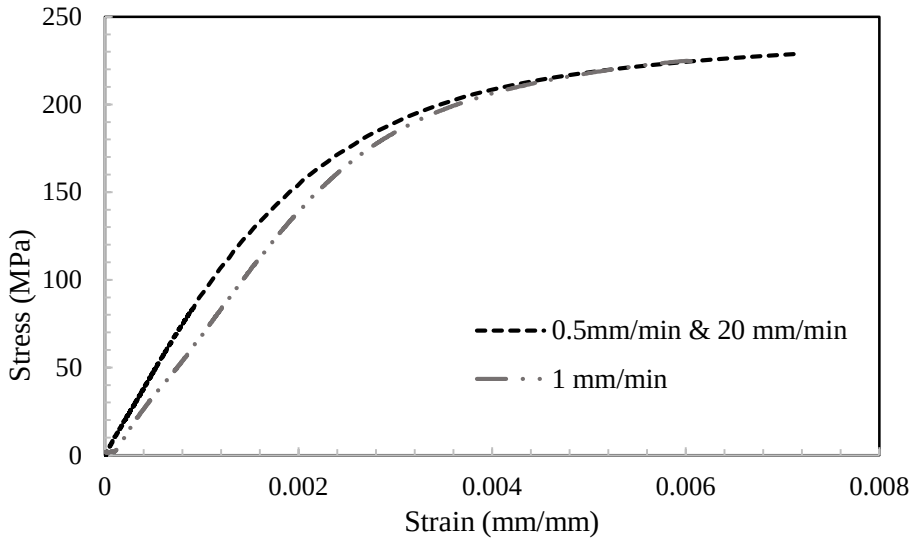

Figure 3.8. Stress–strain response of Sample 1 with the loading rate change

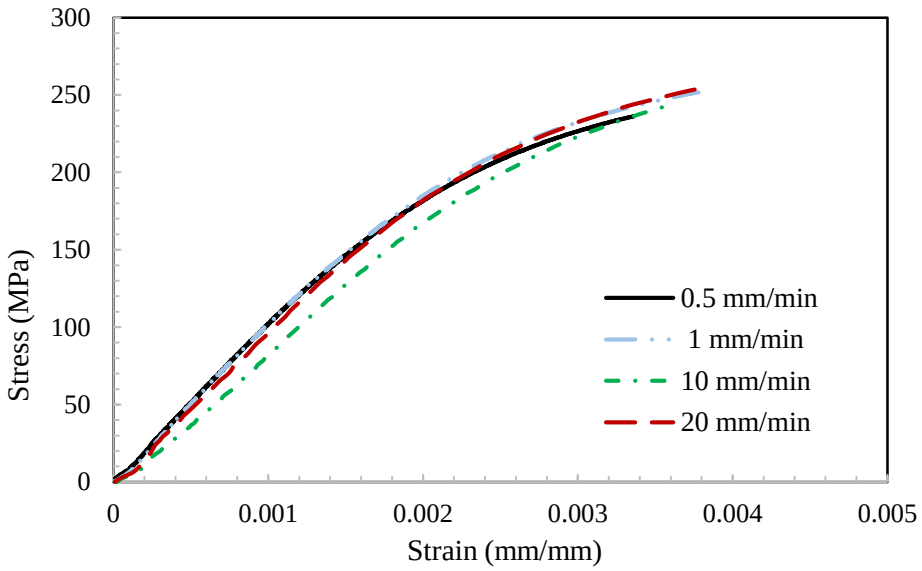

Figure 3.9. Stress–strain behaviour of Sample 2

Variabilities in the tensile strength of cast iron pipe materials were also identified earlier (Seica and Packer 2004, Makar and McDonald 2007, Zhang et al. 2017a) where the tensile strength was reported to vary from less than 50 MPa to over 300 MPa. Therefore, pipe specific material parameters should be used for the structural integrity assessment of cast iron water mains. Failed segments of pipes can be exhumed and tested to determine the material parameters and their statistical distributions for the integrity assessment of pipes in existing water main networks.

The stress–strain response of cast iron pipe material is nonlinear. Hyperbolic relations were used to capture the nonlinear relation for cast iron water mains (Rajani 2012, Zhang et al. 2017b). The hyperbolic model as suggested by Attewell et al. (1986) is:

$$\varepsilon/\sigma = a + b\,\varepsilon \qquad (3.3)$$

Where ε and σ are strain and stress, respectively, and *a* is the reciprocal of the initial tangent modulus, and *b* is the slope of strain/stress–strain curve. The hyperbolic parameters from the stress–strain relation presented in Figures 3.8 and 3.9 are determined. Table 3.3 summaries the mechanical parameters obtained from tensile tests along with hyperbolic model parameters.

Table 3.3: Mechanical parameter obtained from tensile test

Foundry	Ultimate strength, σ_u (MPa)	Failure strain, ε_u (mm/mm)	*a* *10^{-5} (MPa^{-1})	*b* (MPa^{-1})
Sample 1	225	0.0065	0.8	0.0028
Sample 2	250	0.0036	0.8	0.0016

3.4.3. Loading-unloading-reloading responses

The uniaxial tensile test is performed to understand the loading-unloading-reloading behavior of cast iron. The specimen is loaded to a 'specified stress level' and then unloaded to zero loads and again loaded until failure. The loading, unloading, and reloading are performed at the

same displacement rates. Tests are conducted at various magnitudes of the 'specified stress level' to identify the elastic limit of the cast iron pipe material. Stress–strain diagrams with the unloading-reloading cycle are illustrated in Figure 3.10. Ideally, at any increment of load, stress–strain diagrams of cast iron show plastic deformation (Angus, 1960). However, the plastic deformation is insignificant in Figures 3.10a to 3.10c, where unloading is applied at a stress level of less than 70 MPa. The reloading responses exactly follow the loading in Figures 3.10a to 3.10c, due to negligible plastic deformation. At the stress levels for unloading of 75 MPa and beyond (Figures 3.10d to 3.10f), significant plastic deformations are observed. In Figures 3.10d to 3.10f, the reloading paths closely follow the unloading path up to the maximum prior stress and then follows the loading response. The maximum stress prior to unloading is reached at the same total strain during unloading. Thus, the progressive damage due to elasto-plastic loading is apparently negligible.

3.4.4. Modulus of elasticity and elastic limit

For cast iron with a nonlinear stress–strain behavior, the initial tangent modulus can be calculated from the slope of the stress–strain curve at zero or near zero stress. The secant modulus corresponding to a stress level is also used to obtain the response at that stress level. The initial tangent modulus for the two samples is calculated as around 125 GPa (same for both samples). The initial tangent modulus for cast iron was reported to vary from 56 MPa to 200 MPa (Seica and Packer 2004, Makar and McDonald 2007). The calculated tangent modulus for the samples are thus within the range reported in the literature.

As there is no exact proportional limit for cast iron, it is recommended to obtain the yield strength using the 0.01% offset method (Angus 1960). Using the 0.01% offset method, the yield stress of Sample 1 and 2 is estimated at around 100 MPa. However, significant plastic deformation

was observed at the stress level of 75 MPa during the test conducted here. The 0.01% offset method can therefore, predict the yield stress which is slightly higher than the elastic limit obtained from the tests.

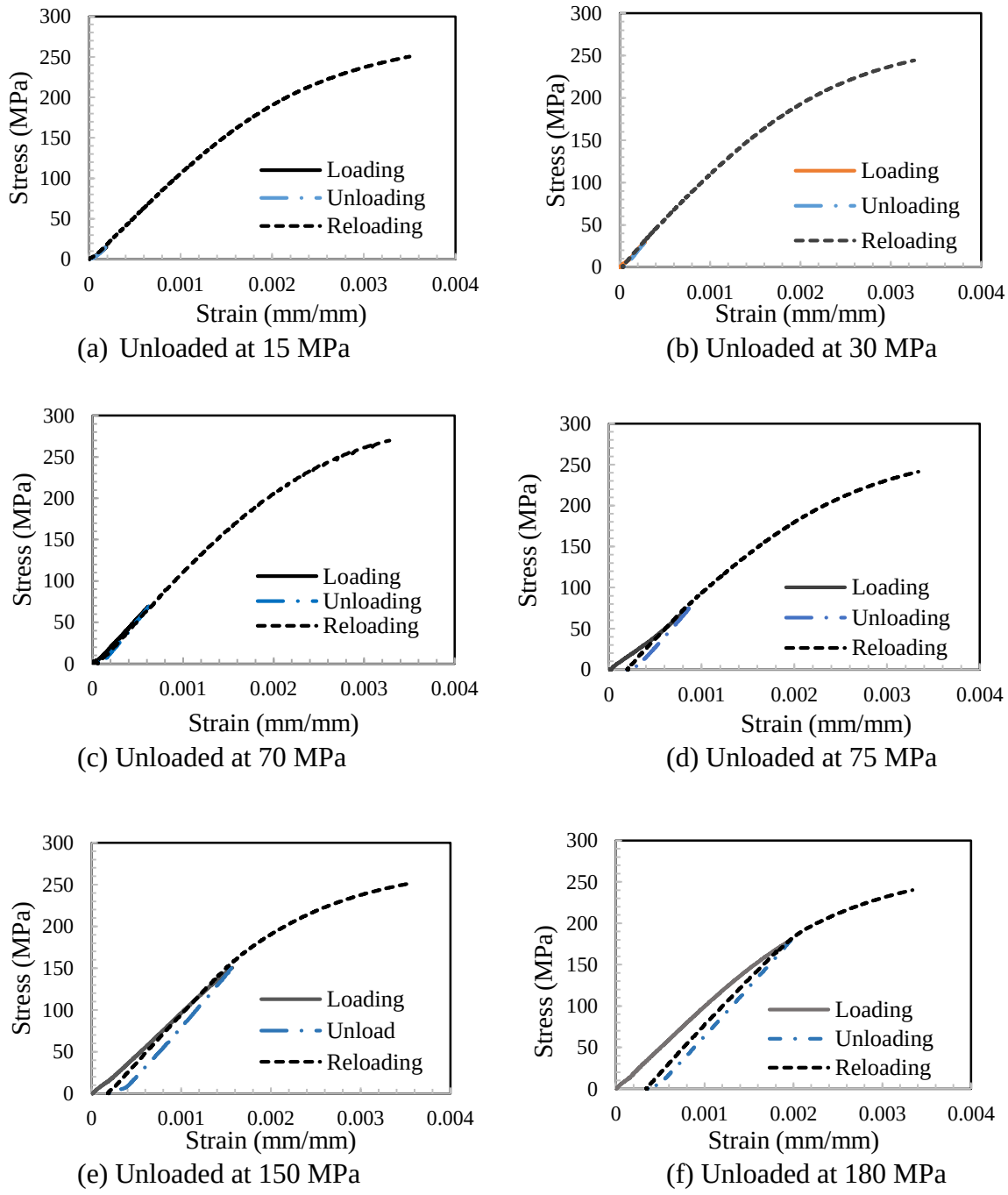

(a) Unloaded at 15 MPa

(b) Unloaded at 30 MPa

(c) Unloaded at 70 MPa

(d) Unloaded at 75 MPa

(e) Unloaded at 150 MPa

(f) Unloaded at 180 MPa

Figure 3.10. Stress–strain behaviour in loading-unloading-reloading (Sample 2)

3.4.5. Poisson's ratio

Longitudinal and transverse strains are measured using a biaxial strain gauge in three of the tests for calculation of Poisson's ratio. An extensometer is also used to measure the longitudinal strain. The longitudinal strains measured using the extensometer and strain gauge are close to each other. Cast iron is not a purely linear elastic material and therefore a constant value of Poisson's ratio may not be applicable. Calculated Poisson's ratio are plotted in Figure 3.11. In the initial stage of loading, the lateral strain measurement shows some instability that results in fluctuation on the calculated Poisson's ratio. Beyond the initial fluctuation, the ratio decreases almost linearly with the increase of longitudinal strain (hence, stress). A linear decrease of Poisson's ratio with stress level was also reported for cast iron in Angus (1960). The initial Poisson's ratio obtained from a backward extension of lines is 0.31 and 0.28 for Sample 1 and 2, respectively. In Figure 3.11, the Poisson's ratio ranges from 0.28 to 0.14 for Sample 1 and 0.31 to 0.17 for Sample 2 within the ranges of stress considered during the tests. Within the elastic region (stress < 75 MPa) the measured Poisson's ratio ranges from 0.28 to 0.24 for Sample 1 and 0.31 to 0.27 for Sample 2. Therefore, a Poisson's ratio of 0.25 to 0.3 can reasonably be used for elastic analysis of cast iron pipes. However, the effects of the Poisson's ratio on overall response should be investigated.

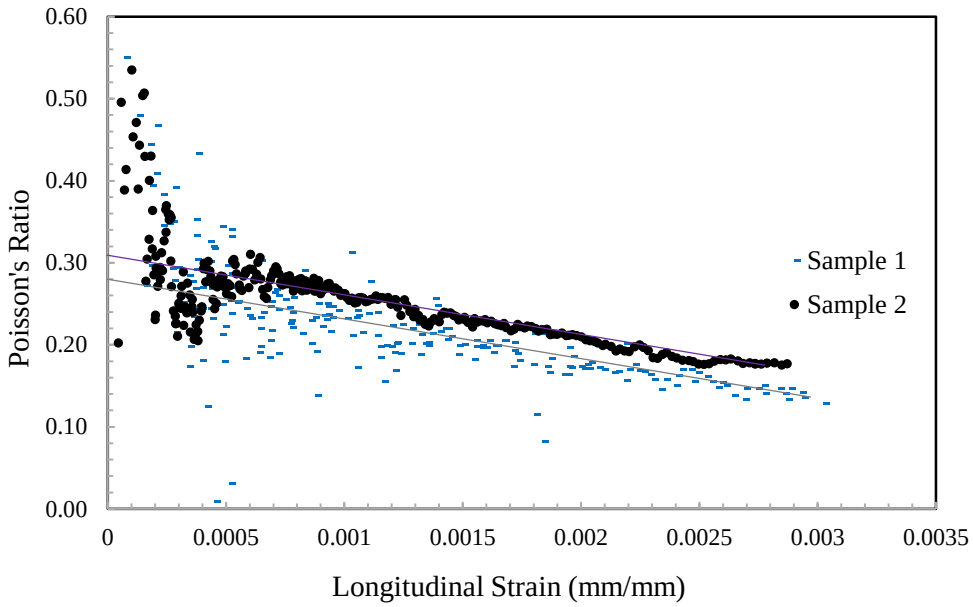

Figure 3.11. Poisson's ratio

3.5. Determination of fracture toughness

3.5.1. Single-Edge Notch Beam (SENB) test

The Single-Edge Notch Beam (SENB) is used for fracture toughness determination of the materials. In the SENB test, a sharp notch is created in the middle of the specimen and the specimen is loaded under a 3-point beam configuration. It is believed that the SENB test provides reliable results if the notch is sharp enough (Rudnayova et al. 1993). To ensure a sharp notch/crack, fatigue pre-cracking of the specimen with a 'straight through notch' is recommended in the fracture toughness test standard (ASTM 2001). However, for the specimen extracted from the pipe wall, it is difficult to create the 'straight through notch'. The application of fatigue pre-cracking is also not feasible due to low fracture toughness of the brittle cast iron pipe material. Therefore, a chevron (V) notch is used for the SENB tests. The obtained fracture toughness is then validated with the calculation of the stress intensity factor at the failure load using FE analysis.

For the SENB tests, the specimens are prepared as a rectangular cross-section with the length parallel to the length of the pipe. Corrosion and other foreign inclusions are removed. The width to depth ratio (W/B) of the specimens is kept in the range of $1 < W/B < 2$. Figure 3.12 shows a schematic view of the specimen used in SENB tests. The clear span (S), depth (W) and thickness (B) of the specimen are 84 mm, 14 mm and 7 mm, respectively. The width of the V notch is 2.4 mm. The depth of the notch is varied at 3.2 mm, 4.7 mm, and 6 mm to examine the effects. Three-point loading was applied on the specimen until failure. A linear voltage displacement transducer (LVDT) is attached to measure the displacement at the center of the beam. The failure load is recorded from the load–displacement response (Ali 2017). The failure load and the crack length are then used for the determination of fracture toughness K_c using the following equation Eq. (3.4) (ASTM 2001):

$$Kc = \frac{PS}{BW^{3/2}} f(a/w) \quad (3.4)$$

$$\text{Here, } f(a/w) = \frac{3(a/w)^{1/2}}{2(1+2a/w)(1-a/w)^{3/2}} [1.99 - (a/w)(1 - a/w)(2.15 - 3.93\, a/w + 2.7\, a^2/w^2)] \quad (3.5)$$

and P is the ultimate load, S is the clear span, B is the thickness, a is the crack length and w is the depth.

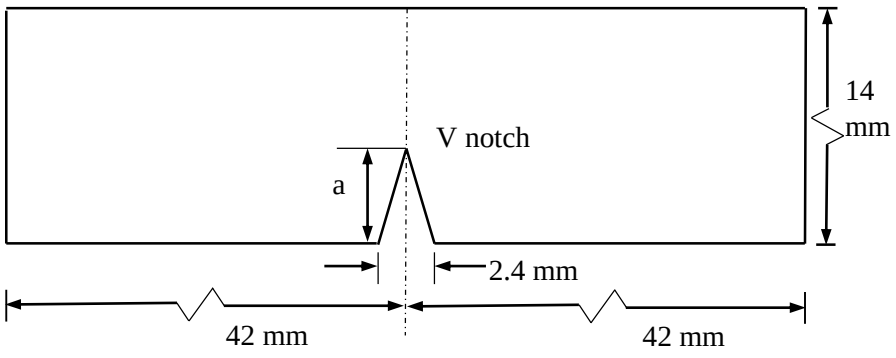

Figure 3.12. Test specimen used

Table 3.4 summaries the fracture toughness obtained from the test that is calculated using Eq. 3.4. The test results show fracture toughness varies from 12 to 19 MPa√m for the pipe material considered. These values are within the range of fracture toughness of cast iron pipe materials reported in the literature, e.g., 10.5 to 17.7 MPa√m (Conlin and Baker 1991), 17 to 24.3 MPa√m (Mohebbi et al. 2010), and 5 to 20 MPa√m (Zhang et al. 2017a).

Table 3.4. Fracture toughness, Kc from SENB tests

Specimen No.	Failure Load (N)	Crack Length (mm)	Kc - Test (MPa√m)	Failure Displacement (mm)
SB1	1869	3.2	17.16	0.17
SB2	2106	3.2	19.33	0.19
SB3	1191	4.7	14.39	0.12
SB4	1068	4.7	12.91	0.12
SB5	1020	4.7	12.33	0.12
SB6	1523	4.7	18.40	0.14
SB7	1179	6	18.34	0.13
SB8	1136	6	17.67	0.11

3.5.2. Validation with FE analysis

To validate the applicability of Eq. 3.4, three-dimensional finite element (FE) analyses are carried out using Abaqus/Standard module (Dassault Systemes 2014) to calculate the stress intensity factor (SIF) at the failure loads of the SENB tests. The results are compared with the fracture toughness obtained from the SENB tests. Linear elastic analyses are performed with a Young's modulus of 125 GPa and Poisson's ratio of 0.25, obtained from the tests discussed above.

FE models of the test specimens are developed with dimensions same as those used in the SENB tests. It is a prismatic member (beam) with a V-notch of various depths located at the mid-span of the specimen (Fig. 3.13). For FE modelling, a 20-node linear brick element (C3D20R) is used. Sufficiently small sizes of element are used based on a mesh sensitivity study as shown in

Figure 3.13a. The specimen is supported with a hinge and a roller at the ends, respectively (as a simply supported beam). A concentrated downward load is applied at the mid-span (shown in Figure 3.13a). The maximum magnitudes of the load are the same as the failure load during SENB tests. .

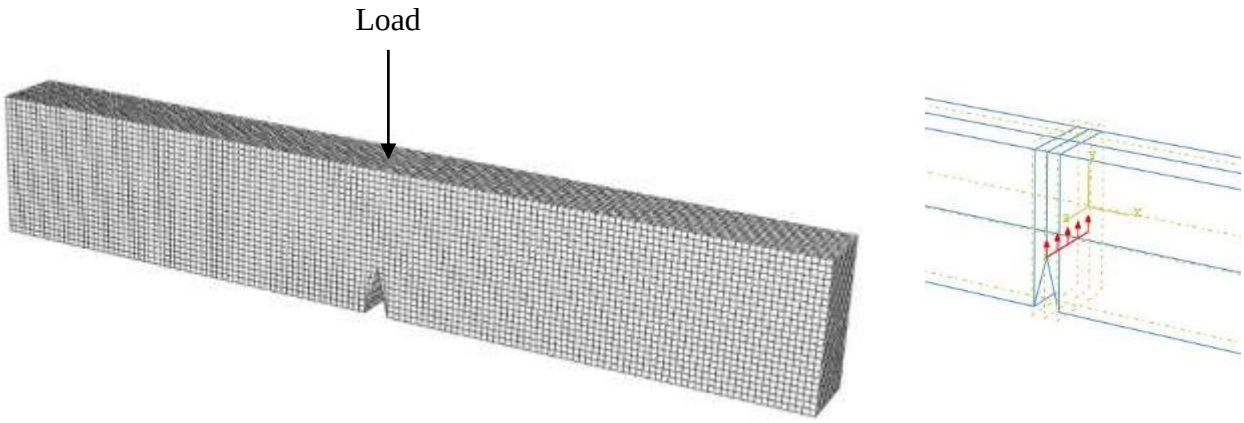

(a) FE mesh (b) Crack direction

Figure 3.13. 3D finite element modeling of single-edge notch beam (SENB) test

The contour integral method is used to determine the stress intensity factor. For the contour integral method, the crack extension direction is defined along the tip of V notch (Figure 3.13b). Five contours are specified using the Abaqus command. Abaqus automatically selects the elements that form each ring from the crack line. Each contour provides an evaluation of the contour integral that is path-independent and has same energy. The first contour usually shows abrupt results and is ignored as it is defined by specifying the nodes at the crack tip (Dassault Systemes 2014).

The failure load obtained from the SENB tests is used to determine the fracture toughness, which is the stress intensity factor at the failure load. Stress intensity factors calculated from FE analysis are compared with the test results obtained using Eq. 3.4 in Figure 3.14. The fracture toughness values obtained from FE analysis are almost identical with the test results in this figure, indicating that Eq. 3.4 is applicable for fracture toughness determination using SENB tests with a

simple chevron (V) notch. Thus, the simple V notch can be used instead of the complex 'straight through notch' for fracture toughness assessment of cast iron pipe material.

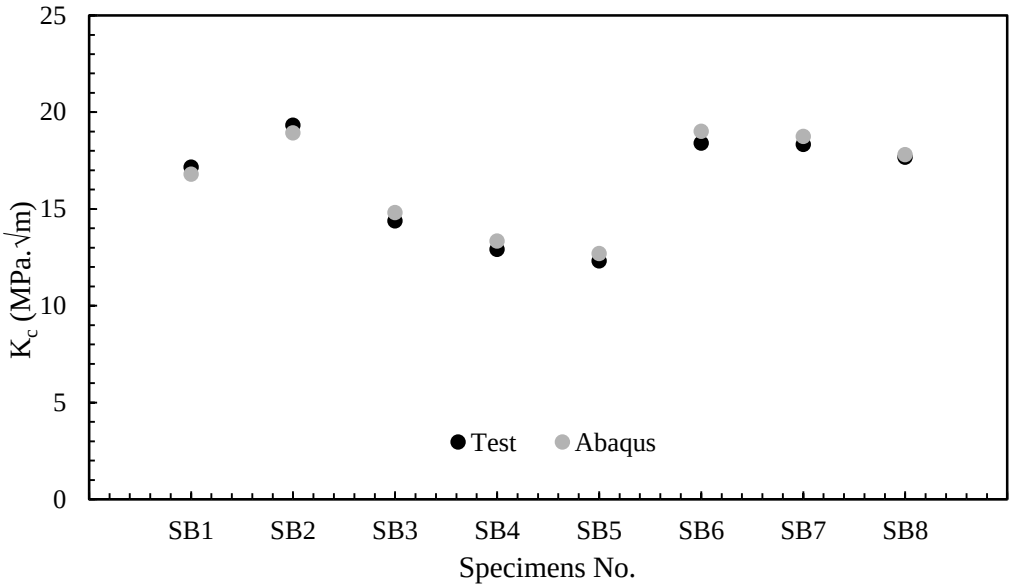

Figure 3.14. Comparison of fracture toughness from test and Abaqus

3.6. Analysis of Pipes with a Corrosion Pit

Fracture mechanics based failure assessment of buried cast iron pipes using the above parameters is demonstrated through application to a pipe with a corrosion pit. Circumferential cracking is the most common type of failure mode observed in cast iron water mains. Makar et al. (2005) postulated that the circumferential cracking in the water main is associated with corrosion pits in the pipe wall. Liyanage and Dhar (2017) employed three-dimensional FE modelling for continuum based failure assessment of a water main with corrosion pit. However, for a pipe in uniform soil, the calculated maximum longitudinal stress was much less than the circumferential stress. Since the longitudinal stress was low, no circumferential cracking was predicted using the method of assessment. Under the loading condition considered, the maximum longitudinal tension was 3.9 MPa, occurring at a distance from the pit, whereas the maximum circumferential stress was calculated as 25.4 MPa. Based on a significantly higher tensile strength of 225 MPa, the factor

of safety against circumferential cracking is 50, based on the continuum based assessment. Liyanage and Dhar (2017) also investigated the effect of pitting corrosion considering a 180° wide, 1 m long void underneath the pipe subjected to an internal pressure (400 kPa) and geostatic stress, and reported the maximum longitudinal and the maximum circumferential stresses as 20.2 MPa and 10.4 MPa, respectively. With the calculated longitudinal stress, the factor of safety against circumferential cracking is greater than 10. Thus, the continuum based modelling approach is not successful in identifying the causes for circumferential cracking of the pipe. Here, a fracture mechanics assessment is employed to investigate the problem from a different perspective.

Three-dimensional finite element analyses are carried out using Abaqus to obtain the pipe stress distribution and stress intensity factor for the pipe with a corrosion pit. Pipe conditions considered in Liyanage and Dhar (2017) are reanalysed using the fracture mechanics approach. The diameter of the cast iron pipe considered is 175 mm and the thickness is 10 mm. The pipe is buried in a medium dense soil with 2 m of soil cover. The pipe is subjected to 400 kN/m^2 internal pressure. Gravity load, snow load of 25 kN/m^2 and a truck load (axle load 14400 kg) are also considered. Gravity load is calculated manually and applied as a pressure at the top of the soil for the calculation of SIF, as the option of gravity type loading is not available for application of contour integral method in the current version of Abaqus.

The length of the pipe considered is 4 m. The corrosion pit is located at the invert position of the pipe. Uniform bedding, as well as a non-uniform bedding condition, is considered. To simulate the non-uniform bedding condition, a 1 m or 2 m long, 50 mm thick void is provided at the invert of the pipe (Figure 3.15). Circular, elliptical and diamond types of corrosion pit are considered, where the diameter of the circular pit is 50 mm, the length of the major axis is 50 mm for the elliptical pit, and the diagonal length is 50 mm for the diamond-shaped corrosion pit. The

void at the bedding is symmetrical to the pit hole and extends 90° or 180° around the pipe circumference. Soil parameters reported in Liyanage and Dhar (2017) are employed in the analyses. Table 3.5 summarizes the material parameters used. Linear elastic material model is used for the pipe material and elastic perfectly plastic model with Mohr-Coulomb plasticity is used for the soil. A parametric study is conducted to investigate the influence of the dilation angle in order to select a suitable dilation angle. The dilation angle is varied from 8º to 15º, and no significant variation in SIF is found.

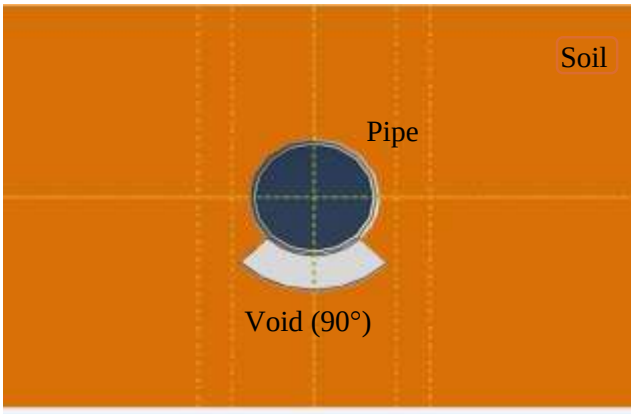

Figure 3.15. Symmetric void (90°) with respect to pit hole

Table 3.5. Material Parameters for FE modelling

Material Properties	Soil	Cast Iron
Density (gm/cm^3)	1.77	7.88
Young's modulus (MPa)	24	125,000
Poisson's Ratio	0.25	0.25
Friction Angle in (°)	38	-
Cohesion Yield Stress (kPa)	0.1	-

Eight-nodded linear brick elements (C3D8R) are used for both the pipe and the soil. Longitudinal displacements of the soil and pipe are restrained at the end planes using roller supports. The bottom surface is fixed in order to restrain horizontal and vertical movements.

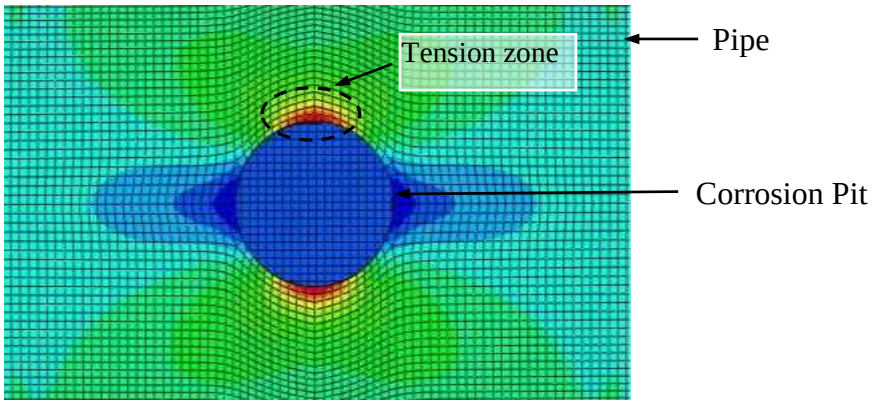

(a) Circular Pit

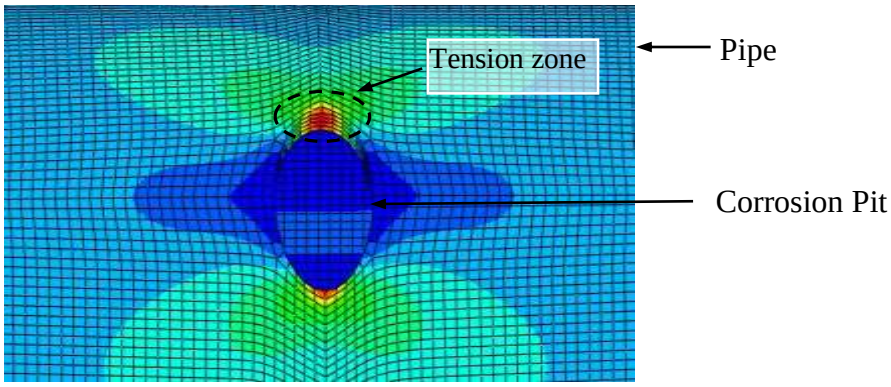

(b) Elliptical Pit

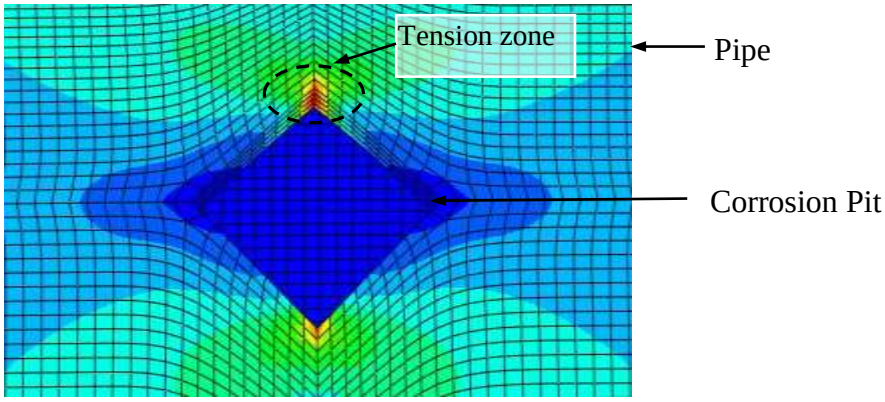

(c) Diamond shaped Pit

Figure 3.16. Major principal stress around a pit

To understand the direction of crack initiations and propagations, the contours of major principal stress are first plotted around the pits of different shapes as shown in Figure 3.16.

Since cracking is generated by tension, the major principal stress from FE analysis provides the direction of cracking. These figures show the highest tensile stress (marked by a dotted line) along the circumferential direction of the pipe across the corrosion pit. Thus, cracking is expected in the circumferential direction of the pipe due to high longitudinal stress. Therefore, crack directions along the circumference are assigned in the contour integral method for calculating SIF. Figure 3.17 shows an example of the crack propagation direction assigned for a circular pit.

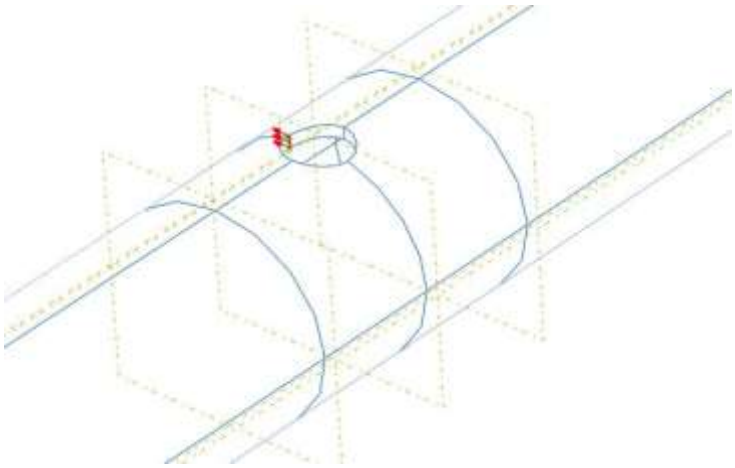

Figure 3.17. Crack extension direction in Contour integral method

The stress intensity factors (SIFs) calculated using the FE analysis for different pipe burial conditions are shown in Tables 3.6. The SIFs in the table suggest that the SIF is highest for a diamond-shaped corrosion pit and lowest for the circular shape. The SIF for the elliptical corrosion pit lies between the diamond and circular corrosion pits. The SIF increases with the decrease of tip radius of the corrosion hole. As a result, the SIF is higher for the diamond shaped pit having

the sharper tip. However, the SIFs under the typical loading conditions of water mains considered here are less than the fracture toughness determined for the cast iron pipe materials. The maximum SIF for circular, elliptical, and diamond-shaped pits are 1.22 MPa√m, 3.67 MPa√m, and 6.65 MPa√m, respectively. Considering the average fracture toughness of 16.4 MPa√m, a factor of safety against fractures of 2.5 to 10 are estimated. However, a crack may propagate at a SIF that can be substantially less than the fracture toughness, due to the stresses in a corrosive environment which is known as 'subcritical crack growth'. Strained bonds at crack tips are weakened due to the chemical action of environmental factors like water that facilitate crack growth during stress corrosion (Atkinson 1984). Cullin et al. (2015) reported that subcritical corrosion fatigue is one of the threats to gray cast iron water pipes, which is mainly due to the cyclic load. A casting defect may cause a microscopic crack on the pipe's interior that may accelerate crack propagation and therefore, a failure may occur at a lower SIF.

Table 3.6. Stress intensity factor in MPa√m

Shape Of the pit	1m hole under the pit, extending 90° around the pit circumference	2m hole under the pit, extending 90° around the pit circumference	2m hole under the pit, extending 180° around the pit circumference
Circular	0.72	0.66	1.22
Elliptical	1.79	1.97	3.67
Diamond	3.29	3.64	6.65

3.7. Conclusion

This paper investigates the strength and deformation properties of cast iron water mains that are required for fracture mechanics based failure assessment. SEM tests are performed to determine the type of cast iron by analyzing the graphite flake shapes and orientations. Coupons extracted from exhumed water mains are tested to determine the tensile strength and deformation

properties such as ultimate strength, yield strength, modulus of elasticity and Poisson's ratio. Test data reveal that mechanical properties of cast iron may vary significantly. The rate of loading is found to have no influence on the stress–strain behavior. The cast iron pipe materials showed negligible plastic strain at a stress less than 75 MPa beyond which the plastic strain is significant. Thus, the elastic limit of the cast iron pipe material is 75 MPa which is around 25% less than the yield strength calculated using the 0.01% offset method. Using the test data, hyperbolic model parameters are developed to represent the nonlinear behavior of cast iron pipe materials. To determine the fracture toughness, SENB tests with simple chevron (V) notch are performed. The test results are evaluated using FE calculation of SIF. The results of FE analysis reveal that chevron (V) notch can be used instead of the complex 'straight through notch' for fracture toughness determination of cast iron pipe materials.

The material parameters determined from the tests are employed for fracture mechanics based strength assessment of a buried water main. The study of the buried cast iron water mains under various loading conditions demonstrates that the SIF is significantly affected by pit shape and the erosion void at the bedding. The SIF is higher in the circumferential direction than in the longitudinal direction across the corrosion pit. As a result, crack propagation is expected along the circumferential direction. Three corrosion pit shapes (circular, diamond and elliptical) are considered in this study where the diamond shaped pit with sharp tips caused the highest SIF. Although the calculated SIF does not exceed the fracture toughness for the pipe material, it may cause failure due to subcritical crack growth in a corrosive environment.

References

Ali, I. (2017). "Mechanical properties of an exhumed cast iron pipe material." M.Eng. Thesis, Memorial University of Newfoundland, St. John's, NL, Canada.

ASTM. (2001). "Standard test method for measurement of fracture toughness." *ASTM E1820-01*. American Society for Testing and Materials, Philadelphia, Pennsylvania.

ASTM. (2016). "Standard test methods for tension testing of metallic materials." *ASTM E8 / E8M -16a*. American Society for Testing and Materials, Philadelphia, Pennsylvania. DOI: 10.1520/E0008_E0008M-16A

ASTM. (2017). "Standard test method for evaluating the microstructure of graphite in Iron casting." *ASTM A247-17*. American Society for Testing and Materials, Philadelphia, Pennsylvania.

Angus, H. T. (1976). "*Cast iron: Physical and engineering properties,*" 2nd Ed., Butterworths, London, UK.

Atkinson, B. K. (1984). "Subcritical crack growth in geological materials." *Journal of Geophysical Research*, 89(B6): 4077-4114.

Attewell, P. B., Yeates, J., and Selby, A. R. (1986). "*Soil movements induced by tunnelling and their effects on pipelines and structure,*" Chapman & Hall, New York.

Collini, L., Nicoletto, G., and Konečná, R. (2008). "Microstructure and Mechanical Properties of Pearlitic Gray Cast Iron." *Materials Science and Engineering: A,* 488(1–2): 529–39.

Conlin, R. M., and Baker, T. J. (1991). "Application of fracture mechanics to the failure behaviour of buried cast iron mains." *Contract Rep. No. 266*, Transport and Road Research Laboratory, London.

Cullin, M. J., Petersen, T.H. and Paris, A. P.E. (2015). "Corrosion Fatigue Failure of a Gray Cast Iron Water Main." Journal of *Pipeline Systems Engineering* and *Practice*,6(2):05014003

Dassault Systemes. (2014). "ABAQUS/CAE user's guide." Dassault Systemes Simulia Corp. Providence, RI, USA.

Fahimi, A., Evans, T. S., Farrow, J., Jesson, D. A., Mulheron, M. J., and Smith, P. A. (2016). "On the residual strength of aging cast iron trunk mains: Physically-based models for asset failure." *Materials Science and Engineering: A, 663, 204–212.*

Folkman, S. (2018). "Water Main Break Rates in USA and Canada: A Comprehensive Study". *Mechanical and Aerospace Engineering Faculty Publications.* Paper 174. https://digitalcommons.usu.edu/mae_facpub/174

Ji J., Zhang C., Kodikara, J., and Yang S. (2015). "Prediction of stress concentration factor of corrosion pits on buried pipes by least squares support vector machine," *Engineering Failure Analysis*, Vol. 55 (2015), 131-138.

Jesson, D. A., Mohebbi, H., Farrow, J., Mulheron, M. J., and Smith, P. A. (2013). "On the condition assessment of cast iron trunk main: The effect of microstructure and in-service graphitisation on mechanical properties in flexure". *Materials Science and Engineering: A*, 576, 192–201. doi:10.1016/j.msea.2013.03.061

Jesson, D.A., Le Page, B.H., Mulheron, M.J., Smith, P.A., Wallen, A., Cocks, R., Farrow, J., and Whiter, J.T. (2010). "Thermally induced strains and stresses in cast iron water distribution pipes: an experimental investigation". *Journal of Water Supply Research and Technology-*Aqua, 59. pp. 221-229.

Lacaze, J., Sertucha, J., and Åberg, L. M. (2016). "Microstructure of As-cast Ferritic-pearlitic Nodular Cast Irons". *ISIJ International, 56(9),* 1606–1615. doi:10.2355/isijinternational.isijint-2016-108

Liyanage, K.T.H and Dhar, A.S. (2017) "Effects of corrosion pits on the wall stresses in cast iron water mains", *ASCE Journal of Pipeline Systems - Engineering and Practice*, 8(4): 04017023.

Liyanage, K.T.H and Dhar, A.S. (2018) "Stresses in Cast Iron Water Main Subjected to Non-Uniform Bedding and Localized Concentrated Forces", *International Journal of Geotechnical Engineering*, 12(4), 368-376.

Makar, J. M., and Rajani, B. (2000). "Gray Cast-Iron Water Pipe Metallurgy". *Journal of Materials in Civil Engineering*, 12(3), 245–253. doi:10.1061/(asce)0899-1561(2000)12:3(245)

Makar, J. M., Rogge, R., McDonald, S., and Tesfamariam, S. (2005). "The Effect of Corrosion Pitting on Circumferential Failures in Grey Iron Pipes." American Water Works Association, Denver.

Makar, J. M., and McDonald, S. E. (2007). "Mechanical Behavior of Spun-Cast Gray Iron Pipe". *Journal of Materials in Civil Engineering*, 19(10), 826–833. doi:10.1061/(asce)0899-1561(2007)19:10(826)

Mohebbi, H., Jesson, D. A., Mulheron, M. J., and Smith, P. A. (2010). "The fracture and fatigue properties of cast irons used for trunk mains in the water industry". *Materials Science and Engineering: A*, 527(21-22), 5915–5923. doi:10.1016/j.msea.2010.05.071

Mondal, B. (2018). "Remaining strength assessment of deteriorating energy pipeline". PhD Thesis, Memorial University of Newfoundland, St. John's, NL, Canada.

Rajani, B. B., Makar, J. M., McDonald, S. E., Zhan, C., Kurakao, S., Jen, C.-K., and Viens, M. (2000). “Investigation of grey cast iron water mains to develop a methodology for estimating service life”. AwwaRF and AWWA, Denver.

Rajani, B., and Kleiner, Y. (2010) “Fatigue Failure of Large-Diameter Cast Iron Mains”, *12th Annual Conference on Water Distribution Systems Analysis (WDSA)*, September 12-15, 2010, Tucson, Arizona.

Rajani, B. (2012). "Nonlinear Stress–Strain Characterization of Cast Iron Used to Manufacture Pipes for Water Supply". *Journal of Engineering Materials and Technology, 134(4), 041005.* doi:10.1115/1.4007213

Rudnayová, E., dusza, J., and kupková, M. (1993). "Comparison of fracture toughness measuring methods applied on silicon nitride ceramics". *Le Journal de Physique IV, 03(C7), C7–1273–C7–1276.*

Seica, M. V., and Packer, J. A. (2004). "Mechanical Properties and Strength of Aged Cast Iron Water Pipes". *Journal of Materials in Civil Engineering*, 16(1), 69–77. doi:10.1061/(asce)0899-1561(2004)16:1(69)

Wang, W., A. Zhou, G. Fu, C.-Q. Li, D. Robert, and Mahmoodian, M. (2017) “Evaluation of stress intensity factor for cast iron pipes with sharp corrosion pits.” *Eng. Fail. Anal*. 81: 254–269. https://doi.org/10.1016/j.engfailanal.2017.06.026.

Yamamoto, K., Mizoguti, S., Yoshimitsu, K., and Kawasaki, J. (1983). “Relation between Graphitic Corrosion and Strength-degradation of Cast Iron Pipe”. *CORROSION ENGINEERING*, 32(3), 157–162. doi:10.3323/jcorr1974.32.3_157

Zhang, C., Rathnayaka, S., Shannon, B., Ji, J., and Kodikara, J. (2017a). “Numerical interpretation of pressurized corroded cast iron pipe tests”. *International Journal of Mechanical Sciences,* 128-129, 116–124.

Zhang, C., Ji, J., Kodikara, J., and Rajani, B. (2017b). “Hyperbolic constitutive model to study cast iron pipes in 3-D nonlinear finite element analyses”. *Engineering Failure Analysis, 75, 26–36.*

CHAPTER 4

Assessment of Stress Intensity Factor for Buried Cast Iron Water Pipes Using Abaqus

4.1 Introduction

A sustainable water supply network plays a vital role in the development of a city. Cast iron pipelines were one of the main components in this system in the past few decades and are still functioning but show deterioration with passes of time. As a result, cast iron pipe failure increases day by day that causes huge economical loss and affects public safety. Corrosion, construction defects, land movement, and cracking are the main causes of pipelines failure. Internal and external corrosion occurs in most of the buried pipeline which are the most predominant causes of pipe incidents (Mohebbi et al. 2011). Corrosive soil is mainly responsible for the corrosion of buried pipes. Most of the buried utilities are affected with moderate to high corrosion risk by the soil (Folkman 2018). Folkman (2018) reported that cast iron pipeline breaks 20 times more in highly corrosive soils than in low corrosive soils. Among the several types of corrosions identified in water mains, pitting corrosion is considered as the most dangerous types. Irregular soil contact and non-uniformities in the metal structure cause pitting corrosion when the pipes are in a hostile soil environment. It is difficult to detect pitting corrosions, which may initiate stress corrosion cracking and lead to failure.

Pipeline failure occurs either due to loss of strength or loss of toughness. Cast iron is a brittle material and may fail due to loss of strength through cracking rather than yielding. Fracture mechanics can be applied in failure (cracking) assessment of the pipe. For brittle material, stress intensity factor (SIF) is used for assessment of crack initiation and crack propagation in fracture mechanics. Several works have been conducted analytically and numerically to calculate the SIFs

for pipes with internal and external cracks. Raju and Newman (1982) determined different influence coefficients and provided an empirical equation to calculate the SIFs for semi-elliptical surface cracks in cylindrical pressure vessels with aspect ratios of defects ranging from 0.2 to 1.0. Lambert et al. (1994) extended the work of Raju and Newman (1982) by conducting three-dimensional finite element analysis (FEA) considering low aspect ratios (0.05 to 0.1) to calculate the SIFs for semi-elliptical cracks. Lin and Smith (1998) worked with crack growth in pressure vessels and revealed that after some cycles the crack forms a semi-elliptical shape. Li at al. (2012) further conducted FEA to find SIFs with high aspect ratio for semi-elliptical cracks in pipes. Similar research has been presented by Diamantoudis and Labeas (2005), Moulick and Sahu (2012), Predan et al. (2013) and Li et al. (2016b). Li et al. (2016a) studies the effect of inclined surface crack in pressurized pipes and determine SIF with mixed modes failure. Most of the studies focused on the crack-only defect of the pipes. Randeniya et al. (2016) considered surface crack along with corrosion for the determination of the influence coefficients. The SIF reported to date considered in-air pipe only. No study is available on the SIF considering the soil effect for buried pipe. In this paper, three-dimensional FE analyses are performed to investigate the SIF of buried cast iron pipe, subjected to cracking or 'corrosion with cracking'.

4.2 Finite element (FE) modelling

The Abaqus/Standard module (Dassault Systemes 2014) is used in this study for calculating the fracture parameters for pipelines containing a crack defect (no metal loss) and a 'cracks with corrosion' defect. For the development of FE modelling, solution for the SIFs reported in Raju and Newman (1982) is first simulated for validation. Pipelines are then analyzed under buried condition subjected to either crack (Figure 4.1) or crack along with corrosion (Figure 4.2).

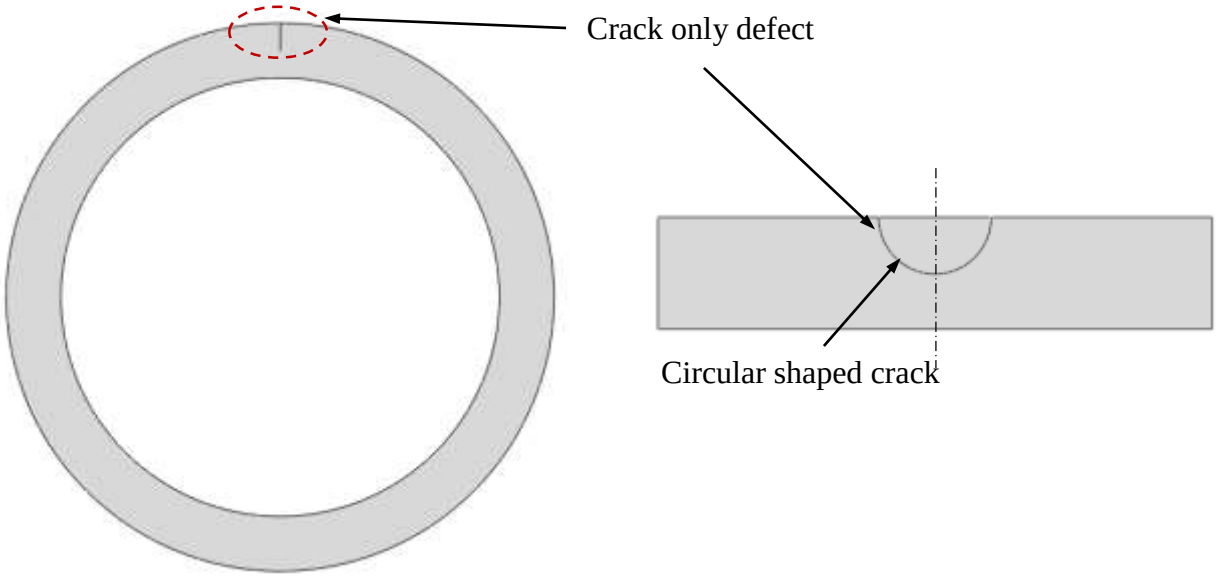

(a) Cross-section (b) Longitudinal section

Figure 4.1: An example of crack only defect

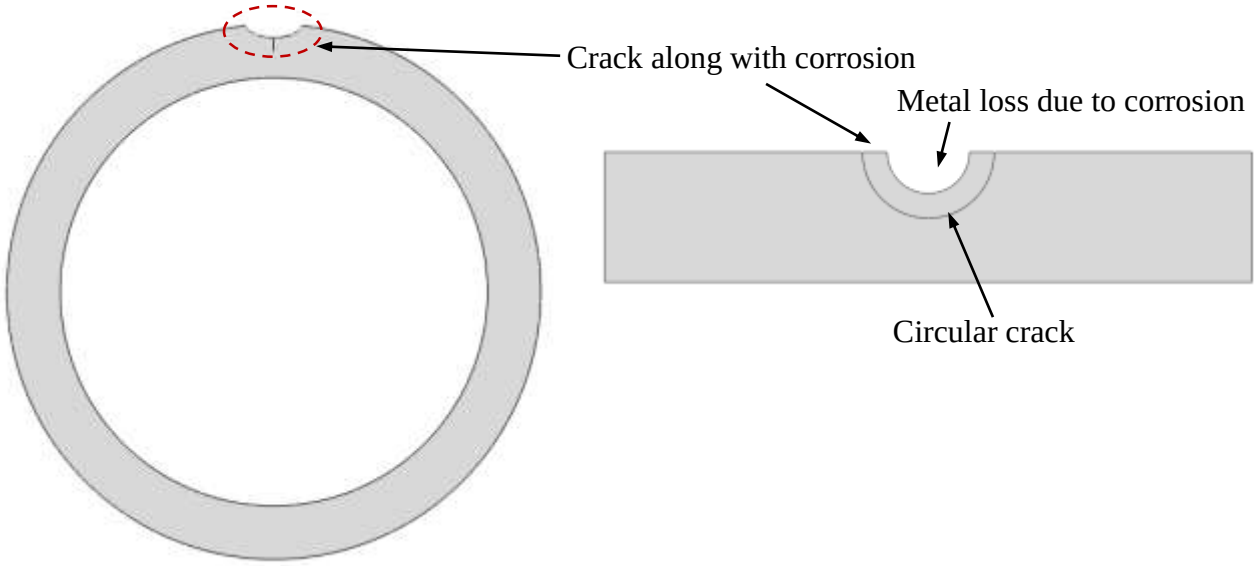

(a) Cross-section (b) Longitudinal section

Figure 4.2: An example of crack in corrosion defect

4.2.1 FE model development

Using extensive FE analyses, Raju and Newman (1982) developed a simplified equation (Equation 4.1) for the calculation of SIF at any point along an elliptical crack of a pipe subjected to internal pressure.

$$K = \frac{PR}{t}\sqrt{\pi \frac{a}{Q}}\, F_e\,(a/c,\ a/t,\ t/R,\ \phi) \qquad [4.1]$$

Where, *PR/t* is the average hoop stress of an uncracked pipe subjected to internal pressure, *a* is the depth of crack, *Q* is the crack shape parameter, F_e is the boundary-correction factor, *t* is the pipe wall thickness, *c* is the half-length of surface crack, *R* is the inner radius of the pipe and ϕ is the parametric angle locating a point on the crack (Figure 4.3).

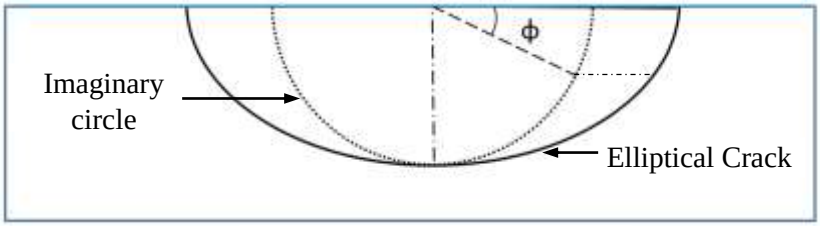

Figure 4.3: Parametric angle (ϕ) of an elliptical crack

The boundary-correction factor, F_e is expressed using influence coefficients of a polynomial function of the crack depth, *a*. For j^{th} order polynomial (j = 0, 1, 2, 3) with influence coefficients G_j, the F_e is given by

$$F_e = \frac{t}{R}\left(\frac{R^2}{R_0^2 - R^2}\right)\left[\,2\,G_0 + 2\left(\frac{a}{R_0}\right)G_1 + 3\left(\frac{a}{R_0}\right)^2 G_2 + 4\left(\frac{a}{R_0}\right)^3 G_3\,\right] \qquad [4.2]$$

Where R_0 is the outer radius of the pipe and G_0, G_1, G_2, G_3 are the influence factors for four polynomial terms for uniform, linear, quadratic and cubic distributions, respectively. The influence coefficients are obtained from FEA. Crack shape parameter, Q in Eq. (4.1) can be found from Eq. (4.3), Raju and Newman (1982):

$$Q = 1 + 1.464 \left(\frac{a}{c}\right)^{1.65} \qquad \text{for } a \leq c \qquad [4.3]$$

In this study, an elliptical external surface crack (a/c =1) on a pipe in the longitudinal direction is considered for validation of the FE model developed using Abaqus. The outer diameter of the cast iron is considered as 220 mm, and the thickness is 10 mm to satisfy the relative wall thickness (t/R) and relative crack depth (a/t) mentioned in Raju and Newman (1982). The depth of crack (a) is considered as 5 mm. During the analysis, an internal pressure of 600 kPa is applied. Although cast iron shows nonlinear stress–strain behavior, it is assumed as a linear elastic material. A Young's modulus of 125 GPa and Poisson's ratio of 0.25 are considered. The pipe is defined as 3D deformable solid bodies. For modelling of the crack, a partition is applied on the pipe's crack face. The crack is then defined using Abaqus command along the partition.

Calculation of SIF along a crack in pressure tube requires fine meshes around the crack tip that result in a large number of elements in the FE model. This large number of elements increases the computational time and the memory requirement of the computer. To overcome the problem, a sub-model technique available in Abaqus is applied. In this approach, a global model is first run with larger element sizes to calculate the stress and displacement fields. A sub-model with fine mesh around the crack is then reanalyzed under the stress and displacement fields from the global model.

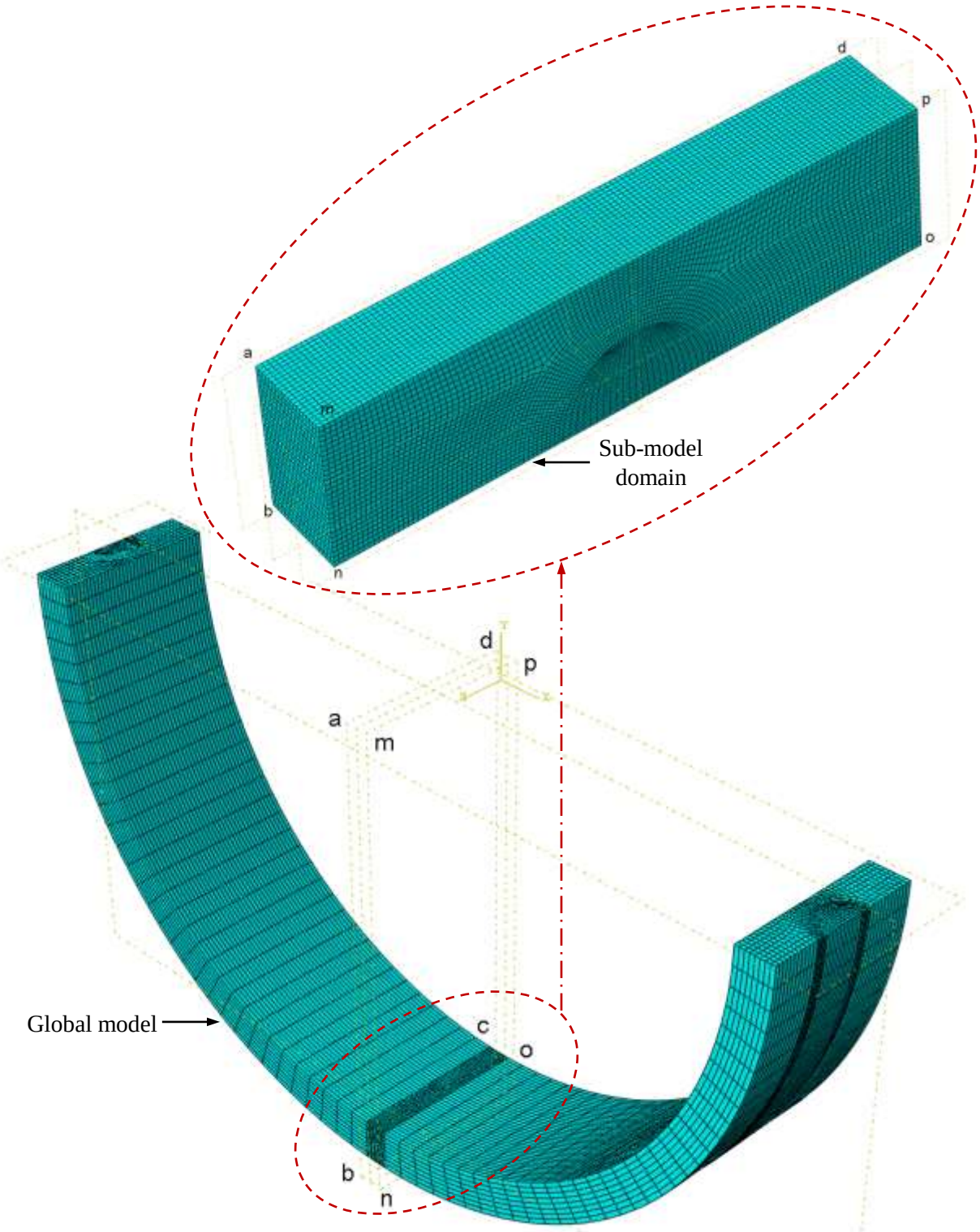

Figure 4.4: Global model and sub-model

To develop the global model, a quarter of the pipe cross-section is first developed and then a model of half cross-section is obtained using mirror tools, available in Abaqus. To take the advantage of symmetry for saving computational time, the pipe cross-section is assumed as symmetric about a diametric plane passing perpendicular to the crack surface. This assumption corresponds to a pipe with two cracks on diametrically opposite locations. Since the SIF for a particular crack is not affected by any other crack located at sufficient distance, it is expected that the calculated SIF will not be affected by the assumption of the symmetric condition. Symmetric boundary conditions are used on the planes of symmetry. Longitudinal displacements of the pipe are restrained at the end planes by using roller supports. Figure 4.4 shows the global model where the volume defined by *abcd* and *mnop* planes in the close vicinity of the crack is used for developing the sub-model. In the global model, within the volume (defined by *abcd* and *mnop* planes) there are 6,720 elements. In the sub-model, the number of elements is increased to 81,840 through re-meshing to ensure higher degree of accuracy in the results.

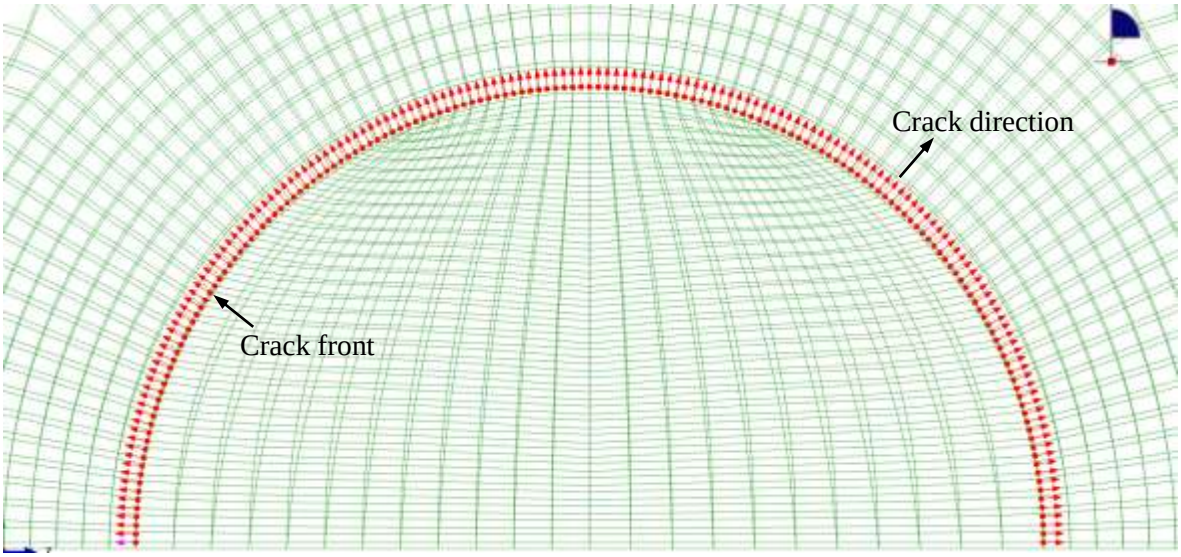

Figure 4.5: Crack extension direction of an elliptical crack (a/c = 1)

For the sub model, the boundary condition option of sub-model, available in Abaqus, is applied at the faces *abcd* and *mnop* and thus the stress and displacement fields from the global model are transferred to these faces. Axially restrained boundary conditions are applied on faces *abmn* and *cdpo.*

The contour integral method is used for calculating the SIFs along the crack tip. The contour integral method requires defining the crack front, and specifying the virtual crack extension direction. The crack extension direction is assigned orthogonal to the crack front (perpendicular to the ellipse) which varies along the elliptical crack front. To specify the crack extension direction in Abaqus, a single *q* vector is first defined. The input file data is then edited to correct the q vectors at each node to make orthogonal to the crack front (Figure 4.5). A seam is assigned that creates overlapping nodes and allows the crack to open when loaded (Figure 4.6).

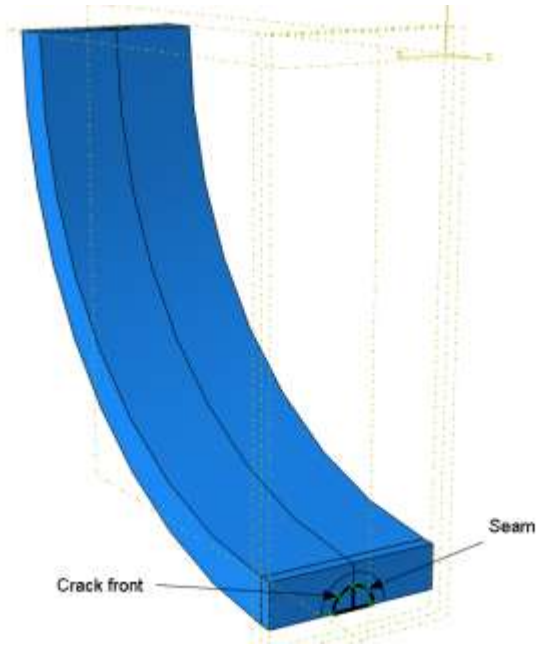

Figure 4.6: Crack front and seam location

In the contour integral method, five contours are specified using the Abaqus command. Abaqus automatically selects the elements that form each ring of contour from the crack line. Each contour provides an evaluation of the contour integral that is path-independent and has same energy. The first contour usually shows abrupt results as it is defined by specifying the nodes at the crack tip and is ignored (Figure 4.7) (Dassault Systemes 2014). Figure 4.7 shows one-half portions of the contours, which are symmetric about the crack plane.

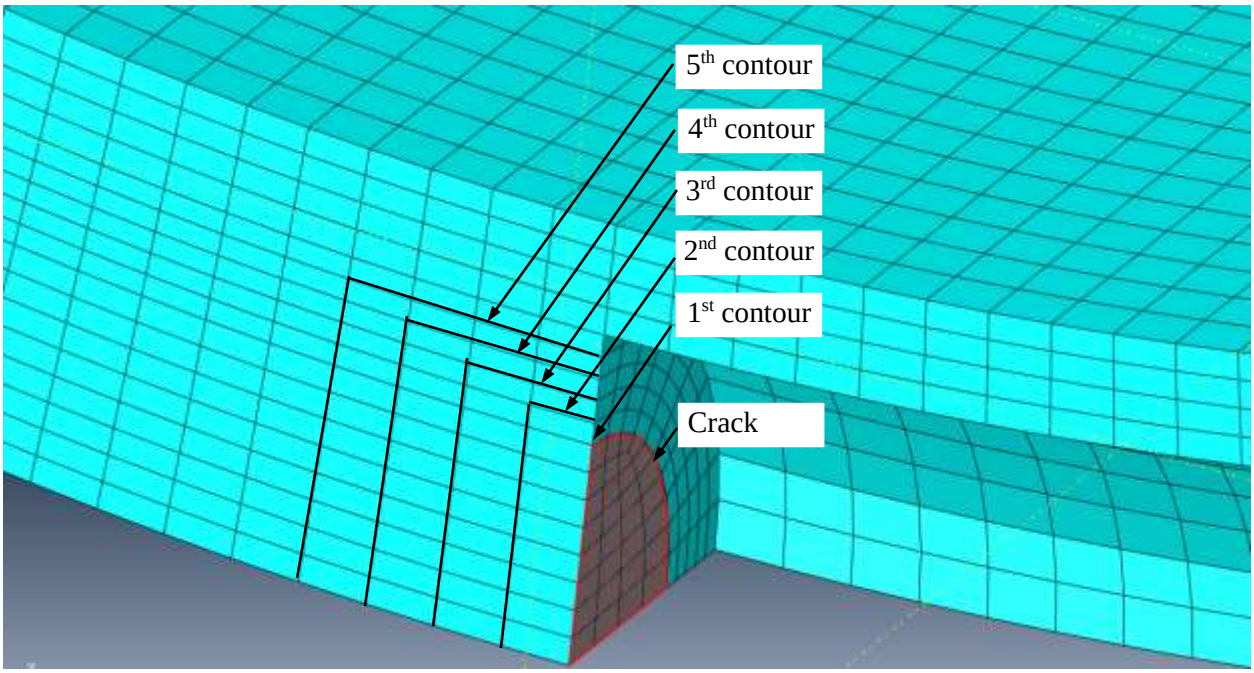

Figure 4.7: Five contours and crack location

Twenty-nodded brick elements with reduced integration (C3D20R) and eight-nodded linear brick elements (C3D8R) are used in the FE analysis to examine the suitability of elements to be used in the analysis. Element size is determined through a mesh sensitivity analysis. The SIFs at the location $\phi = 0$ along the crack calculated using C3D20R elements are plotted in Figure 4.8 for four contours (except the first one). In Figure 4.8, the SIFs calculated from each of the contours

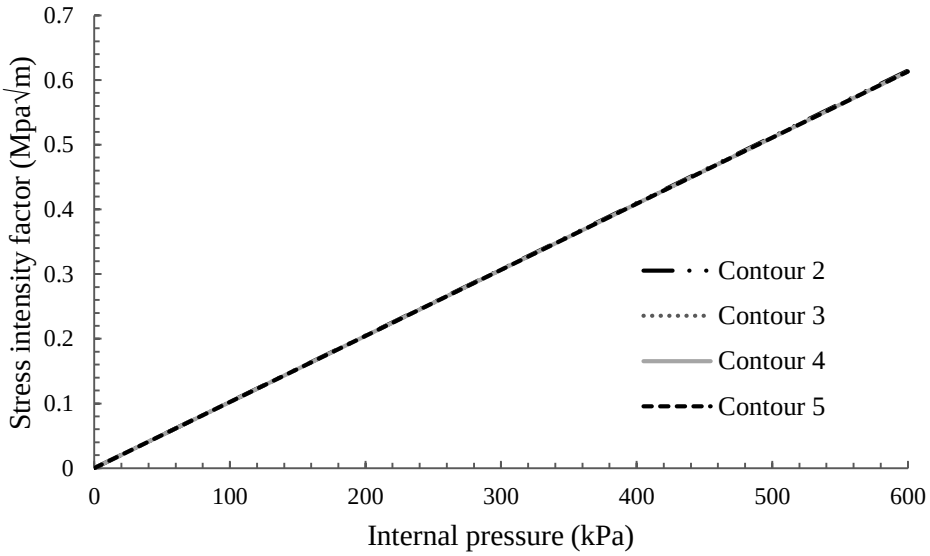

Figure 4.8: SIFs of four contour around the crack front ($\phi = 0$)

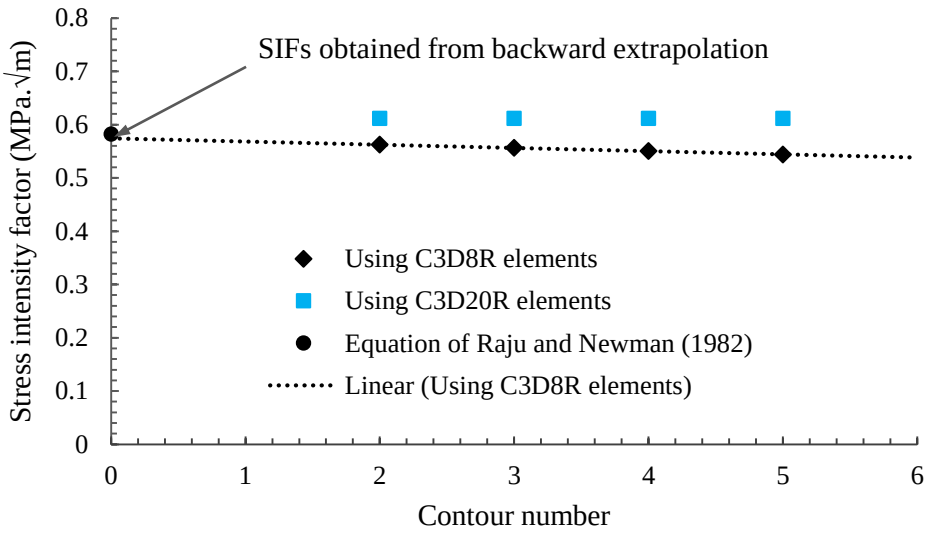

Figure 4.9: SIF at various contour ($\phi = 0$)

are the same. The FE analysis with C3D20R elements thus simulated successfully the path-independent contour integrals. However, the use of C3D20R elements require higher calculation effort and sometimes it is not possible to perform analysis due to lack of computational capacity for complex problems involving a large number of elements. On the other hand, the use of C3D8R elements provide constant strain in the elements and requires less computational effort. The SIFs calculated using C3D8R elements is found to vary from contour to contour as shown in Figure 4.9, which is potentially due to the errors in the calculated stress field in the vicinity of the crack tip. However, the variation of SIFs in Figure 4.9 is not significant. Recognizing the limitations of FE analysis in accurately calculating the stress field in the vicinity of crack tip, Fisher-Cripps (2007) proposed to plot the SIF obtained for different contours located at various distances from the crack tip against the distance from the tip and extrapolate the best fit curve backward to the tip (distance = 0) to estimate the SIF. The SIF is obtained using the method proposed in Fisher-Cripps (2007) as shown in Figure 4.9 from FE analysis with C3D8R elements. This SIF is around 4% less than the SIF calculated using C3D20R elements and matched with the value calculated using the equation of Raju and Newman (1982). The SIFs estimated from FE analysis using this method throughout the crack length are compared with those calculated using the equation of Raju and Newman (1982) in Figure 4.10. The comparison shows good agreement (<5% error) of the results of FE analysis with those from the equation of Raju and Newman (1982). Randeniya et al. (2016) also found FE calculations of SIFs within 5% of the values calculated using the equation of Raju and Newman (1982). FE analysis with C3D8R elements is therefore used for buried pipes where the method proposed in Fisher-Cripps (2007) is used for estimating the SIFs.

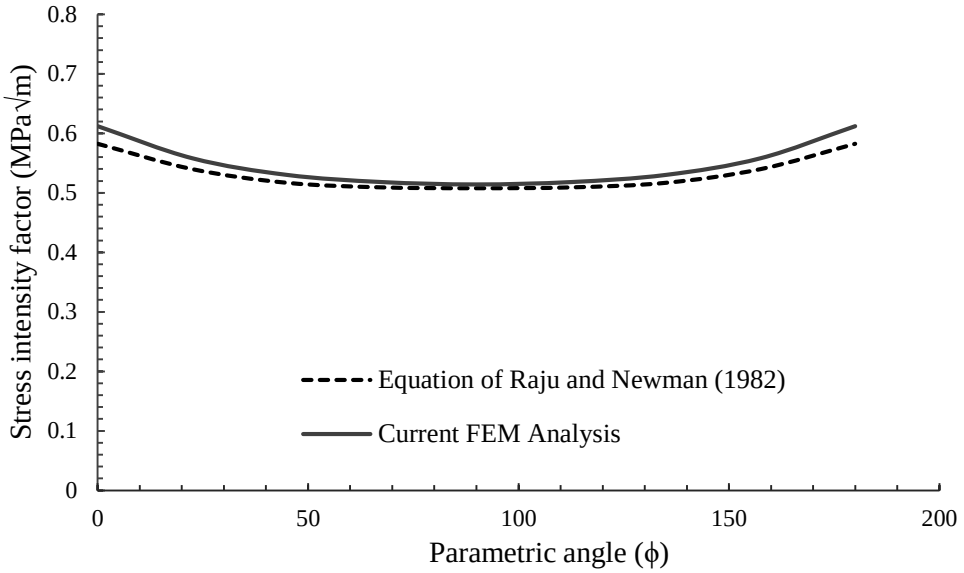

Figure 4.10: Comparison of SIFs (obtained from the equation of Raju and Newman (1982) and current FEA)

4.2.2 SIF calculation for buried pipeline

Three-dimensional pipeline-soil interaction analysis is performed using Abaqus to assess the SIFs for buried pipes with a wall crack. The soil and pipe are modelled as a 3D deformable solid body. The pipeline and crack geometries similar to those discussed above for in-air pipe are considered. Soil is assumed as an elasto-plastic material and defined by the Mohr–Coulomb failure criteria. Material parameters typical for medium dense sand are used, as shown in Table 4.1.

Table 4.1. Material Parameters

Material Properties	Soil	Cast Iron
Density (gm/cm^3)	1.77	7.88
Young's modulus (MPa)	24	125,000
Poisson's Ratio	0.25	0.25
Friction Angle in (°)	38	-
Dilation Angle in (°)	8	-
Cohesion Yield Stress (kPa)	0.1	-

General contact algorithm that automatically select master and slave surface is used for soil-pipe interaction. For the interface, the Coulomb's friction model is used that defines the critical shear stress at which sliding of the surfaces occurs. The friction coefficient (μ) depends on interface characteristics and the slip rate between the soil and the pipe. Larger value of μ indicates rough surface, and lower value represents a smooth surface. In this study, μ is assumed to be 0.30. The locations of the bottom and side boundaries of the problem with respect to the location of the pipe are sufficiently large in order to avoid the boundary effects. As the pipe is lying on uniform soil, the bending of the pipe due to vertical load is expected to be negligible. The length of the model (L) is thus selected as 100 mm so that $L/c > 20$, which is small to reduce computational time, yet sufficient to minimize the length effect on SIFs (Randeniya et al. 2016). Crack locations at the crown, springline and invert of the pipe are considered for the calculation of the SIFs. For analysis, horizontal and vertical movements are restrained at the bottom boundary, while the lateral movement of soil is restrained at side boundaries using roller supports. A typical FE model used for the determination of SIFs for a crown or invert crack is shown in Figure 4.11. Springline SIFs are calculated by taking the advantage of symmetry. Therefore, half of the soil-pipe system is considered for the analysis where the symmetric boundary condition is applied at the plane of symmetry. Figure 4.12 shows a typical FE model used for the determination of SIFs for springline crack.

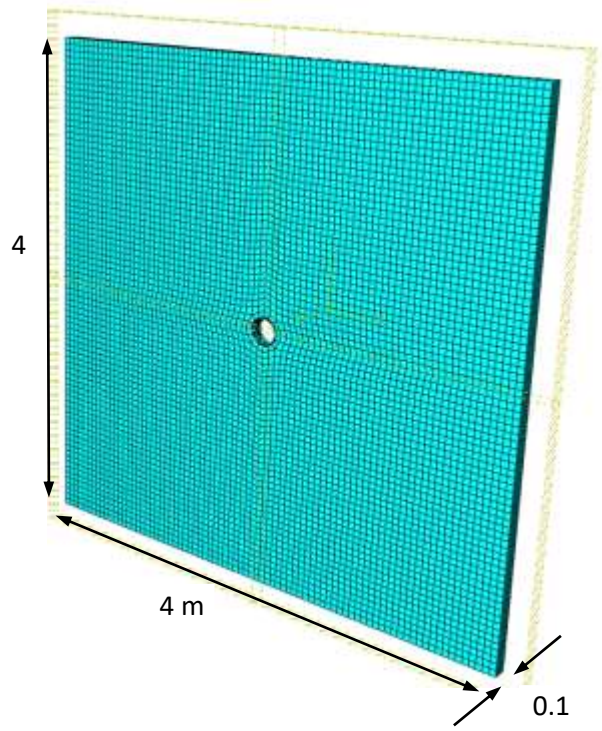

Figure 4.11: Global model of a buried pipeline for the determination of SIFs for a crown or invert crack

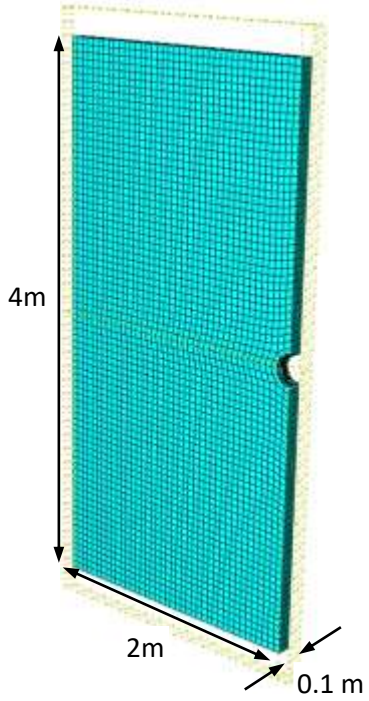

Figure 4.12: Global model of a buried pipeline for springline SIFs calculation

The global model and sub-model approach is again applied to save computational time. Figure 4.13 shows the sub-model considered for SIFs calculation of a springline crack.

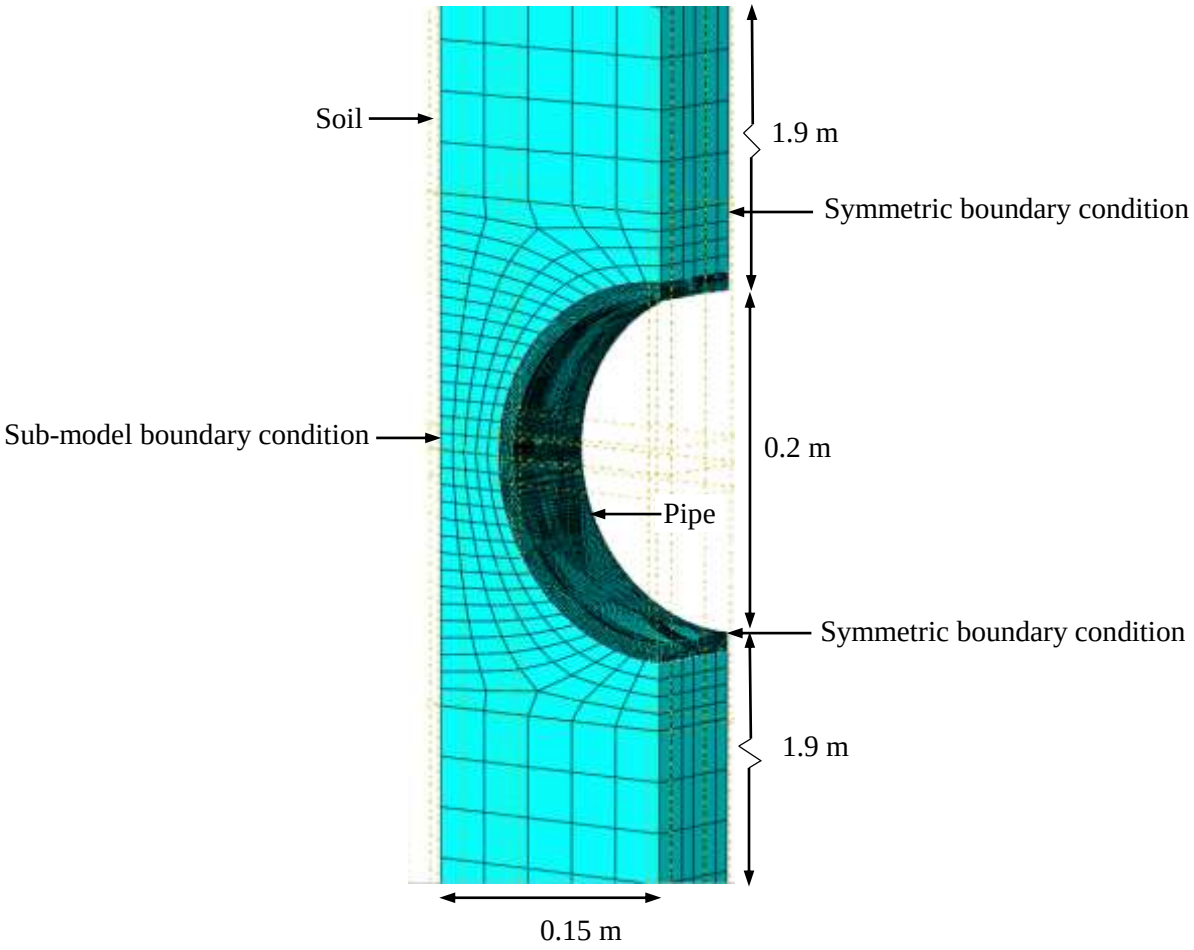

Figure 4.13: Sub-model boundary condition

Numerical analysis is carried out in two main steps. In the first step, 600 kPa internal pressure is applied to obtain SIFs and compared with the analytical solution of Raju and Newman (1982). In the second step, a surface load is applied at the top boundary to account for the surface load including gravity load. A surface pressure of 34.73 kPa, equivalent to the weight of 2 m of soil is applied.

It is to be noted that SIFs for pipelines subjected to surface load has not been extensively investigated earlier. Existing literature focused on calculating SIFs for pipelines subjected to internal pressure only. In the current study, the SIFs of buried pipes under internal pressure and surface load are examined at various locations of an elliptical crack. SIFs for a crack in corrosion defect for a buried water main is also calculated considering half ellipsoidal shape of corrosion (Figure 4.14).

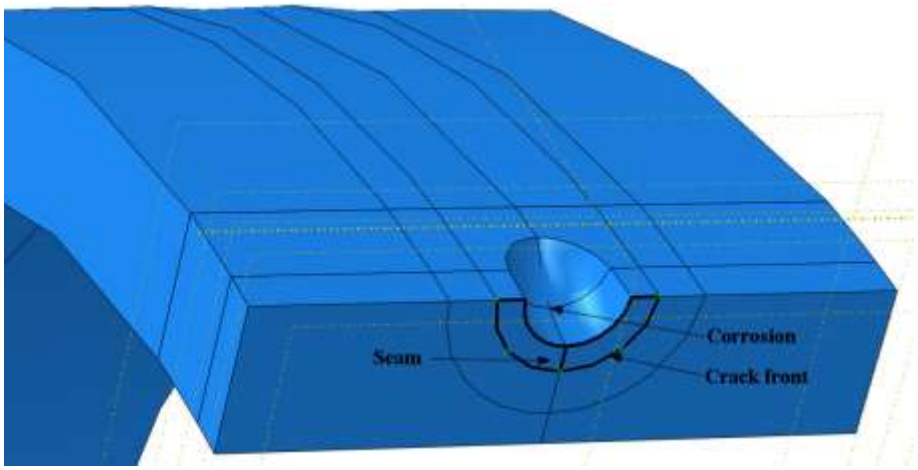

Figure 4.14: Crack front and corrosion location for a crack in corrosion defect

To identify the crack propagation direction for assigning during application of contour integral method, analyses with extended finite element method (XFEM), available in Abaqus, are first performed. Figure 4.15 shows a crack predicted using the XFEM analysis, which is essentially in the longitudinal direction. Therefore, longitudinal crack is assigned at the location determined from XFEM in the SIF calculation using the contour integral method. Table 4.2 shows the pipe dimensions and defect geometries considered.

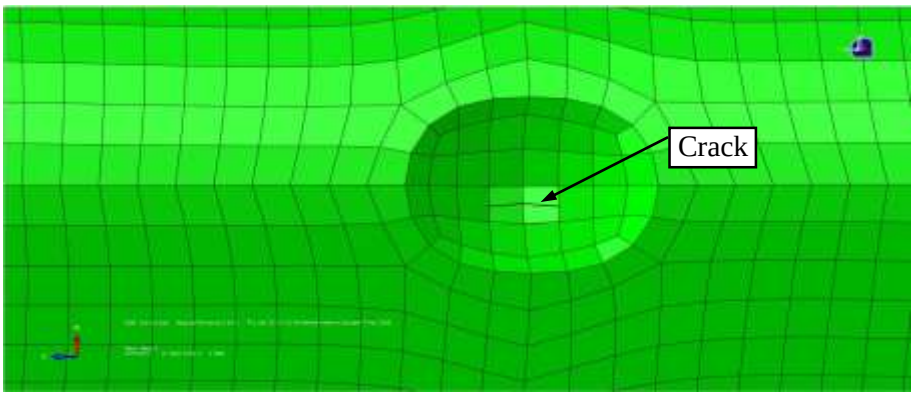

Figure 4.15: Crack propagation using XFEM

Table 4.2. Pipe dimensions and defect geometries

Geometries	Values
Pipe diameter, *D* (mm)	220
Wall thickness, *t* (mm)	10
Corrosion depth, *d* (mm)	3.3
Corrosion length, *l* (mm)	13
Corrosion width, *w* (mm)	6.5
Crack depth, d_c (mm)	1.7
Crack length, l_c (mm)	10

4.3 SIF for buried pipes

Numerical analysis is first performed to investigate the critical SIFs for longitudinal and circumferential cracks of a buried cast iron pipeline. Figure 4.16 shows that SIFs is much higher for longitudinal crack than the circumferential crack. As a result, longitudinal crack is considered for further analysis.

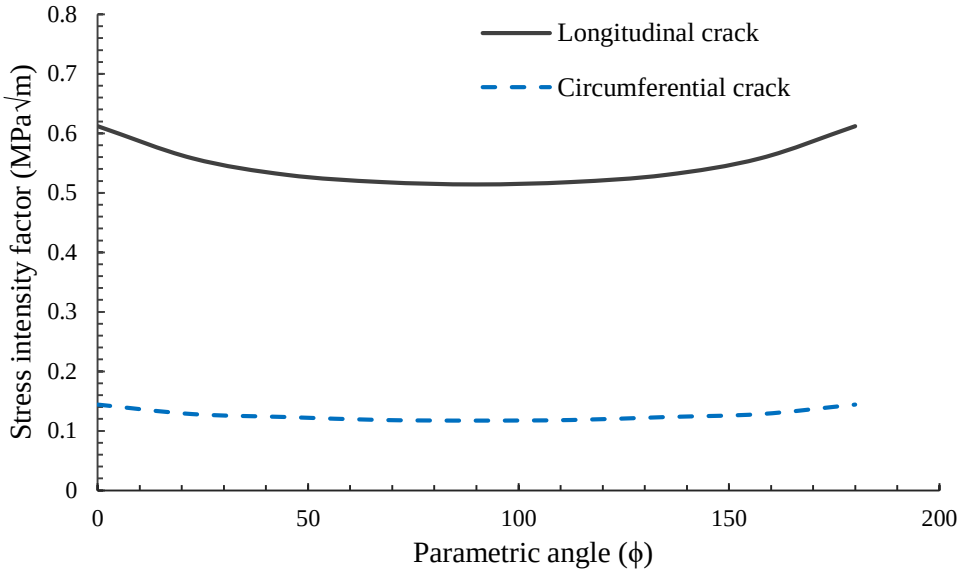

Figure 4.16: SIFs for a longitudinal and circumferential crack

The SIFs calculated for a longitudinal crack located at the springline and crown/invert of a buried pipeline are compared in Figure 4.17. Figure 4.17 shows that the SIF is higher for the springline crack than for a crown or invert crack. The SIFs calculated using the equation of Raju and Newman (1982) are also included in the figure. It is to be noted that the equation of Raju and Newman (1982) is only applicable under the loading of internal pressure. Due to the application of surface load, the SIFs at the springline is increased and SIFs at the crown/springline is decreased from the values under the internal pressure load only (calculated using the equation of Raju and Newman 1982).

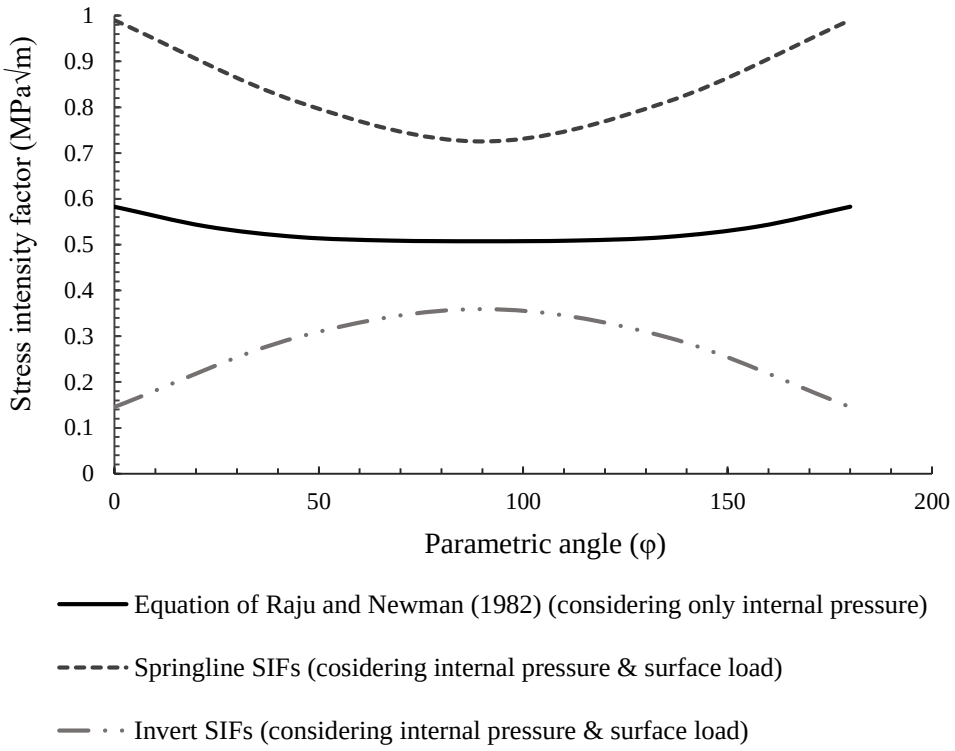

Figure 4.17: SIFs in springline and invert position, considering combined loading condition

The contribution of the internal pressure and external load independently on the SIFs are also obtained from FE calculations, as plotted in Figure 4.18. Figure 4.18 shows that FE calculation of SIFs under internal pressure matches reasonably with the values calculated using the equation of Raju and Newman (1982), which was developed for the in-air pipe. This implies that the surrounding soil does not have a significant effect on the SIFs due to the internal pressure. The equation of Raju and Newman (1982) can be used for calculation of SIFs under internal pressure of buried pipe. The SIFs under the surface can be separately calculated and added to the SIFs under the internal pressure to obtain the total SIFs. The SIFs for a buried pipe can be expressed as:

$$K = K_{pressure} + K_{surface} \quad [4.4]$$

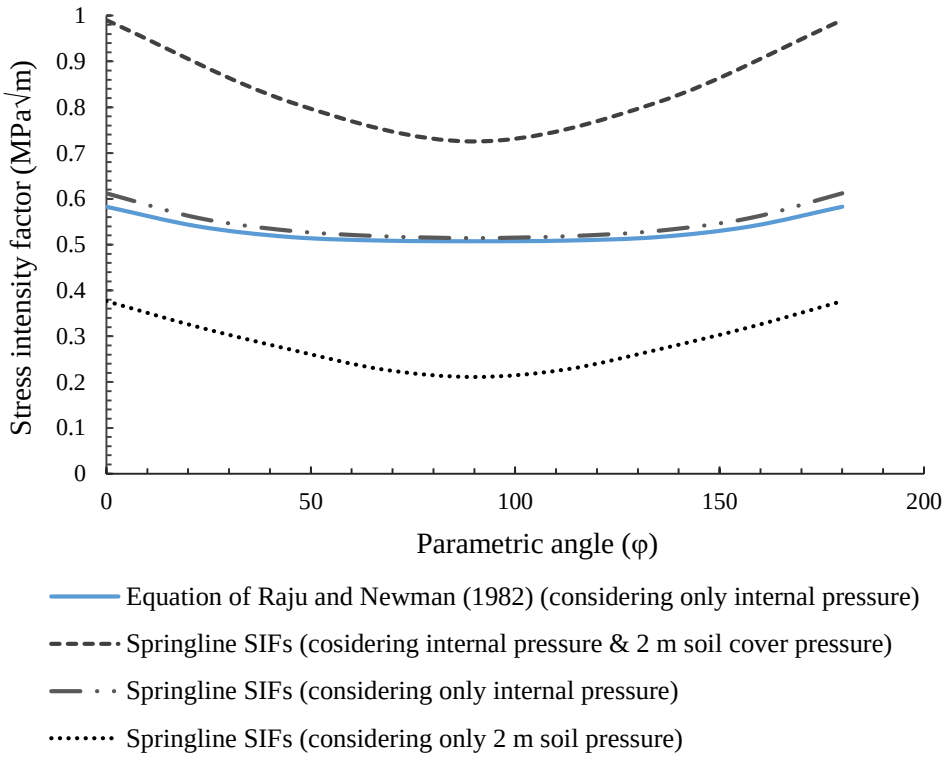

Figure 4.18: SIF for 'crack only defect' for a springline crack

Where, $K_{pressure}$ corresponds to the SIF due to internal pressure and $K_{surface}$ corresponds to the SIFs due to surface load. $K_{pressure}$ can be calculated using the equation of Raju and Newman (1982). For $K_{surface}$, the results of FE analysis are used to develop a simplified equation as shown in Equation (4.5).

$$K_{surface} = q\sqrt{\pi \frac{a}{Q}}\, F_s\,(a/c,\ a/t,\ t/R,\ \phi) \qquad [4.5]$$

Where, q is the surface load, and F_s is the influence coefficient of soil. The crack shape parameter, Q is recommended in Ichsan (1994) is assumed to be applicable for this case.

The parameter can be accurately approximated by Equation 4.6 and 4.7 (Ichsan 1994).

$$Q = 1 + 1.464 \left(\frac{a}{c}\right)^{1.65} \quad \text{for } a \leq c \qquad [4.6]$$

$$Q = 1 + 1.464 \left(\frac{c}{a}\right)^{1.65} \quad \text{for } c \leq a \qquad [4.7]$$

To simulate the gravity load, the surface load can be estimated as $q = \rho gh$, where ρ, g, h is the density, specific gravity, depth of soil cover, respectively.

The influence coefficients along the surface crack are determined using the results of FE analysis and listed in Table 4.3 for the particular crack considered (a/c=1, t/R =1).

Table 4.3. Influence coefficient for external surface crack (t/*R* =1)

a/c	parametric angle (ϕ)	Springline influence coefficient, F_s	Crown or invert influence coefficient, F_s
1	0	135.783	- 168.209
	$\pi/8$	115.350	- 120.583
	$\pi/4$	97.711	- 83.598
	$3\pi/8$	82.078	- 62.318
	$\pi/2$	76.120	- 55.732

SIFs for corroded pipe subjected to crack ('crack in corrosion defect') are also calculated and are presented in Figure 4.19. In this study, a total 5 mm defect depth is considered by assigning 3.3 mm of corrosion depth and 1.7 mm of crack depth. SIFs in Figure 4.19 are similar to those obtained for the crack only defect (presented in Figure 4.18). SIFs for internal pressure calculated using the equation of Raju and Newman (1982) with the crack depth as 5 mm (total of the corrosion and crack depths) is included in Figure 4.19. The equation with a total depth of defect can therefore, be used to calculate the SIFs for 'crack in corrosion defect' using the simplified equations.

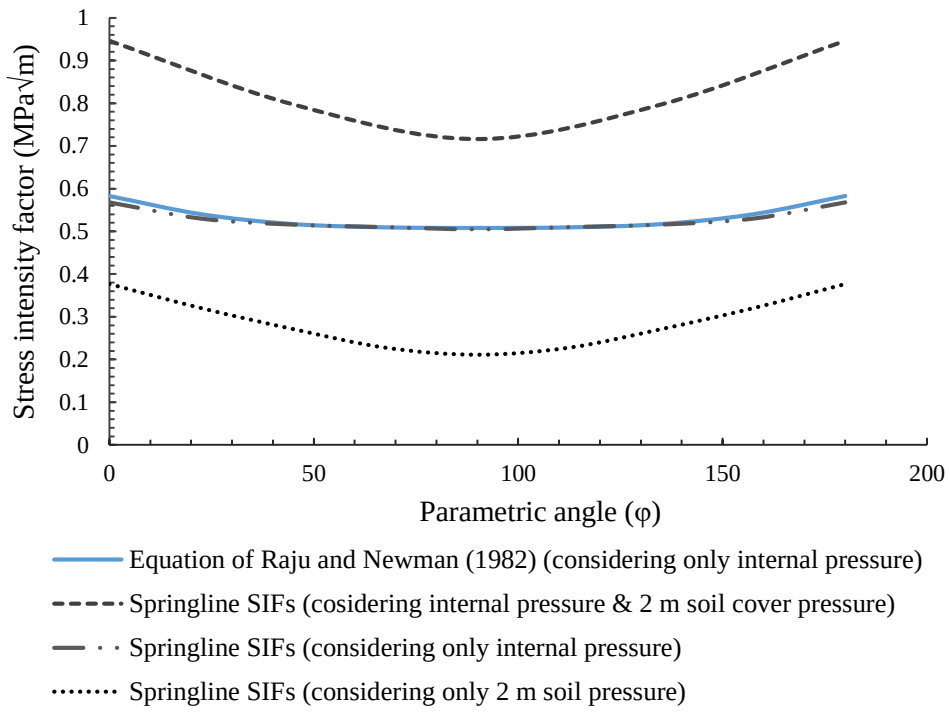

Figure 4.19: SIF for 'crack in corrosion defect' for a springline crack

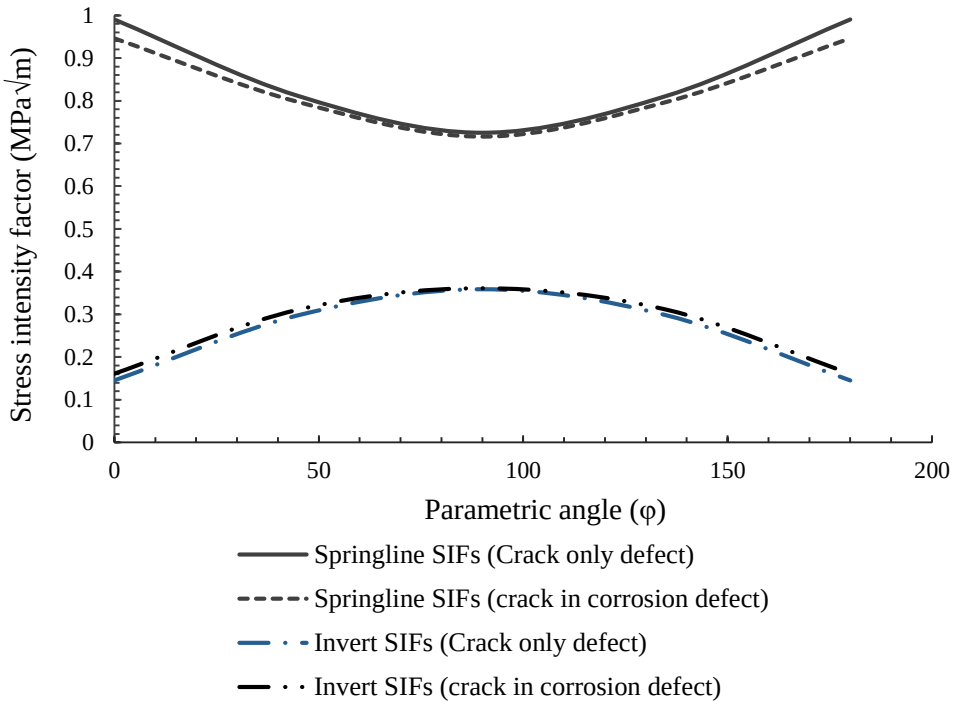

Figure 4.20: Comparison of 'crack only defect' and 'crack in corrosion defect'

Figure 4.20 compares the SIFs for 'crack only defect' and 'crack in corrosion defect' obtained from FE analysis. The calculated SIFs for the 'crack only defect' and the 'crack in corrosion defect' are almost same in the figure. This reveals that the solution developed for crack only defect (presented in Table 4.3) can be used for 'crack in corrosion defect' using total depth of defect as the crack depth.

4.5 Conclusion

In this study, FEA is used to investigate SIFs for a buried pipeline subjected to wall crack and 'crack in corrosion' defects. The analysis is performed using the contour integral method available in Abaqus FE software. Major numerical issues for the application of the contour integral method in calculating SIFs includes assignment of crack location, defining crack propagation direction and the computational requirements to deal with fine mesh requirements. XFEM analysis is performed to identify the crack location to assign during the analysis for calculation of SIFs. A sub-model technique is used to deal with the computational requirement to use fine mesh in a smaller region around the crack. The key finding from this study is presented below:

- The proposed FE modelling technique can be used to calculate SIF for buried pipeline. However, for properly calculating SIFs, one should be careful in assigning crack propagation direction which must be perpendicular to the crack face. The FE analysis with C3D8R elements successfully simulated the SIFs obtained from the equation of Raju and Newman (1982) for the in-air pipe.

- The SIFs due to internal pressure is not affected by the surrounding soil and therefore can be calculated using the equation of Raju and Newman (1982).

- A new equation is developed for calculating the SIFs due to the effect of surface load, which can be added to the SIFs due to the internal pressure to calculate the total SIFs.
- For the pipe with 'crack in corrosion defect', the simplified equation for SIFs can be used using the total depth of the defect (including corrosion depth and crack depth) in the equation.

References

Dassault Systemes. (2014). ABAQUS/CAE user's guide. Dassault Systemes Simulia Corp. Providence, RI, USA.

Diamantoudis, A.T. & Labeas, G.N. (2005). "Stress intensity factors of semi-elliptical surface cracks in pressure vessels by global-local finite element methodology." *Engineering Fracture Mechanics*, vol. 72, no. 9, pp. 1299-312.

Fisher-Cripps, C.A. (2007). "*Introduction to Contact Mechanics*," 2nd Ed., New South Wales, Australia.

Ichsan S.P. (1994). "Fatigue crack growth predictions of surface cracks under constant amplitude and variable amplitude loading." Faculty of Aerospace Engineering. Delft University of Technology.

Folkman, S. (2018) "Water Main Break Rates in the USA and Canada: A Comprehensive Study". *Mechanical and Aerospace Engineering Faculty Publications.* Paper 174.

Li, C.Q., & Yang, S.T. (2012). "Stress intensity factors for high aspect ratio semi-elliptical internal surface cracks in pipes". *International Journal of Pressure Vessels and Piping*, vol. 96–97, pp. 13-23.

Li, C.Q., Fu, G., & Yang, W. (2016a). “Stress intensity factors for inclined external surface cracks in pressurised pipes”. *Engineering Fracture Mechanics*, 165, 72–86. doi:10.1016/j.engfracmech.2016.08.014

Li, Y., Hasegawa, K., & Udagawa, M. (2016b). “Development of Stress Intensity Factors for Cracks with Large Aspect Ratios in Pipes and Plates”. *Journal of Pressure Vessel Technology*, 139(2), 021202.

Lin, X.B. and Smith, R.A. (1998). “Fatigue growth prediction of internal surface cracks in pressure vessels.’’ *Journal of Pressure Vessel Technology-Transactions of the ASME*, Vol. 120, pp. 17–23, 1998

Mohebbi, H., & Li, C. Q. (2011). “Experimental Investigation on Corrosion of Cast Iron Pipes”. *International Journal of Corrosion*, 2011, 1–17. doi:10.1155/2011/506501

Moulick, S.K. & Sahu, Y.K. (2012). “Stress Intensity Factor for Cracks in Thick Pressure Vessels using Weight Function Technique”. *National Conference on Innovative Paradigms in Engineering and Technology (NCIPET 2012*)

Predan, J., Močilnik, V., & Gubeljak, N. (2013). “Stress intensity factors for circumferential semi-elliptical surface cracks in a hollow cylinder subjected to pure torsion”. *Engineering Fracture Mechanics*, vol. 105, pp. 152-68.

Raju, I. S., & Newman, J. C. (1982). “Stress-Intensity Factors for Internal and External Surface Cracks in Cylindrical Vessels”. *Journal of Pressure Vessel Technology*, 104(4), 293. doi:10.1115/1.3264220

Randeniya, C., Robert, D., Fu, G., and Li, C. (2016). “The effect of corrosion patch geometry on stress intensity factors for external surface cracks in cast iron water mains”. *Proceedings of the*

4th International Conference on Sustainable Construction Materials and Technologies (SCMT4), Nevada, United States, 7-11 August 2016, pp. 1673-1680.

CHAPTER 5

Conclusions and Recommendations for Future Research

5.1 Conclusions

Cast iron water mains cover a significant portion of the municipal water distribution system. Assessing the structural strength of the deteriorating water mains has been a challenge for the municipalities. Due to the limitations of existing continuum based analysis in the failure assessment of the water main, a fracture mechanics approach is gaining attention for the failure assessment of the pipes. However, the tools for applying the fracture mechanics approach such as available material parameter and a method of assessing stress intensity factor (SIF) are not well developed. This research focuses on developing a method for calculating stress intensity factors for buried pipe and developing materials parameters for fracture mechanics based strength assessment of municipal cast iron water mains. Finding from this research are summarized as follow.

5.1.1 Assessment of material parameter

Two cast iron water mains exhumed from two nearby cities (City of St. John's and City of Mount Pearl) in the Province of Newfoundland and Labrador in Canada are considered to investigate the properties of cast iron. The samples are first scanned with an electron beam to produce a magnified image in SEM lab of Memorial University to determine the type of cast iron by analyzing the graphite flake shapes and orientations. In the SEM tests, both of the specimens show a very fine pattern of flakes with the surrounding areas without graphite and therefore, are classified as a spun cast iron.

Flat coupons extracted from the two separate exhumed cast iron water mains are also tested to determine the tensile strength and deformation properties such as ultimate strength, yield strength, modulus of elasticity and Poisson's ratio. Test data reveal that mechanical properties of cast iron may vary significantly. The rate of loading is found to have no influence on the stress–strain behavior. The cast iron pipe materials showed negligible plastic strain at a stress less than 75 MPa beyond which the plastic strain is significant. Thus, the elastic limit of the cast iron pipe material is 75 MPa which is around 25% less than the yield strength calculated using the 0.01% offset method. SENB tests are performed to determine the fracture toughness by using simple chevron (V) notch instead of the complex 'straight through notch' as it is difficult to fabricate the 'straight through notch' and the application of fatigue pre-cracking is also not feasible due to low fracture toughness of the brittle cast iron pipe material. The test results are evaluated using FE calculation of SIF. The results of FE analysis reveal that chevron (V) notch can be used instead of the complex 'straight through notch' for fracture toughness determination of cast iron pipe materials. The material parameters determined from the tests are employed for fracture mechanics based strength assessment of a buried water main. The study of the buried cast iron water mains under various loading conditions demonstrates that the SIF is significantly affected by pit shape and the erosion void at the bedding. The SIF is higher in the circumferential direction than in the longitudinal direction across the corrosion pit. As a result, crack propagation is expected along the circumferential direction. Three corrosion pit shapes (circular, diamond and elliptical) are considered in this study where the diamond shaped pit with sharp tips caused the highest SIF. Although the calculated SIF does not exceed the fracture toughness for the pipe material, it may cause failure due to subcritical crack growth in a corrosive environment.

5.1.2 Method for calculating SIFs

In this study, fracture mechanics approach is used to investigate SIFs for a buried pipeline subjected to 'crack only defects' and 'crack in corrosion defects'. The contour integral method available in Abaqus FE software is used for the analysis. Major numerical issues for the application of the contour integral method in calculating SIFs includes assignment of crack location, defining crack propagation direction and the computational requirements to deal with fine mesh requirement. To identify the crack location and crack propagation direction, XFEM analysis is performed as the contour integral method requires defining the crack front, and specifying the virtual crack extension direction. The study shows that for properly calculating SIFs on an elliptical crack, crack propagation direction must be assigned perpendicular to the crack face. A finer mesh in a smaller region around the crack is created to deal with the computational requirement by using sub-model technique, available in Abaqus. The FE analysis with C3D8R and C3D20R elements are considered and the study reveals that C3D8R elements along with C3D20R elements successfully simulated the SIFs obtained from the equation of Raju and Newman (1982) for the in-air pipe. The FE analysis is also performed for a buried pipe and shows that the SIFs due to internal pressure has no influence by the surrounding soil and therefore the equation of Raju and Newman (1982) can be used. A new equation is developed for calculating the SIFs due to the effect of surface load, which can be added to the SIFs due to the internal pressure to calculate the total SIFs. For the pipe with 'crack in corrosion defect', the simplified equation for SIFs can be used using the total depth of the defect (including corrosion depth and crack depth) in the equation.

5.2 Recommendations for Future Study

The study presented here investigates the mechanical properties for two cast iron water main segments extracted from two municipalities in Canada. The study reveals that mechanical

properties vary significantly for cast iron pipe materials. Therefore, further laboratory investigations are recommended to develop a more comprehensive database to examine the variability in the material parameters. Some specific recommendation for future research in this area included below:

i. Perform additional tests to determine the mechanical properties of a wide variety of cast iron pipe material.
ii. Conduct a statistical analysis to determine the statistical distribution of the material parameters.
iii. Conduct a reliability assessment of cast iron water main considering statistical distribution of mechanical parameters and loads.

This research also develops numerical modelling techniques for the assessment of stress intensity factors for buried pipelines. SIFs determined for a limited crack geometry (a/c =1) are presented. The developed technique can be used to develop tools for SIF assessment of wide variations of pipe and corrosion geometries. A few recommendations for future research in this area are outlined below:

i. SIFs can be determined for the different shape of crack (a/c), relative wall thickness (t/R) and relative crack depth (a/t) for external as well as internal surface crack.
ii. Fatigue failure may occur in cast iron pipeline that can be considered for future studies.
iii. Conduct field monitoring to obtain more information on corrosion geometries and develop design tools for failure assessment for these geometries.

References (for Chapter 1 and 2)

Arias-González, F., del Val, J., Comesaña, R., Penide, J., Lusquiños, F., Quintero, F., Pou, J. (2016). "Fiber laser cladding of nickel-based alloy on cast iron". *Applied Surface Science, 374, 197–205*.doi:10.1016/j.apsusc.2015.11.023

Caproco Corrosion Prevention Ltd. (1985). Underground corrosion of water pipes in Canadian cities. Case: The city of Calgary. Report prepared for CANMET, Ottawa, Canada.

CES Edupack 2013. Granta Design Limited, Cambridge.

Conlin, R. M., and Baker, T. J. (1991). "Application of fracture mechanics to the failure behaviour of buried cast iron mains." *Contract Rep. No. 266*, Transport and Road Research Laboratory, London.

Dowling N.E. (2013). "*Mechanical Behavior of Materials, Engineering Method for Deformation, Fracture and Fatigue*". Fourth edition. Pearson Education Limited, Essex, England.Fahimi, A., Evans, T. S., Farrow, J., Jesson, D. A., Mulheron, M. J., & Smith, P. A. (2016). "On the residual strength of aging cast iron trunk mains: Physically-based models for asset failure". *Materials Science and Engineering:* A, 663, 204–212. doi:10.1016/j.msea.2016.03.029

Granta (2018) "CES Edupack 2018 Installation Guide." http:www.grantadesign.com/education/

Griffith, A.A., (1921). "*The phenomena of rupture and flow in solids"*. Philosophical Transactions. Series A, 221, 163-198.

Jesson, D.A., Le Page, B.H., Mulheron, M.J., Smith, P.A., Wallen, A., Cocks, R., Farrow, J., and Whiter, J.T. (2010). "Thermally induced strains and stresses in cast iron water distribution pipes: an experimental investigation". *Journal of Water Supply Research and Technology-*Aqua, 59. pp. 221-229.

Ji J., Zhang C., Kodikara, J., and Yang S. (2015) "Prediction of stress concentration factor of corrosion pits on buried pipes by least squares support vector machine", *Engineering Failure Analysis*, Vol. 55 (2015), 131-138.

Koeble, T. F. and Hogan, T.W. (1967). "*Cast iron soil pipe and fittings handbook*". Cast iron soil pipe institute, Chattanooga, Tennessee.

Finkel L. M. (2018). "*Pipeline Politics: Assessing the Benefits and Harms of Energy Policy*". Santa Barbarana, California.

Folkman, S. (2018). "Water Main Break Rates in USA and Canada: A Comprehensive Study". *Mechanical and Aerospace Engineering Faculty Publications.* Paper 174.

Inglis, C. E., (1913). "Stresses in a plate due to the presence of cracks and sharp corners", *Transactions of the Institute of the Naval Architects* 55, 219-241.

Irwin, G.R., (1957). "Analysis of stress and strain near the end of a crack traversing a plate". *Journal of Applied Mechanics* 24, 361-364.

Kamel S., Meguid M.A. (2008). "An experimental study of soil erosion around leaking pipes". North American Society for Trenchless Technology, Dallas, Texas.

Liyanage, K.T.H (2016). Numerical investigation of failure mechanics of cast iron water mains. M.Eng. Thesis, Memorial University of Newfoundland, St. John's, NL, Canada.

Liyanage, K.T.H and Dhar, A.S. (2017). "Effects of corrosion pits on the wall stresses in cast iron water mains." *ASCE Journal of Pipeline Systems - Engineering and Practice*, 8(4): 04017023

Liyanage, K.T.H and Dhar, A.S. (2018) "Stresses in Cast Iron Water Main Subjected to Non-Uniform Bedding and Localized Concentrated Forces", *International Journal of Geotechnical Engineering*, 12(4), 368-376.

Ma, Z., and Yamada, K. (1994). "Durability evaluation of cast iron water supply pipes by sampling tests" *Proc., Structural Engineering,* Japan Society of Civil Engineers, Tokyo, 40A.

Makar, J.M., Desnoyers, R. and McDonald, S.E. (2001). "Failure modes and mechanisms in gray cast iron pipe." *Proceedings of the International Conference on Underground Infrastructure Research*, pp. 303-312. Netherlands.

Makar, J. M., Rogge, R., McDonald, S., and Tesfamariam, S. (2005). "The Effect of Corrosion Pitting on Circumferential Failures in Grey Iron Pipes." American Water Works Association, Denver.

Makar, J. M., & McDonald, S. E. (2007). "Mechanical Behavior of Spun-Cast Gray Iron Pipe". *Journal of Materials in Civil Engineering*, 19(10), 826–833. doi:10.1061/(asce)0899-1561(2007)19:10(826)

Mondal, B. (2018). "Remaining strength assessment of deteriorating energy pipeline". PhD Thesis, Memorial University of Newfoundland, St. John's, NL, Canada.

Rajani, B. and McDonald, S., (1995) "Water main break data for different pipe materials for 1992 and 1993", Report A-7109.1, Ottawa, Ontario, National Research Council.

Rajani, B. B., Makar, J. M., McDonald, S. E., Zhan, C., Kurakao, S., Jen, C.-K., and Viens, M. (2000). "Investigation of grey cast iron water mains to develop a methodology for estimating service life". AwwaRF and AWWA, Denver.

Seica, M. V., & Packer, J. A. (2004). "Mechanical Properties and Strength of Aged Cast Iron Water Pipes". *Journal of Materials in Civil Engineering*, 16(1), 69–77. doi:10.1061/(asce)0899-1561(2004)16:1(69)

Talbot, A.N. (1926). "Strength Properties of Cast Iron Pipe Made by Different Processes as Found by Tests", *Journal of the American Water Works Association*, Vol. 16, July, pp.1- 44

Terfas, O. A. (2010). “Quantification of constraint in three-dimensional fracture mechanics”. PhD thesis university of Glasgow.

Wang. W., Zhou. A., Robert. D.J. and Li.C.Q (2017). “Assessment of stress intensity factors for cast iron pipes with pitting corrosion.” *International Conference on Geomechanics, Geo-energy and Geo-resources*, Clayton, Monash University

Westergaard, H. M. (1939). “Bearing Pressures and crack”. *Journal of Applied Mechanics* 6, 49-53

Yamamoto, K., Mizoguti, S., Yoshimitsu, K., & Kawasaki, J. (1983). Relation between Graphitic Corrosion and Strength-degradation of Cast Iron Pipe. *CORROSION ENGINEERING*, 32(3), 157–162. doi:10.3323/jcorr1974.32.3_157

Zhang, C., Rathnayaka, S., Shannon, B., Ji, J., & Kodikara, J. (2017). “Numerical interpretation of pressurized corroded cast iron pipe tests”. *International Journal of Mechanical Sciences*, 128-129, 116–124. doi:10.1016/j.ijmecsci.2017.04.015

APPENDIX A

Failure Analysis of Buried Cast Iron Water Main Using Fracture Mechanics

This research work has been published as Debnath S., and Dhar A. S. 2018. “Failure analysis of buried cast iron water main using fracture mechanics” in the 71th Canadian Geotechnical Conference, GeoEdmonton 2018, Alberta, Canada, September 23–26, 2018. Most of the research presented in this chapter has been conducted by the first author. The other author, my supervisor Dr. Ashutosh Dhar supervised the research by provided support in developing the idea, guidance on finite element modelling and reviewed the manuscript.

Failure analysis of buried cast iron water main using fracture mechanics

Suborno Debnath, & Ashutosh Sutra Dhar
Department of Civil Engineering – Memorial University of Newfoundland, St. John's, NL, Canada

ABSTRACT
Water main failure, particularly for cast iron pipes, has been identified as a major concern for municipalities, as a number of water main breaks occur every year. Despite numerous past studies, pipe failure mechanisms observed in the field are not well understood. Conventional analyses using continuum based and Winkler spring based finite element methods calculate higher circumferential stress on the pipe wall which might lead to longitudinal wall cracking. However, circumferential cracking is the most commonly observed failure mode in water mains. In this paper, fracture mechanics is applied to study the stress concentrations in the buried pipe and offer new insights into the failure mechanisms of buried pipelines. Stress intensity factors for cast iron water mains with different shapes of corrosion defects are investigated using finite element analysis for crack assessment of the pipelines. The stress intensity factors are compared with the fracture toughness determined from laboratory tests.

Keywords: Water main, Cast iron pipe, Stresses intensity factor, Failure mechanisms, Fracture mechanics, Finite-element analysis

RÉSUMÉ

La principale défaillance des conduites d'eau, en particulier pour les tuyaux en fonte, a été identifiée comme une préoccupation majeure pour les municipalités, étant donné qu'un certain nombre de bris de conduites d'eau se produisent chaque année. Malgré de nombreuses études antérieures, les mécanismes de rupture des conduites observés sur le terrain ne sont pas bien compris. Les analyses conventionnelles utilisant des méthodes d'éléments finis à base de continuum et de ressorts de Winkler calculent une contrainte circonférentielle plus élevée sur la paroi de la conduite, ce qui peut conduire à une fissuration de la paroi longitudinale. Cependant, la fissuration circonférentielle est le mode de rupture le plus couramment observé dans les conduites d'eau. Dans cet article, la mécanique de la rupture est appliquée pour étudier les concentrations de contraintes dans le tuyau enterré et offrir de nouvelles perspectives sur les mécanismes de défaillance des pipelines enfouis. Les facteurs d'intensité des contraintes pour les canalisations d'eau en fonte présentant différentes formes de défauts de corrosion sont étudiés à l'aide d'une analyse par éléments finis pour l'évaluation des fissures des canalisations. Les facteurs d'intensité de contrainte sont comparés à la ténacité à la rupture déterminée à partir d'essais en laboratoire.

Mots clés: Conduite d'eau, Conduite en fonte, Facteur d'intensité des contraintes, Mécanismes de rupture, Mécanique de la rupture, Analyse par éléments finis

INTRODUCTION

Buried pipelines are used to transport drinking water, waste water or other fluids. There are different kinds of pipe materials used to carry water. Gray cast iron is one of them, which was generally installed in Canada in the middle of the 19th century. The aged pipes show deterioration and are prone to failure. Rajani et al. (1995) estimated that approximately 50% of water mains were gray cast iron, in their survey of 21 cities in Canada. Gray cast iron shows a tendency to corrode in the buried condition and may create corrosion pits which cause stress concentration around the pits. According to Folkman (2012), nearly 75 percent of all utilities have corrosive soil conditions. Corrosion is thus considered one of the main reasons for water main failure in Canada and the USA. Due to water main failure, 50% of the water has been reportedly lost in the city of Mount Pearl, Canada, which causes huge economic loss (Frick and Manuel, 2005). Cast iron water mains may fail due to circumferential cracking, longitudinal cracking, joint failure or blowouts (Rajani et at, 1996). Circumferential failures mainly occur due to corrosion pits and it is the most common mode of failure for water distribution networks (Makar et al, 2005). Liyanage and Dhar (2015, 2017) showed that the stress concentration can be higher in the circumferential direction than the longitudinal direction around a pit of a pipe that is subjected to non-uniform bedding, which may create cracks in the longitudinal direction. The failure of the pipe occurs when the applied stresses in the pipe exceed the capacity of the pipe material (Gould et al, 2011). Trickey et al. (2016) showed that circumferential cracking in water mains may be caused due to longitudinal bending that results from non-uniform bedding support or a frost load in the soil above the pipe. Differential soil movement occurs due to frost penetration, which causes ring failure. The lack of ground support causes additional stresses on the pipe wall near the unsupported zone (Balkaya et al. 2012). Pipe stresses are

significantly affected by leaks opening, which may exceed the material strength and may fail in the vicinity of an opening where stress increases exponentially with the increase of crack length (Cassa et al, 2009). Dhar et al. (2004) revealed that the lack of soil support within a localized zone can lead to stress or strain concentration in flexible pipes. The stress or strain concentration was higher for pipes with higher stiffness relative to the soil (Dhar et al. 2004). Although these approaches are widely used to assess pipeline failure, fracture mechanics has not been extensively applied to investigate the failure of a pipeline. In fracture mechanics, the stress intensity factor (SIF) is generally used for the assessment of brittle fracture. The stress intensity factor was found to provide less error and is a more accurate way than using stress concentration for failure assessment (Dipen et al. 2015).

Limited research information is currently available in the literature on circumferential crack assessment in water mains using fracture mechanics. Some recent papers on stress intensity factor show that for a surface crack, the maximum stress intensity factor occurs at different points, leading to different modes of failure, because the type of loading affects the stress intensity factors (Li and Yang, 2012). However, no study on the effect of pit shape and non-uniform bedding with various lengths is available in the literature. In this paper, a three-dimensional finite element analysis is developed to determine the stress intensity factor for different shapes of corrosion pits of a cast iron water main that is supported by non-uniform bedding. A three-dimensional finite-element analysis is also performed to calculate the stress intensity factor of cast iron and compare it with the lab results, which helps to understand the failure mechanism.

FRACTURE TOUGHNESS FROM LABORATORY TESTS

Single-edge notch beam (SENB) tests were conducted in the lab by the research group at Memorial University of Newfoundland (Ali, 2017) with 3.2 mm, 4.7 mm and 6 mm pre-crack notches (V-notch) using ASTM E 1820-01(2001) where the width to depth ratio (W/B) of the specimens was kept in the range of $1 < W/B < 2$. In those tests, a simple chevron (V) notch was used rather than a complex straight through notch, recommended in the ASTM standards (Figure 1). The main advantage of using a V notch is that the fabrication procedure is easier. Figure 2 shows the specimen used in SENB tests.

The clear span (S), depth (W) and thickness (B) of the specimen were 84 mm, 14 mm and 7 mm, respectively. Three-point loading was applied on the specimen and a linear voltage displacement transducer (LVDT) was attached to measure the displacement. The width of the V notch was 2.4 mm. The failure load was recorded for each specimen. Details of the test procedure are available in Ali, (2017). Fracture toughness K_c was then calculated from the failure load and crack length (ASTM E 1820-01, 2001) using the following equation Eq. (1).

$$Kc = \frac{PS}{BW^{3/2}} f(a/w) \quad [1]$$

where $f(a/w) = \frac{3(a/w)^{1/2}}{2(1 + 2a/w)(1 - a/w)^{3/2}} * [1.99 - (a/w) * (1 - a/w) * (2.15 - 3.93 * a/w + 2.7 * a^2/w^2)$

and P is the ultimate load, S is the clear span, B is the thickness, a is the crack length and w is the depth.

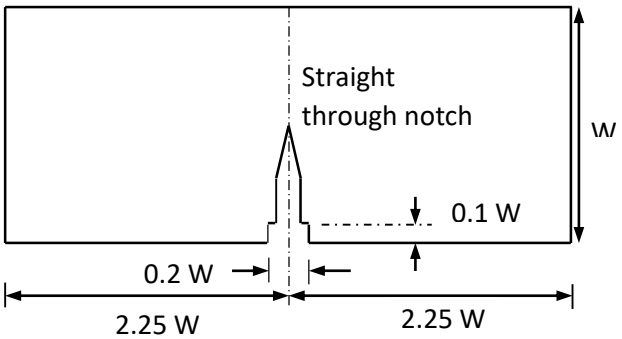

Figure 1. ASTM E 1820-01 recommended specimen

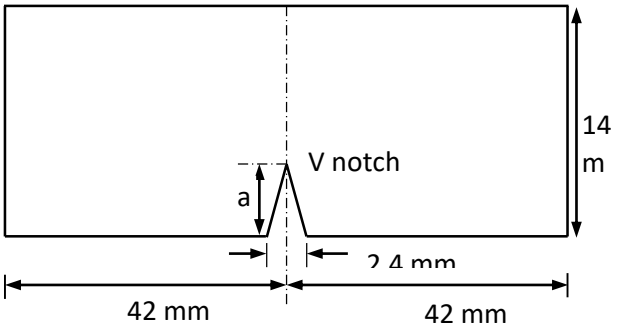

Figure 2. Test specimen used

However, Eq. (1) is recommended in the ASTM standards for the specimen shape shown in Figure 1. To validate the applicability of Eq. (1), a 3D finite element model is developed using Abaqus to determine the fracture toughness of the specimen in the single-edge notch beam (SENB) tests. The cast iron specimen is defined as a 3D deformable solid body. For FE modeling, an 8-node linear brick element (C3D8R) is used. A Young's modulus of 121 GPa and Poisson's ratio of 0.25 are considered in this model, based on the data reported in Ali, (2017). The specimen is simply supported. The clear span (S), depth (W), and thickness (B) of the specimen are 84 mm, 14 mm and 7 mm, respectively. Pre-crack notches (V-notch) of 3.2 mm, 4.7 mm and 6 mm depth are considered as crack lengths. The width of the V notch is 2.4 mm. Figure 3 shows the finite element mesh considered in the model.

The contour integral method is used to determine the fracture toughness where the crack extension direction is along the normal to the crack plane. For each integral, five contours are specified. Figure 4 shows the crack extension direction.

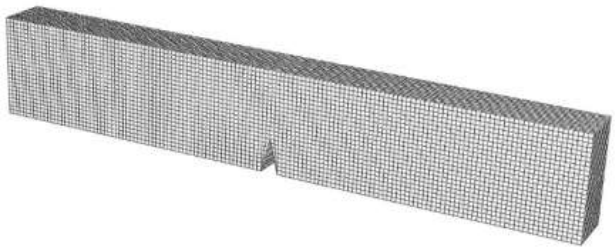

Figure 3. 3D finite element modeling of single-edge notch beam (SENB) test

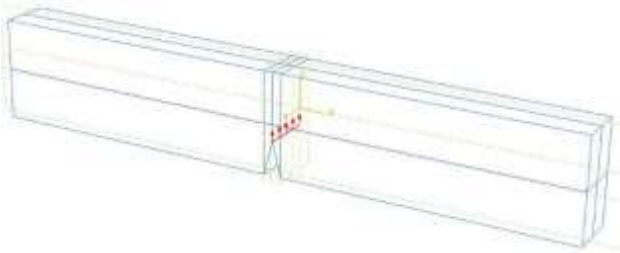

Figure 4. Crack extension direction in Contour integral method

The failure load is taken from single-edge notch beam (SENB) tests to determine the fracture toughness and deflection using finite element analysis. In finite element modeling, a finer mesh typically results in a more accurate solution than coarser mesh. However, as a mesh is made finer, the computation time increases. Therefore, a mesh convergence analysis is performed to increase speed and obtain sufficient accuracy and to ensure that the result is no longer dependent on mesh size. The h-method (varying the element size) is implemented. Stress intensity factors calculated from finite element analysis are compared with the test results obtained using Eq. (1), as shown in Table 1 and Figure 5.

Table 1. Fracture toughness, Kc from tests and Numerical model

Specimen	Failure Load (N)	Crack Length (mm)	Kc Test (MPa√m)	Kc Abaqus (MPa√m)
SB1	1869	3.2	17.16	16.80
SB2	2106	3.2	19.33	18.93
SB3	1191	4.7	14.39	14.81
SB4	1068	4.7	12.91	13.35
SB5	1020	4.7	12.33	12.70
SB6	1523	4.7	18.40	19.01
SB7	1179	6.0	18.34	18.75
SB8	1136	6.0	17.67	17.80

The fracture toughness of cast iron varies between 12 to 19 MPa√m (Figure 5) where the maximum deflection is 19 mm (Figure 6). The fracture toughness obtained from Abaqus is almost identical with the test value, indicating that Eq. (1) is applicable for a simple chevron (V) notch, which can be used instead of the complex straight through notch. Finite element calculations of deflections also match the measurements (Figure 6). Finite element models thus reasonably represent the test conditions.

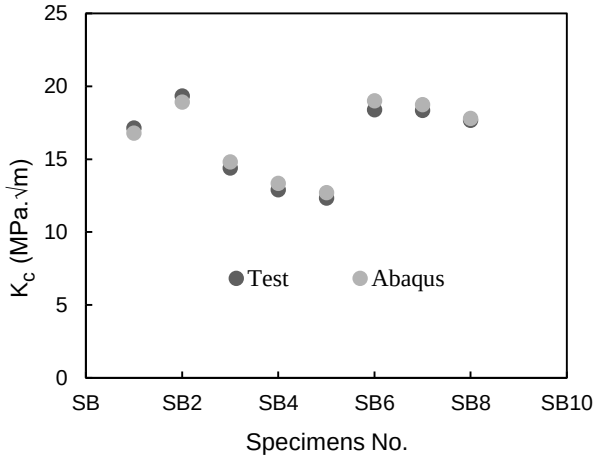

Figure 5. Comparison of fracture toughness from test and Abaqus

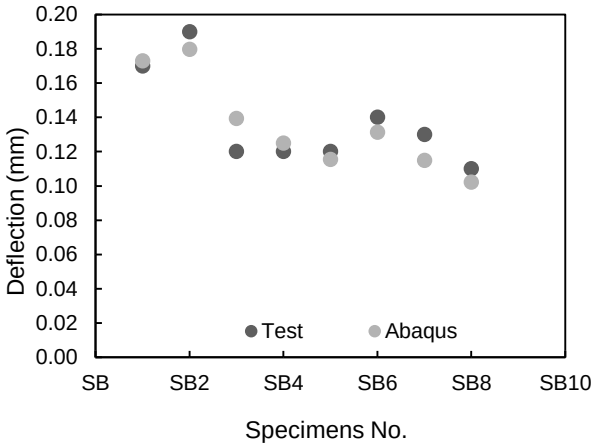

Figure 6. Comparison of deflection from test and Abaqus

FINITE ELEMENT MODELING OF CAST IRON WATER MAIN

Three-dimensional finite element analyses are carried out using Abaqus to obtain the pipe stress distribution and stress intensity factor of the pipe. The model is developed so that the pipeline and the soil model are defined as 3D deformable solid bodies. An 8-node linear brick element (C3D8R) is used. First, an extended finite element method is used to determine the crack propagation direction. The contour integral method is used to determine the stress intensity factor around the corrosion pit, for which the crack

direction needs to be assigned. For the contour integral method, the crack extension direction is defined along the normal to the crack plane and for each integral, five contours are specified. Figure 7 shows the crack extension direction applied, obtained from finite element analysis, discussed later in this paper. Soil load, internal pressure, surcharge (snow load) and traffic load affect the cast iron pipeline, which is buried in an elastoplastic soil.

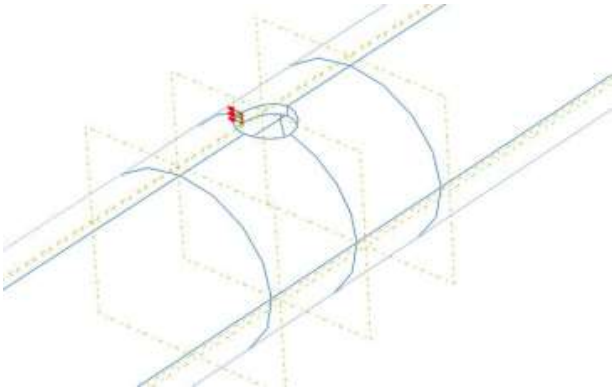

Figure 7. Crack extension direction in Contour integral method

Lack of ground support is also considered using a void (Figure 8). For soil, two boundary conditions are used and for pipeline, one boundary conditions is considered. Longitudinal displacements of soil and pipe are restrained at the end plane by roller support, because an infinite or semi-infinite medium of soil can be assumed to move in a vertical direction. The bottom surface of the 3D finite-element soil model is required to be completely fixed in order to restrain horizontal and vertical movement. The diameter of the cast iron is assumed to be 175 mm and the thickness is 10 mm, buried in a medium dense soil with 2 m of soil cover. The pipe is subjected to 400 kN/m^2 internal pressure. Gravity load, snow load (25 kN/m^2) and truck load (axle load 14400 kg) are also considered in the model. Gravity load is calculated manually and applied as a pressure at the top of the soil in the contour integral method.

The length of the pipe considered is 4 m. The corrosion pit is located at the invert position of the pipe. Uniform bedding, as well as a non-uniform bedding condition, are considered. To simulate the non-uniform bedding condition, a 1 m or 2 m long, 50 mm thick void is provided at the invert of the pipe. Circular, elliptical and diamond types of corrosion pit are considered, where the diameter of the circular pit is 50 mm, the length of the major axis is 50 mm for the elliptical pit and the diagonal length is 50 mm for the diamond shaped corrosion pit. The void at the bedding is symmetrical to the pit hole and extends 90° or 180° around the pit circumference. The FE model is first validated through simulation of data available in the literature (Liyanage and Dhar, 2017). Soil parameters reported in Liyanage and Dhar (2017) are employed in the analyses. A parametric study is conducted to investigate the influence of the dilation angle in order to select a suitable dilation angle. The dilation angle is varied from 8º to 15º and no significant variation in SIF is found. Table 2 summarizes the material parameters used in the analysis.

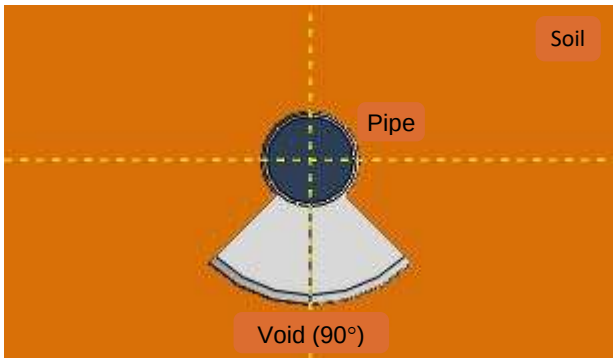

Figure 8. Symmetric void (90°) with respect to pit hole

Table 2. Material Parameters

Material Properties	Soil	Cast Iron
Density (kN/m^3)	1.77	7.88
Young's modulus (MPa)	24	138,000
Poisson's Ratio	0.25	0.21
Friction Angle in (°)	38	-
Dilation Angle in (°)	15	-
Cohesion Yield Stress (kPa)	0.01	
Max Principal Stress (MPa)	-	180
Tolerance	-	0.05

RESULTS

As discussed earlier, in the contour integral method for calculating stress intensity factor, the direction of crack propagation has to be defined. To understand the direction of stress propagation, an extended finite element method (XFEM) is employed using Abaqus. In XFEM, the maximum principal stress criterion is used to identify the direction of crack propagation. Figure 9 shows the direction of crack propagation for a pipe with a circular corrosion pit. The pit is located at the invert of the pipe where a 2 m long void which extends 90° around the pit circumference, in the bedding soil. To ensure initiation and propagation of the crack, a high pressure (i.e. 400 kPa) is applied at the ground surface. Figure 9 demonstrates that a crack initiates and propagates in the circumferential direction of the pipe.

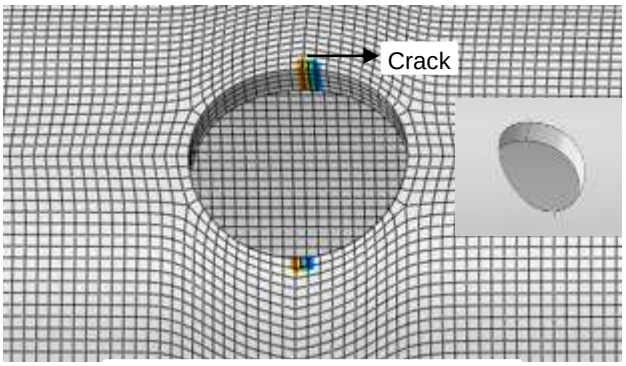

Figure 9. Crack propagation direction (philsm)

The distribution of major principal stress around the circular pit is plotted in Figure 10. Since cracking is generated by tension, the major principal stress from Abaqus provides the direction of cracking. Figure 10 shows the highest tensile stress along the circumferential direction of the pipe across the circular corrosion pit. Thus, cracking is expected in the circumferential direction of the pipe due to high longitudinal stress, which is consistent with the crack direction observed in Figure 9.

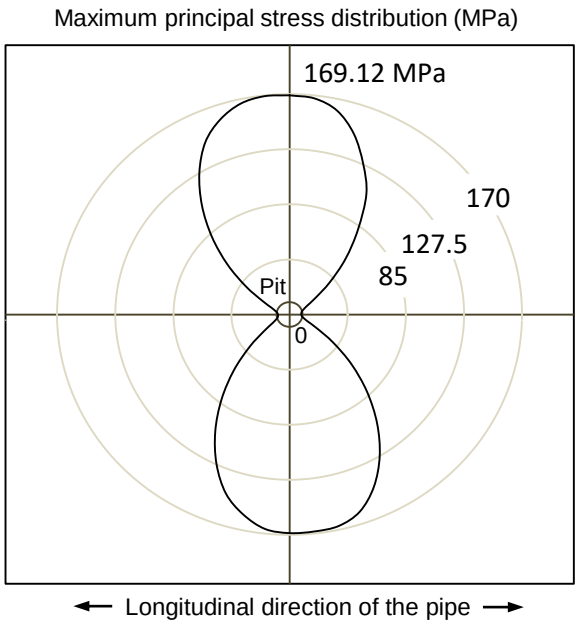

Figure 10. Distribution of maximum principal stress around a circular pit

To determine the direction of crack initiations and propagations for different shapes of corrosion pits, the contours of major principal stress are plotted against the pit in Figures 11 to 13. These figures demonstrate high tensile stress (red colour in the figure) in the circumferential direction of the pipe. Therefore, crack directions along the circumference are assigned in the contour integral method, as shown in Figure 7.

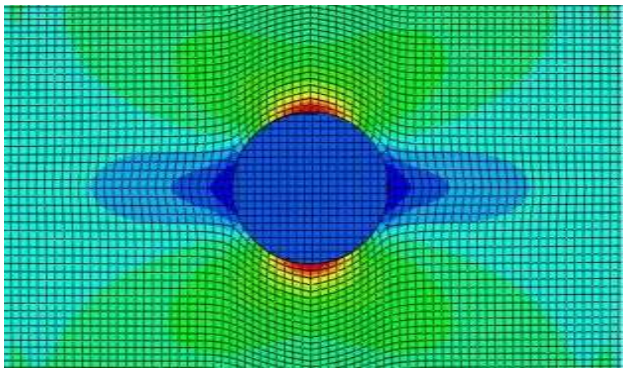

Figure 11. Maximum principal stress around a circular pit

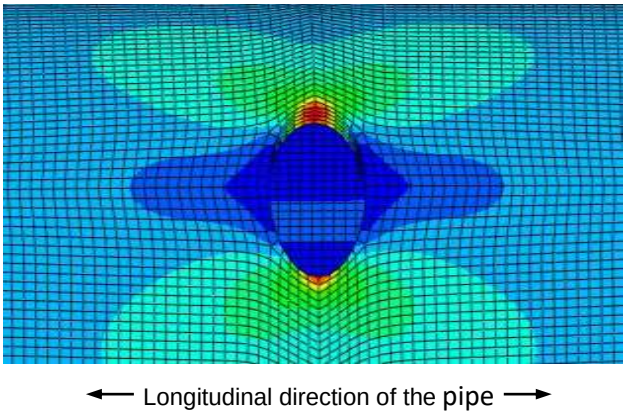

Figure 12. Maximum principal stress around an elliptical pit

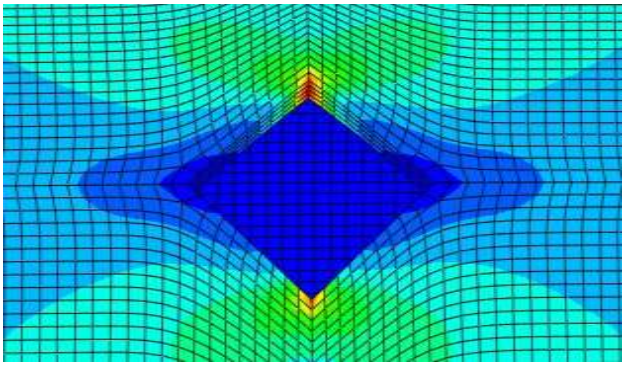

Figure 13. Maximum principal stress around a diamond shaped pit

The stress intensity factors (SIFs) calculated using finite element analysis, for different pipe installation and loading conditions are shown in Tables 3 to 5. The SIFs in

the tables suggest that the SIF is highest for a diamond shaped corrosion pit and lowest for the circular shape. The SIF for the elliptical corrosion pit lies between the diamond and circular corrosion pits. The SIF increases with the decrease of tip radius of the corrosion hole. SIF increases due to gravity, surcharge (snow load) and traffic load but decreases due to internal pressure. SIF increases 40 % due to traffic load and decreases 6% due to internal pressure for the 1 m hole under the pit. Thus, for fracture, the critical condition is when the cast iron water main is empty and has internal pressure.

However, the SIFs under typical loading conditions of water mains (Tables 3 to 5) are less than the fracture toughness determined for cast iron pipe materials shown in Table 1. The maximum calculated SIF (i.e. 6.80 MPa√m) is about 45% of the mean value of the fracture toughness (i.e. 15 MPa√m). A crack may propagate at values of SIF that can be substantially below fracture toughness, which is known as subcritical crack growth, stable cracking or quasi-static crack propagation, due to stress corrosion. Strained bonds at crack tips are weakened due to the chemical action of environmental factors like water that facilitate crack growth during stress corrosion (Atkinson, 1984). Cullin et al (2014) reported that subcritical corrosion fatigue is one of the threats to gray cast iron water pipes which is mainly due to the cyclic load. A casting defect may cause a microscopic crack on the pipe's interior that may accelerate crack propagation and failure may occur before fracture toughness is reached.

Table 3. Stress intensity factor in MPa√m (1m hole under the pit and extending 90° around the pit circumference)

Shape of the pit	Gravity and Surcharge	Gravity, Surcharge and Traffic	Gravity, Surcharge, Traffic and Internal pressure
Circular	0.56	0.77	0.72
Elliptical	1.37	1.91	1.79
Diamond	2.49	3.48	3.29

Table 4. Stress intensity factor in MPa√m (2m hole under the pit and extending 90° around the pit circumference)

Shape of the pit	Gravity and Surcharge	Gravity, Surcharge and Traffic	Gravity, Surcharge, Traffic and Internal pressure
Circular	0.56	0.77	0.66
Elliptical	1.44	2.09	1.97
Diamond	2.62	3.81	3.64

Table 5. Stress intensity factor in MPa√m (2m hole under the pit and extending 180° around the pit circumference)

Shape of the pit	Gravity and Surcharge	Gravity, Surcharge and Traffic	Gravity, Surcharge, Traffic and Internal pressure
Circular	0.99	1.38	1.22
Elliptical	2.71	3.77	3.67
Diamond	4.91	6.80	6.65

CONCLUSION

In this study, finite element analysis is used to calculate stress intensity factors for a pipeline subjected to corrosion pits. Stress intensity factors are compared with fracture toughness, determined from laboratory tests for fracture assessment of a cast iron water main. A finite element method is used to determine the fracture toughness of the cast iron specimen and compared with the single-edge notch beam (SEBN) tests results. In this study, a simple chevron (V) notch is used instead of a complex straight through notch, which is recommended by ASTM E 1820-01. From those results, the conclusion can be drawn that a complex straight through notch can be successfully replaced with a chevron (V) notch that will reduce fabrication difficulty.

The study of buried cast iron water mains under various loading conditions subjected to non-uniform bedding demonstrates that the pipe SIF is significantly affected by pit shape and the erosion void at the bedding. The SIF is higher in the circumferential direction than in the longitudinal direction across the corrosion pit. As a result, crack propagation is expected along the circumferential direction. Three corrosion pit shapes (circular, diamond and elliptical) are considered in this paper. The round hole corrosion pit is the safest among the three types of corrosion pits, and the diamond shape is the least safe. SIF increases with the gravity, surcharge (snow load) and traffic load but decreases due to internal pressure. Although the SIF does not exceed the fracture toughness for the pipe considered, it may fail due to subcritical crack growth. This study can be extended by investigating the effect of subcritical crack growth in a cast iron water main.

ACKNOWLEDGEMENTS

Funding of this research project was provided by the Natural Sciences and Engineering Research Council of Canada (NSERC) through its Collaborative Research and Development Grants and the city of Mount Pearl in the province of Newfoundland and Labrador. This financial support is gratefully acknowledged.

REFERENCES

Ali I. 2017. “Mechanical properties of an exhumed cast iron pipe material”. M.Sc. Thesis, Memorial University, Newfoundland and Labrador, Canada.

ASTM E1820-01 2001. “Standard test method for measurement of fracture toughness.” *American society for testing and materials*.

Atkinson B. K. 1984. “Subcritical crack growth in geological materials.” *Journal of Geophysical Research*, vol. 89, no. B6: 4077-4114.

Balkaya, M., Moore, I. D., and Sağlamer, A. 2012. “Study of Nonuniform Bedding Support Because of Erosion under Cast Iron Water Distribution Pipes.” *Journal of Geotechnical and Geoenvironmental Engineering*, 138(10): 1247–1256.

Cassaa A.M., Zylb J.E. van and Laubsche R.F. 2010. “A numerical investigation into the effect of pressure on holes and cracks in water supply pipes.” *Urban Water Journal*, Vol. 7, No. 2: 109–120.

Cullin M. J., Petersen T.H. and Paris A. P.E. 2015. “Corrosion Fatigue Failure of a Gray Cast Iron Water Main”. Journal of *Pipeline Systems Engineering* and *Practice*,6(2):05014003.DOI:10.1061/(ASCE)PS.19491204.0000188.

Dhar, A. S., Moore, I. D., & McGrath, T. J. 2004. “Two-dimensional analyses of thermoplastic culvert deformations and strains.” *Journal of Geotechnical and Geoenvironmental Engineering*, ASCE, 130(2): 199-208.

Dipen B., Ketul B. and Dipal P. 2015. “Stress Concentration Factor Converts Into Stress Intensity Factor Using ANSYS.” *European Journal of Advances in Engineering and Technology*, 2015, 2(1): 46-49.

Folkman S. 2012. “Water Main Break Rates in the USA and Canada: A Comprehensive Study.” *Research Report, Utah State University Buried Structures Laboratory*, Logan, UT, USA.

Frick, G.R. and Manuel, J. 2005. “Leak Detection Program: The City of Mount Pearl”, Proc. Leakage 2005, Halifax, NS, Canada

Gould, S.J.F., Boulaire, F.A., Burn, S., Zhao, X.L. & Kodikara, J.K., 2011, Seasonal factors influencing the failure of buried water reticulation pipes*, Water Science & Technology:* 2692-2699.

Li C.Q., Yang S.T. 2012. “Stress intensity factors for high aspect ratio semi-elliptical internal surface cracks in pipes.” *International Journal of Pressure Vessels and Piping* 96-97: 13-23.

Liyanage, K., and Dhar, A. S. 2015. “Three Dimensional Finite Element Analyses of Partially Supported Water Mains.” *68th Canadian Geotechnical Conference*. Quebec City, Canada.

Liyanage, K., and Dhar, A. S. 2017. “Stresses in Cast Iron Water Main Subjected to Non-Uniform Bedding and Localized Concentrated Forces”. In press.

Liyanage, K.T.H and Dhar, A.S. 2017. “Effects of corrosion pits on the wall stresses in cast iron water mains.” *ASCE Journal of Pipeline Systems - Engineering and Practice*, 8(4): 04017023.

Makar, J. M., Rogge, R., McDonald, S., and Tesfamariam, S. 2005. “The Effect of Corrosion Pitting on Circumferential Failures in Grey Iron Pipes.” American Water Works Association, Denver.

Rajani B. and McDonald S. 1995. *Water mains break data on different pipe materials for 1992 and 1993*. Report No. A-7019.1, National Research Council, Ottawa, ON.

Rajani, B., Zhan, C. and Kuraoka, S. 1996. “Pipe Soil Interaction Analysis of Jointed Water Mains.” *Canadian Geotechnical Journal* 33 (3): 393–404. Doi: 10.1139/t96- 061.

Trickey, S. A., Moore, I.D. and Balkaya, M. 2016. “Parametric study of frost-induced bending moments in buried cast iron water pipes”, *Tunnelling and Underground Space Technology* 51: 291-300.